Design Optimization, Control, and Testing of a Powered Ankle Foot Orthosis

Master Thesis
to acquire the academic grade of
Master of Science in Engineering (MSc)

University of Applied Sciences Vorarlberg
Mechatronics

submitted to
Dipl. Ing. Dr. Johannes Steinschaden
Dr. Thomas Sugar
Geir Hovland
presented by
Philipp Pasolli BSc

Dornbirn, August 2014

To my parents Eveline and Andreas,
as well as to my siblings Vanessa and Alexander,
who have always supported me in my doings.

Abstract

DESIGN OPTIMIZATION, CONTROL, AND TESTING OF A POWERED ANKLE FOOT ORTHOSIS

The aim of this thesis was to develop a Powered Ankle Foot Orthosis, specifically designed to help treat patients suffering from foot ulceration caused by diabetes. The device is supposed to support its user with 50% active gait support for patients of up to 150kg. Also, it is designed for multiple usage. The modeling was performed in a way, to make it modular so that essential parts can be reused. The necessary power is generated by a combination of motor, pullies, ball screw, spring and leverarm.

Research was performed on diabetes ulceration as well as on already existing wearable robots and their working principles. After gaining the necessary information, concepts were generated to tackle certain problems, which arose during research of the topics. From them the most promising concepts where chosen and modeled in SolidWorks. Stress calculations were performed by hand and utilizing Abaqus CAE for FEA.

The electronics run on an MC710AWA μ-Controller. The motor controller is an EPOS2 40/12, which was custom designed by Maxon Motors to SpringActive's specifications. For programming and data monitoring, a CB-OBS421I Bluetooth module was implemented. As control strategy the Tibia Controller was used, facilitating signals from a rate gyro sensor located on the patients tibia.

Acknowledgement

First of all i want to thank Alexander Böhler and Dr. Thomas Sugar for offering me the possibility to perform my Master Thesis at ASU on such an interesting topic. Throughout my project, Alexander provided me with the basic knowledge and helped me to get familiar with the certain peculiarities of this field of work.

Also i want to thank Jeff Ward, Kevin Hollander and all other members of the team for their continuous support of my project and their invaluable inputs. Their feedback was essential for the project to come together.

Contents

List of Figures **8**

List of Tables **12**

1 Introduction **13**

1.1 Diabetes . . . 13
1.2 Wearable Robots . . . 13
1.3 Objective of the Study . . . 14
1.4 Organization of the Thesis . . . 15

2 Literature Review **16**

2.1 Diabetes . . . 16
2.1.1 Causes and Consequences . . . 16
2.1.2 Foot Ulceration . . . 17
2.1.3 Methods of Treatment up to now . . . 18
2.2 Wearable Robots . . . 20
2.2.1 RUPERT . . . 21
2.2.2 MIT's active ankle foot orthosis . . . 22
2.2.3 MRF Brake Lower Limb Orthosis . . . 22
2.2.4 MR Fluid Damper AFO . . . 23
2.2.5 Artificial Pneumatic Muscle Powered AFO . . . 24
2.2.6 Powered Ankle Foot Orthosis (PAFO) . . . 25
2.2.7 Exosuit . . . 25
2.2.8 Hybrid Assistive Limb (HAL) . . . 26
2.3 Gait cycle . . . 27
2.3.1 General Movmement . . . 29
2.3.2 Ankle Movement in Detail . . . 30
2.3.3 Ankle Graphs . . . 32

3 Powered Ankle Foot Orthosis (PAFO) 34
3.1 Kinematics, Kinetics and Motor Layout . . . 36
3.1.1 Nut Pattern . . . 38
3.1.2 Power and Energy Consumption . . . 42
3.1.3 Motor Layout . . . 47
3.1.4 Motor Evaluation . . . 53
3.2 Modeling . . . 55
3.2.1 Concepts . . . 55
3.2.1.1 Sole . . . 55
3.2.1.2 Ankle Joint . . . 58
3.2.1.3 Actuator . . . 60
3.2.1.4 Interface Leg - Calf Shell . . . 64
3.2.1.5 Eversion/Inversion . . . 67
3.2.1.6 Connection Rods . . . 69
3.2.1.7 Morphological Box . . . 71
3.2.2 CAD . . . 73
3.2.2.1 Foot . . . 73
3.2.2.2 Actuator . . . 78
3.2.2.3 Slider . . . 87
3.2.2.4 Main Assembly . . . 89
3.2.2.5 Bill of Materials . . . 90
3.2.3 Stress Calculation and Finite Elements Analysis . . . 93
3.2.3.1 Footplate . . . 94
3.2.3.2 Foot - Actuator Bolt . . . 100
3.2.3.3 Chain Element . . . 103
3.2.3.4 Chain Bolts . . . 105
3.2.3.5 Screw for Ball Screw - Screwmount Connection . . . 107
3.2.3.6 Ball Screw . . . 107
3.3 Electronics . . . 109
3.3.1 Wiring . . . 110
3.3.2 Component Specifications . . . 112
3.4 Controls . . . 116
3.4.1 Formerly Used Controllers . . . 116
3.4.1.1 Lever Control . . . 116
3.4.1.2 Basic Nut Control . . . 117

3.4.1.3 Nut Control with Time Modulation 117
3.4.1.4 Impedance Control 118
3.4.1.5 Equilibrium Controlled Stiffness (ECS) 118
3.4.1.6 Dynamic Pace Controller 119
3.4.1.7 Robust Control 121
3.4.2 EPOS2 Controller 122
3.4.3 Tibia Controller 123
3.4.4 Signal Conditioning 127

4 Testing and Data Analysis **129**

5 Discussion and Outlook **137**

Bibliography **140**

Affidavit **144**

List of Figures

2.1 Stepwise process from callus formation to ulceration and infection 18
2.2 RUPERT 21
2.3 Active Ankle Foot Orthosis 22
2.4 Osaka MRF Brake 23
2.5 MR Fluid Damper Orthosis 24
2.6 Artificial Air Muscle Powered AFO 24
2.7 Powered Ankle Foot Orthosis 25
2.8 Exosuit 26
2.9 HAL 27
2.10 Anatomical planes 28
2.11 Ankle movements 29
2.12 Gait cycle 30
2.13 Joint angle 32
2.14 Joint moments 33
2.15 Joint power 33

3.1 Main assembly 35
3.2 Electronics schematic 36
3.3 Kinematic model of the PAFO 37
3.4 PAFO orientations 38
3.5 Ankle angle 39
3.6 Ankle moment 40
3.7 Nut and leverarm position during gait cycle 41
3.8 Optimal spring stiffness 43
3.9 Optimal leverarm length 44
3.10 Minimum overall power consumption 45
3.11 Power needed by the motor and the ankle 46
3.12 Optimal leverarm and motornut position 46

3.13 Motor circuit . . . 48
3.14 Transmission limitations . . . 51
3.15 Optimal transmission ratio . . . 52
3.16 M-ω-diagram . . . 53
3.17 Sole concept 1 . . . 55
3.18 Sole concept 2 . . . 56
3.19 Sole concept 3 . . . 56
3.20 Sole concept 4 . . . 57
3.21 Ankle joint concept 1 . . . 58
3.22 Ankle joint concept 2 . . . 59
3.23 Ankle joint concept 3 . . . 59
3.24 Ankle joint concept 4 . . . 60
3.25 Actuator concept 1 . . . 61
3.26 Actuator concept 2 . . . 61
3.27 Actuator concept 3 . . . 62
3.28 Actuator concept 4 . . . 62
3.29 Actuator concept 5 . . . 63
3.30 Actuator concept 6 . . . 63
3.31 Calf shell concept 1 . . . 64
3.32 Calf shell concept 2 . . . 65
3.33 Calf shell concept 3 . . . 65
3.34 Calf shell concept 4 . . . 66
3.35 Concept joint 1 . . . 67
3.36 Concept joint 2 . . . 67
3.37 Concept joint 3 . . . 68
3.38 Concept joint 4 . . . 68
3.39 Concept joint 5 . . . 68
3.40 Concept joint 6 . . . 69
3.41 Connection rod schematic . . . 70
3.42 Concept slider 1 . . . 70
3.43 Concept slider 3 . . . 71
3.44 Morphological box . . . 72
3.45 Foot assembly . . . 73
3.46 Footplate . . . 74
3.47 Flexible front of foot plate . . . 75

3.48 Ankle joint exploded view . . . 75
3.49 Chain connection . . . 76
3.50 Actuator connector . . . 77
3.51 Actuator connector in assembly . . . 77
3.52 Actuator assemblies . . . 78
3.53 Actuator assembly bottom . . . 81
3.54 Actuator spring connector cross section . . . 81
3.55 Actuator top cross section . . . 83
3.56 Actuator top connector . . . 85
3.57 Actuator motorplate . . . 86
3.58 Slider . . . 87
3.59 Slider markups . . . 88
3.60 Powered Ankle Foot Orthosis . . . 89
3.61 Slider mounting . . . 90
3.62 Actuator mount . . . 90
3.63 FEA linear and quadratic elements . . . 94
3.64 FAE footplate assembly . . . 95
3.65 FAE constraints and connectors . . . 96
3.66 FAE footplate stress analysis . . . 96
3.67 Ankle angle and ankle moment . . . 97
3.68 FAE footplate assembly. Boundary condition during maximum ankle moment . . . 98
3.69 FAE footplate assembly stresses during maximum moment . . . 99
3.70 FAE footplate balljoint . . . 100
3.71 Foot - Actuator Bolt handcalculation . . . 101
3.72 FAE foot balljoint bolt stresses . . . 102
3.73 FAE chain element . . . 103
3.74 FAE chain element - stress . . . 104
3.75 FAE chain bolt . . . 105
3.76 FAE chain bolts - stresses . . . 106
3.77 FAE mesh ball screw . . . 108
3.78 FAE ball screw - stresses . . . 108
3.79 Electronics mounted . . . 109
3.80 Electronics layout . . . 110
3.81 Electronics detailed wire layout . . . 111

3.82 Motor controller output current as a function of temperature 114
3.83 Schematic of a robotic actuator 116
3.84 Profiles of Dynamic Pace Controller 120
3.85 Split up of gait cycle for robust control 121
3.86 Tibia angle during one gait cycle 123
3.87 Tibia angular velocity as a function of tibia angle 124
3.88 Polar angel as function of gait percent 124
3.89 Polar radius as function of gait percent and stride length 125
3.90 Ankle angle as function of gait percent and stride lenght 126
3.91 Pseudo integrator Bode Diagram 127
3.92 Accelerations of original and fitted nut pattern 128
3.93 Original and fitted nut position 128

4.1 PAFO 130
4.2 Reference vs. real motor position 131
4.3 Moments, deflections and positions of the ankle, spring and leverarm at 3mph 132
4.4 Ankle moment comparison 2mph vs. 3mph 133
4.5 Real vs. theoretical ankle moment 134
4.6 Motor input and output power and efficiency over two consecutive cycles 136

List of Tables

3.1 Symbols of fig. 3.3 39
3.2 table:simulation values for figure 3.3 41
3.3 Motor circuit symbols 48
3.4 Final motor, values 54
3.5 Chosen motor, values 54
3.6 Springs for 20kg intervals 80
3.7 Parts to interchange for distinct weight categories 91
3.8 Number of parts per category 91

1 Introduction

"Today, diabetes is now epidemic, according to the Centers for Disease Control, the National Institutes of Health, the American Diabetes Association and other national healthcare leaders." - Tim Holden [Holden, 1957]

1.1 Diabetes

Back in 1935, 15 million people were affected by diabetes, while that number grew to about 150 million by 2004. So at the beginning of the 21st century, 5% of the world's population was affected. By that time this disease was already called the disease of the 21st century. [Nazarko, 2009]

As a matter of fact, there are currently 347 Million people suffering from diabetes worldwide. 80% of those are located in countries with a low- to mid average income. Up until 2010, India was the leading country with most people affected by diabetes. Meanwhile, China has taken its place with 92 million diabetics.

It gets even worse by taking a look at the economical costs caused by this disease. The total costs for the global economy in 2010 was about 376 billion US Dollars, making up 11.6% of the world wide health care expenditure!

The WHO furthermore estimates, that the number of people affected by diabetes will increase to about 366 million by 2030, which is 10 times the number of patients affected by HIV/AIDS. Also it is predicted, that during the time period from 2005 to 2030 the deaths caused by diabetes will double. This is mainly because around 298 million of the people affected, are living in developing countries with no access to adequate health care. [Einstein, 2014], [WHO, 2014]

1.2 Wearable Robots

A few years ago, wearable robots were still considered as devices which still have to go a long way until they will make it on the market to be used by people in a daily fashion.

Nowadays, we are closer to the use of wearable robots than we would have ever imagined back then. The technological improvements in different areas as microprocessors, power supplies, motor size and efficiency have propelled the development of such devices dramatically.

Wearable robots are already used in a variety of different areas of application, spanning from medicine all the way to military usage. However, most of the devices are still in either their prototype or beta stages and are not used on a daily basis. Nevertheless, the achieved results are already highly promising.

One of the biggest challenges for wearable robots are to interface with the human body. Early stages of these robots were called exoskeletons, using a rigid frame surrounding the user to mount the necessary devices on to and providing the desired support. However, recent tendencies show a movement towards more flexible systems, where the robot tries to fit the person's anatomy. Constant research and development and the combination of new materials led to new actuator methods, which are quite different to the commonly known directly connected electrical motors and gearboxes. By introducing power storing elements like e.g. springs, the size of the actuator as well as the device's power consumption could be reduced dramatically.

1.3 Objective of the Study

In 2008 Alexander Böhler, former student at the University of Applied Sciences in Vorarlberg, developed an powered Ankle Foot Orthosis at Arizona State University in the course of his Master's Degree. A prototype was manufactured and tested but never was used for commercial purposes.

The purpose of this thesis is to incorporate new theories and the improvements in different areas over the last few years into a new orthosis. The first version was intended for the use of rehabilitation of stroke patients, while this one aims for treatment of diabetic patients.

The goal of the project, is to build a fully functioning prototype, which then can be tested on able bodied, or, if possible, on subjects already affected by foot ulceration. The objectives listed below were derived during the course of several meetings and discussions with some of the student advisors:

- model and construct a new Powered Ankle Foot Orthosis which suits the needs of a diabetic patient

- take into account existing information and mechanical models and improve these if possible and/or necessary
- for control, the Tibia Controller developed by SpringActive should be incorporated
- SpringActive's custom developed MC710AWA microprocessor board and EPOS2 40/12 motor controller shall be used
- the orthosis should be able to support a diabetic patient of 150kg with 50% of the power needed for normal gait behavior. A safety factor of 1.2 should be included.
- because of long lead times, standard ball screws should be used instead of roller screws
- the orthosis should be built and tested on able bodied people, or, if possible, on patients affected by foot ulceration
- a mode should be implemented which moves the foot in plantar and dorsal direction while the patient is sitting, "pumping" blood into the foot.

1.4 Organization of the Thesis

Chapter 2, Literature review: Important facts - Consequences and appropriate treatment of Diabetes - Wearable Robots
Chapter 3, PAFO: Kinematics and Kinetics - Motor Dimensioning - Design and Concepts - CAD Modeling - FEA verification - Electronics - Controls
Chapter 4, Testing and data analysis
Chapter 5, Discussion and outlook

2 Literature Review

2.1 Diabetes

2.1.1 Causes and Consequences

So what is diabetes, what is the cause, why is it so severe and when did it emerge? In the past, there was no guaranteed, everyday food supply. If harvests failed due to environmental issues, food could be short in supply. Also, most of the people had to exercise every day, even if it only was to check the crops, get some water or just perform their work. Nowadays we have plenty of food almost everywhere. So we end up eating more and exercising less. As our society became more obese, diabetes emerged.

Diabetes mellitus, which translates into 'sweet' diabetes is a chronicle disease caused by a deficiency, inherited or acquired, of insulin production by the pancreas. This deficiency results in an increased amount of glucose in our body's bloodstream, damaging multiple of our body's systems, in particular the nerves and vessels.

Diabetes can be classified into two different groups:

- Type 1: formerly also known as insulin dependent diabetes.
- Type 2: also known as non-insulin dependent diabetes.

Type 1 diabetes leads to the destruction of the beta cells of the pancreas. However, only 10% of all diabetes patients are affected by type 1 diabetes. The cause is not fully understood yet, although it seems that there are multiple factors causing it. Nevertheless it is certain, that type 1 diabetes is an autoimmune disease leading to an increased risk of developing type 2 diabetes.

90% of all diabetes patients are affected by type 2 diabetes, meaning, that one out of 20 persons, is affected by type 2 diabetes. This type of diabetes is most common among overweight people, for example, the appearance of the disease is twice as frequent in the US as in the UK. In general diabetes can cut your life expectancy by about 10-15 years. [Nazarko, 2009]

"When we digest carbohydrate, the body breaks it down into simple sugars (glucose). Glucose is then absorbed by the intestine into the blood supply, causing blood glucose levels to rise. The pancreas responds to this by producing insulin, which is released directly into the blood stream and acts quickly." [Nazarko, 2009, Page 534]

Diabetes can act on our body in many ways. Some of the most common ones are the following:

- Increased risk of cerebrovascular disease and stroke by about 12 times.
- Increased risk of coronary heart disease by about 12 times.
- Increased risk of peripheral neuropathy by about 16 times.
- Increased risk of blindness.

[Nazarko, 2009]

2.1.2 Foot Ulceration

The consequence of diabetes directly related to the topic of this thesis is neuropathy. It is a complication affecting nerves and can be distinguished into sensory, autonomic and motor neuropathy.

As already described, diabetes affects the bloodflow to nerves and in vessels. Sensory neuropathy is related to the nerves and therefore the sensing of our environment. One of the most affected areas is the foot, where the patient has almost no or no sensation at all any more. [Jeffcoate and Harding, 2003]

Autonomic neuropathy causes dryness of the skin, while motor neuropathy affects the muscle movement. The patient is not able to move appropriately any more, causing an uneven force distribution throughout the foot. This leads to thickening of the skin, developing callus. The next stage in development of the disease on a patient's foot would be an ischeamic necrosis, meaning the breakdown of the skin tissue and subcutaneous tissue, finally resulting in a neuropathic ulcer which has a punched out appearence.

This is getting even more dramatic, taking into consideration that the patient is walking all day with an open wound and therefore exposed to an extremely high risk of severe infection of the affected area or even the whole foot, if not treated accordingly within time.

A stepwise process from callus formation to ulceration and infection can be seen in figure 2.1. [Jeffcoate and Harding, 2003]

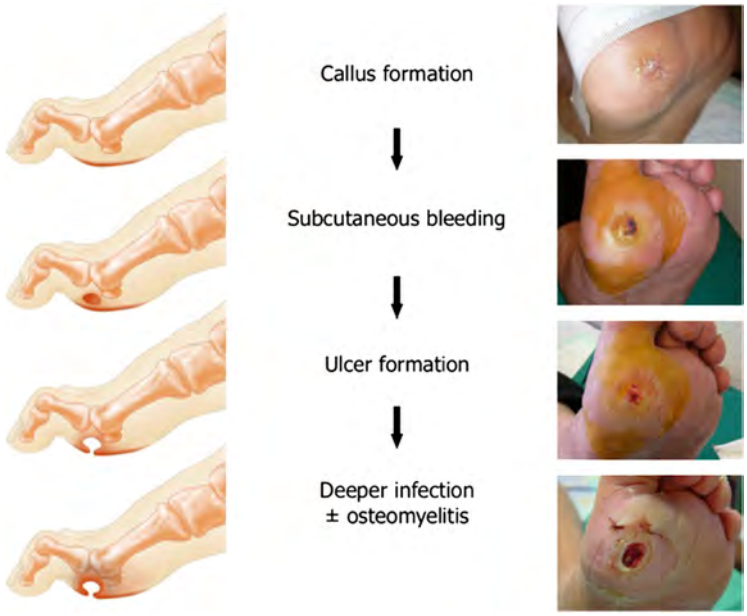

Figure 2.1: Stepwise process from callus formation to ulceration and infection [Alavi et al., 2014]

Furthermore, diabetic foot ulcers can be divided into neuropathic, ischemic and neuroischemic ulcers, where ischemia is a restriction in blood supply and therefore causing shortage of oxygen. If ischemia is detected, the patient must be transferred to a vascular surgeon immediately, attempting a revascularization. However, the latter two mentioned categories have a less favorable prognosis, often resulting in amputation.

Neuropathy makes the patient almost completely unaware of his condition until it is almost too late. Statistics show, that half of the persons with diabetes are not even aware of their disease. However, early recognition of the high-risk foot and timely treatment is absolutely crucial to prevent foot ulceration, saving limbs and potentially lives. [Alavi et al., 2014]

2.1.3 Methods of Treatment up to now

The process of healing off an ulceration area is often really slow. On average it will take around two months, even in centers specialized on foot ulceration. In general 20% to 25% of all hospital admission days for patients with diabetes, are related to foot ulcerations. The risk of an amputation of the lower extremity for a diabetic patient is about 15 to 46 times higher than for their non-diabetic counterparts.[Alavi et al., 2014]

The worst case scenario, death of the patient set aside, is the amputation of the affected limb. However, the healing costs for an amputation sum up to around 45,000$, while costs for the healing process without an amputation are roughly around 6,600$. Besides the economic costs, an amputation is obviously not desirable for the patient either. [Alavi et al., 2014]

The main priority of treating foot ulceration is to restore vascular blood flow to ensure, that the healing process can start. Also an early detection of the ulceration is necessary. Therefore the people have to be sensitized to get checked out, if they think there might be something wrong. In such a case it is better to check once too often than too seldom. Finally the pressure on the affected area has to be redistributed, meaning lifting weight off from the ulceration area.

Naturally the area surrounding the ulceration, as well as the ulcer itself has to be treated for infection and the callus area has to be removed surgically.

Devices for treatment and lifting off weight from the affected area are:

- Total Contact Cast (TCC)
- Removable Cast Walker (RCW)
- Half Shoe (forefoot)
- Padding
- Custom made Orthotics
- Custom Braces, Ankle and Foot Orthoses.

The most common treatment method, used all over the world, is the total contact cast. for that, fiberglass or casting material is applied to the whole lower leg including the foot with minimal padding, in order to get as close to the shape of the foot as possible. However, the areas affected have to be hollowed out to redistribute pressure. The patient is not able to remove the cast by himself, which is positive for the healing process. Furthermore the patient is limited in his daily activities causing him to take fewer steps and applying less stress on the affected area.

However, the rocker bottom of the cast and the limitations in ankle joint movement, forces the patient into an abnormal gait behavior, affecting the knees and the hips. This is even more critical, if the patient has a preexisting arthritis. Despite that, the time necessary to heal off the affected area remains the shortest by utilizing the TCC. Studies

showed, that the healing time is between 28 and 38 days. However, the total contact cast is not recommended to be used on ulcerations at the heel.

The Removable Cast Walker (RCW) serves the same purpose as the TCC, but gives the user the ability to remove the device whenever necessary. However, studies have indicated, that patients wear the device only 25% to 28% percent of their total ambulatory time. Most of the time the device is worn outside the house, but is then removed when back at home. In order to ensure a fast and optimal healing process, the device has to be worn almost all day. Removing the cast at home basically negates all the benefits gained from wearing it outside. But not only this, some patients even report that they walk around in stockings or even barefoot throughout the house. This behavior increases the risk of infections dramatically. Also, the RCW does not fit the leg of the patient as well as a TCC, introducing shear forces to the skin. That, in combination with the reduced blood flow and therefore a slower healing process, can cause further wearing of the skin at high stress contact areas between cast and foot. Like the TCC, the RCW is not suited to be used for heel ulceration treatment.

The Half Shoe is also often used in treating ulcerations. This device is highly affordable and lifts off weight from the forefoot and redistributes it to the middle and rear section of the foot. It is often used with inlays, padding or custom made orthotics. However, the shoe is unstable compared to the other devices mentioned, which is highly counterproductive, if the patient has an unstable gait behavior already.

Custom Braces serve the same purpose as the RCW, with an improved fit for the patient's leg and foot. It has to be kept in mind, that this device will only suit one patient and cannot be used by any other one. Therefore the price tag for such a device is very high in comparison to the other mentioned ones. [Alavi et al., 2014]

While the main purpose of ulceration treatment is to save the foot, in selected cases an amputation may offer a better functional outcome for the patient. However, most of the time it is not clearly defined, what the better solution would be. [Alavi et al., 2014]

2.2 Wearable Robots

This section of the thesis deals with the literature review of already existing robots. The main focus hereby is on wearable robots which are not necessarily in need for a tethered power source.

2.2.1 RUPERT

RUPERT (fig. 2.2) stands for Robotic Assisted Upper Extremity Repetitive Therapy and was developed at the Arizona State University. This robot is used for rehabilitation purposes of patients suffering from stroke. The robot has four actuated degrees of freedom and is able to extend the arm and move it around in 3D space. Several pneumatic muscles are responsible for the different movements, placed on the shoulder, elbow and wrist. [Sugar et al., 2007]

The device was modeled in a lightweight, safe and easy to use fashion. It can also be worn by a person standing or sitting. The sensors' feedback signals are evaluated by a portable laptop running Matlab to calculate the accelerations and necessary torques. The data for evaluation of the movement is collected by several sensors, including inertial sensors and potentiometers. The data from testing shows, that the active support of the robot helped the patient in performing his tasks. It is important to mention, that gravity is not compensated for.

For therapy the device can be used in both places, at home or in the clinic. The application of the robot mainly focuses on stroke patients. [Sugar et al., 2007]

Figure 2.2: RUPERT developed by ASU, Tempe, AZ, US [Sugar et al., 2007]

2.2.2 MIT's active ankle foot orthosis

The active ankle foot orthosis (AAFO) (fig. 2.3), developed at MIT, is designed for patients with foot drop gait. The main components of the device are a standard passive orthosis with an ankle joint and the actuator, where the actuator consists of a motor connected to a screw, which is in series with a spring. The shell can be custom fitted for the patient's needs, while the actuator is attached on the backside of the patient's tibia.

An angular potentiometer at the ankle joint and a linear potentiometer attached to the spring, provides the necessary data for controlling. Furthermore, capacitive force sensors were embedded in the bottom of the shell to monitor ground reaction forces. The device was tested on two different persons in three different control modes: zero, constant and variable impedance control. The resulting data showed, that the best results were achieved by using the constant impedance control, based on the occurrence of foot drag at slow and self selected speeds. [Blaya and Herr, 2004]

Figure 2.3: Active Ankle Foot Orthosis developed by MIT [Ostrovsky, 2005]

2.2.3 MRF Brake Lower Limb Orthosis

This device was developed by the Osaka Electro-Communication University and combines a standard orthosis with an intelligently controlled MRF (Magneto-Rheological-Fluid) brake. Its main area of application is for people suffering from paralyzation of their lower extremities due to stroke. The purpose of the device is to prevent the foot from dropping and dragging during the swing phase. In order to do so, the compact MR brake is controlled in a fashion to adopt the brake torque to the individual walking conditions. This system does not provide active support to the user's gait. The device presented on the 13th ISPO World Congress is shown in fig. 2.4. [Morimoto et al., 2014]

Figure 2.4: MRF AFO developed by Osaka University [Morimoto et al., 2014]

2.2.4 MR Fluid Damper AFO

This AFO developed by Svensson and Holmberg at the Univerity of Halmstad does not only support walking on even ground, but also on ascending and descending surfaces as well as stairs. It is mainly made of composite materials and a steel joint for the ankle movement. The magnetorheological damper restricts the ankle movement and is placed at the posterior side of the leg. The orthosis allows an ankle movement of 8°of dorsiflexion and 26°of plantarflexion and is powered by a 40MHz microprocessor.

The damper has four different modes:

- Damp: Foot slap is prevented by moderate damping during foot down
- Free: Almost no damping, for example during stance phase to allow free motion
- Lock: High dampening factor to keep the toes up during swing phase
- Free down: Very small dampening during swing phase in order to allow the foot do drop.

The control algorithms distinguish automatically if the surface is ascending, descending, even or if the person is walking stairs, by analyzing the ankle angle during the gait cycle. The device is shown in fig. 2.5. [Svensson and Holmberg, 2008]

Figure 2.5: MR Fluid Damper Orthosis developed by the University of Halmstad.[Svensson and Holmberg, 2008]

2.2.5 Artificial Pneumatic Muscle Powered AFO

The University of Michigan came up with an active, powered orthosis (fig.2.6), which differs from all the ones mentioned so far. The device consists mainly of a carbon shell with a metallic hinge to allow the ankle movement. The support for the user is generated by two artificial pneumatic muscles. One of the muscles situated behind the leg at the tibia provides plantarflexion movement, while the other one, placed above the foot, provides dorsiflexion. As control strategy a proportional myoelectric control was inplemented, measuring the bodies EMG signals and using them as a reference to control the device. [Sawicki et al., 2005]

Figure 2.6: Artificial Air Muscle Powered AFO developed at the University of Michigan [Sawicki et al., 2005]

2.2.6 Powered Ankle Foot Orthosis (PAFO)

In 2008 Alexander Boehler developed an PAFO in the course of his Master Thesis. The device is built in a way, so that the user can step in and strap his foot into place. The foot and the shell of the device are connected with a hinge, allowing the ankle to plantar- and dorsiflex. An ankle sensor at the ankle joint provides the controller with information, to set the motor position according to the gait. The actuator is located behind the patient's leg and consists of a motor linked to a leadscrew, in series with a spring system, introducing a force to a lever arm in order to provide torque to the ankle joint. The device is displayed in fig.2.7.

For the control strategy, the dynamic pace controller as well as a new robust control strategy were tested. Furthermore a graphical user interface was developed to simplify the testing procedure and provide feedback about the status of the robot. [Boehler, 2008]

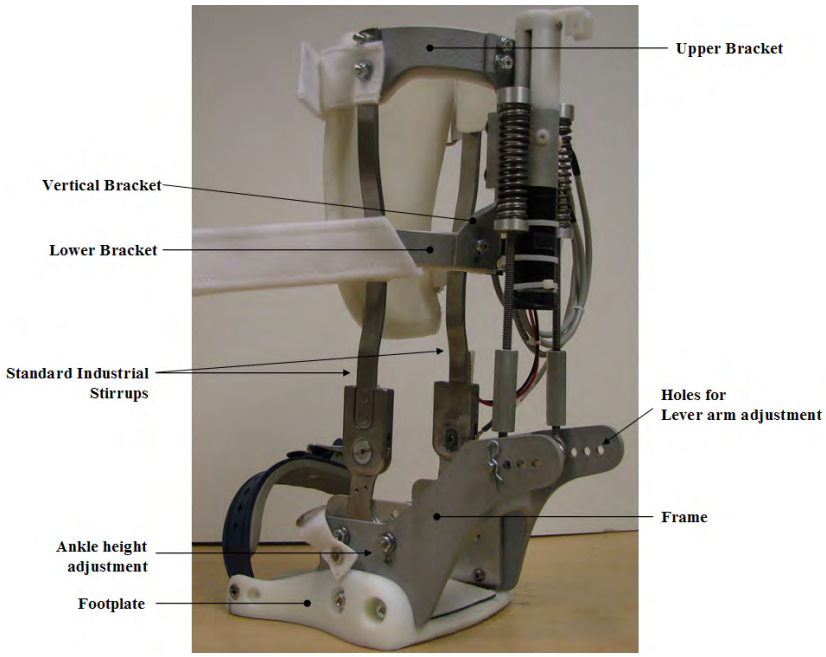

Figure 2.7: Powered Ankle Foot Orthosis, developed by Alexander Boehler at ASU, Tempe, AZ, US [Boehler, 2008]

2.2.7 Exosuit

At Harvard University, the lab of Conor Walsh designed an Exosuit (fig. 2.8) aimed to assist and enhance the endurance of soldiers, routinely carrying heavy packs over long

distances. The approach for the Exosuit is rather different from the typical exoskeletons, not having any rigid structural elements. The suit is mainly built from nylon, polyester and spandex and utilizes the normal, pendulum like gait movement of humans, only providing small, well-timed power bursts to support its wearer.

Sensors in the insole of the shoe support the necessary information for the controller, to time the assistive bursts. The whole suits runs on approximately 50 Watts of continuous power, providing assistance for about 4 hours. Its weight, including actuators, batteries, and the suit itself, sums up to around 6kg, nearly all carried around the waist area. [Xue, 2014]

Figure 2.8: Exosuit developed at Harvard University [Xue, 2014]

2.2.8 Hybrid Assistive Limb (HAL)

The HAL (see, fig. 2.9) is a full bodysuit to assist its user in moving, developed by Dr. Sankai, president of Cyberdine and professor of the University of Tsukuba, Japan. The Robot has rotational actuators placed at the joints, moving the robot. The movement is

triggered by the signals from the brain heading to the muscles themselves. Sensorpads on the wearer's skin sense these signals and processors translate them accordingly to the different movements of the motors. The joints of the robot move towards the desired direction, slightly before the user himself starts to move his limbs, ensuring to support the wearer in his daily activities.

The HAL is controlled by two types of controllers. First the one mentioned above, sensing the nerve signals and second a robot-like, cybernic, autonomous control system that provides human-like movement. [Zelinsky, 2009]

Figure 2.9: Hybrid Assistive Limb (HAL), developed by Dr. Sankai [Ficarra, 2009]

2.3 Gait cycle

In order to develop an orthosis, with the goal in mind, to give its wearer the most comfortable and normal gait behaviour as possible, one first has to understand what the gait cycle looks like and what its movement patterns are.

First of all, the human body is divided in three different planes:

- Sagittal Plane: Dividing the body into left and right
- Frontal Plane: Dividing the body into front and back
- Transverse Plane: Dividing the body into top and bottom

The feet are therefore in the lower part of the body, split by the transverse plane, also called inferior part of the body. See fig. 2.10.

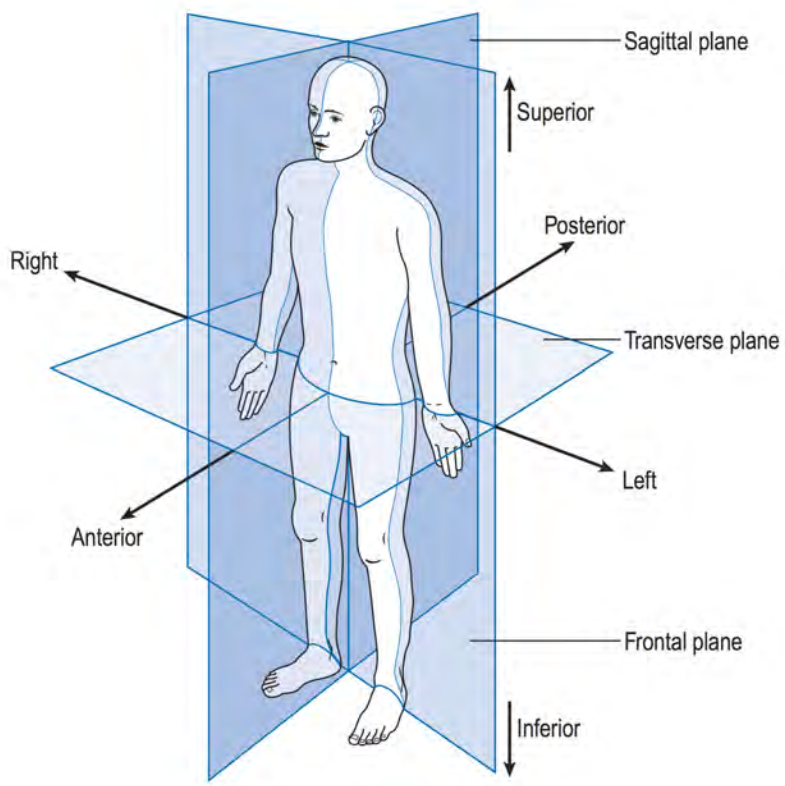

Figure 2.10: Anatomical position and reference planes [Whittle, 2002]

To go into more detail, the movement of the whole body is involved to provide normal gait because of shifting the center of mass. Also the joint bending at the hip and the knee is necessary. However, all these areas are not affected by foot ulceration and are not directly influenced by the orthosis. Analyses of these parts were made in order to fully understand gait behavior, but will not be presented in this thesis.

2.3.1 General Movmement

The foot's movement, is the most important part in the gait cycle regarding the topic of this thesis, because the device will directly influence its freedom and movement. In general the ankle has 3 DOF (compare fig. 2.11)

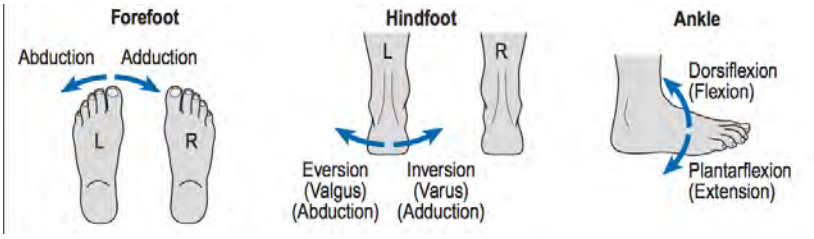

Figure 2.11: Ankle movements [Whittle, 2002]

Although most people think that it is only necessary to lift and push the front of the foot down in order to walk, many more movements of the ankle are involved, not to mention the rest of the body. In addition to the movements of the ankle, shown in fig. 2.11, there are another two important combinations of ankle movements which occur regularly:

- Supination: A combination of Inversion, Plantarflexion and Adduction
- Pronation: A combination of Eversion, Dorsiflexion and Abduction

The gait cycle describes the movement of one foot in the cycle of one step. Typically the gait cycle begins shortly before heel strike and ends at the same point of the same foot again. Figure 2.12 provides an overview of the different stages of the cycle.

The illustration shows the initial position of the human at RHC (Right Heel Contact). Until the next LTO (Left Toe Off), we experience DS (Double Support). After LTO, the whole body's weight is on the right foot. The body roles over the ankle until LHC (Left Heel Contact) occurs. That phase is called RSS (Right Side Support). From LHC until RTO (Right Toe Off), we experience DS again, preparing our right foot to push off to accelerate our body. At RTO the right foot loses contact to the ground, shifting all weight to the left foot. This is maintained until the same point again, known as LSS (Left Side Support). From there on the whole cycle starts all over again.

The phase of the foot having contact with the ground, supporting our movement is called Stance Phase, while the time between Toe Off and Heel Strike is known as Swing

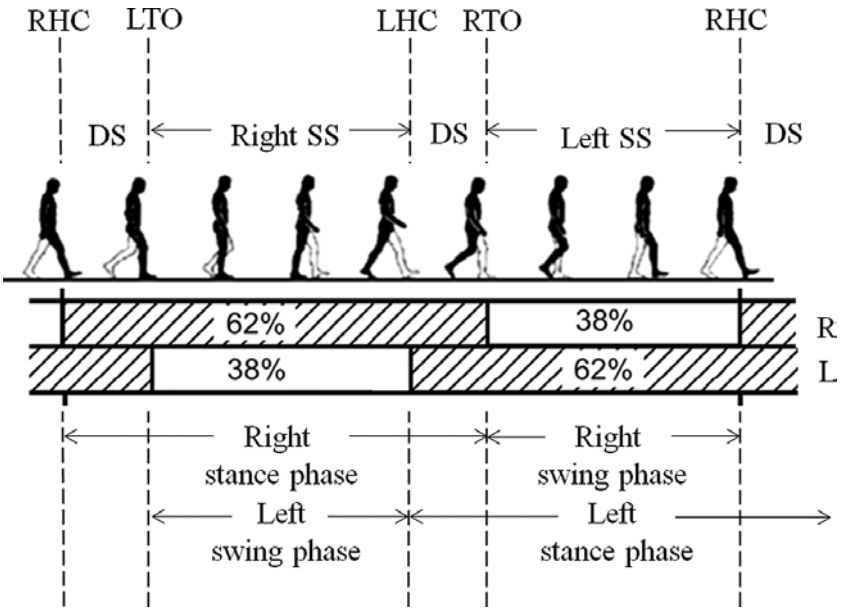

Figure 2.12: Gait cycle and its different stages [Mummolo et al., 2013]

Phase.

The explanations above, describe the general movement from an outside observer's position. Also, the faster the pace we choose, the shorter the time of double support gets. Once we start running, double support is not present any more but a time of no support at all is introduced, where both feet are in the air. One could say that during that time we are flying.

However, to fully understand the movement of the ankle, we have to take a deeper look into the actual positioning of the foot in the discrete positions. [Whittle, 2002]

2.3.2 Ankle Movement in Detail

Initial Contact - Heel Strike

At that time the ankle is normally in its neutral position, meaning no plantar- or dorsiflexion. In general, the foot points upwards, so that the heel strikes the ground first. Usually the foot is slightly supinated at that time, showing a wear pattern on the lateral (outer) side of one's shoe. Muscles for dorsiflexion are still active to hold the foot in its neutral position, preparing for heel strike and plantarflexion movement. **Movements:** Inversion, Adduction.

Loading Response - 20ms after Initial Contact

This position is also called the 'initial rocker' where the foot moves into plantarflexion. The plantarflexion is furthermore accompanied by pronation of the foot. **Movements:** Plantarflexion, Eversion, Abduction.

Opposite Toe Off
When the foot is on flat ground, its angle changes from plantarflexion to dorsiflexion while the tibia is rolling over the ankle angle. **Movements:** Dorsiflexion.

Mid-Stance
The foot is still flat on ground but in a dorsiflexed position. **Movements:** Dorsiflexion.

Heel Rise
This is the point when the foot reaches maximum dorsiflexion and begins to move into a plantarflexed position. In addition to that, the foot starts to supinate as soon as heel off starts. **Movements:** Plantarflexion, Inversion, Adduction.

Opposite Initial Contact
The ankle remains moving into a plantarflexed position. It reaches maximum supination with hindfoot inversion. **Movements:** Plantarflexion, Inversion, Adduction.

Toe Off
Shortly after toe off, the ankle reaches maximum plantarflexion. The ankle's maximum plantarflexion angle is about 25 degrees. **Movements:** Plantarflexion.

Feet Adjacent
The foot moves from the maximum plantarflexed position into a more neutral or dorsiflexed position. This is so, that the toes do not drag on the ground. Also the foot is slightly supinated. **Movements:** Dorsiflexion.

Terminal Contact
The gait cycle ends at the next initial contact of the same foot.
[Whittle, 2002, Pages 52-80]

The explanations above clearly state, that in order to maintain a normal gait behavior not only one rotational joint is necessary, as regular in most of today's orthosis, but 3

of them to give the ankle maximum freedom to move freely.

2.3.3 Ankle Graphs

In order to develop an orthosis correctly to give the user the necessary freedom in ankle movement, but provide safety measures at the same time due of the active power introduced by a motor, one has to know more about the gait cycle than presented so far. The following graphs show the angles (2.13), the moments (2.14) and the power (2.15) for each the hip, knee and the ankle. However, we are merely interested in the curves for the ankle.

From the graphs we notice, that the ankle angle varies between about +10 degrees in dorsiflexion and about -25 degrees in plantarflexion. Furthermore the peak moment, results in about $1.5Nm/kg$, while the peak power is measured at around $4W/kg$

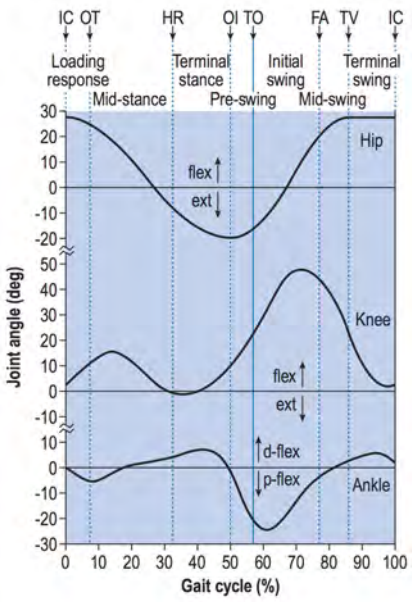

Figure 2.13: Joint angles during a single gait cycle, showing knee, hip and ankle. IC = initial contact, OT =Opposite Toe Off, HR = Heel Rise, OI = Opposite Initial Contact, TO = Toe Off, FA = Feet Adjacent, TV = Tibia Vertical [Whittle, 2002]

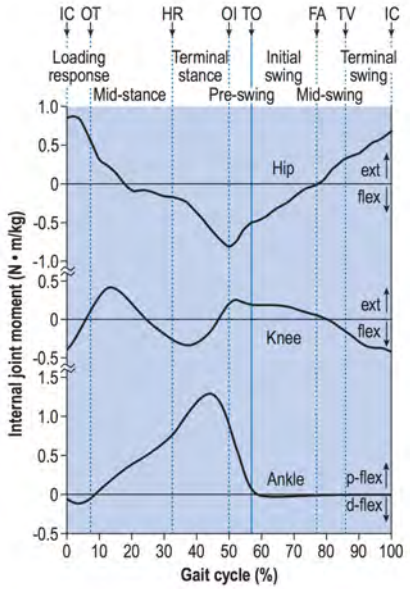

Figure 2.14: Joint moments for hip, knee and ankle during a single gait cycle. IC = initial contact, OT =Opposite Toe Off, HR = Heel Rise, OI = Opposite Initial Contact, TO = Toe Off, FA = Feet Adjacent, TV = Tibia Vertical [Whittle, 2002]

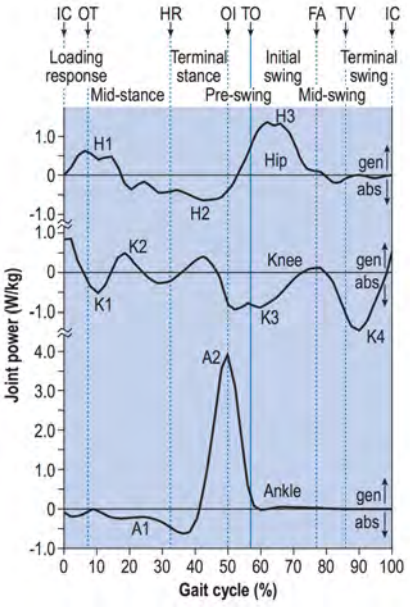

Figure 2.15: Joint power during one single gait cycle needed for hip, knee and ankle. IC = initial contact, OT =Opposite Toe Off, HR = Heel Rise, OI = Opposite Initial Contact, TO = Toe Off, FA = Feet Adjacent, TV = Tibia Vertical [Whittle, 2002]

3 Powered Ankle Foot Orthosis (PAFO)

Despite the fact, that there are many different devices on the market to assist the patient in healing off the affected limb of its ulceration, there are no robots available by now. However, a robotic device would have several positive aspects regarding the healing process and especially the mobility of the patient throughout the day.

First of all the device supports the patient in his gait and his foot movement, allowing the patient to use less of his energy to have the same movement speed. Furthermore due to the active support, the moment for push off and therefore the stress applied on the ulceration area is supposed to be reduced by a significant amount. To take that even one step further, the robot was designed in such a way that it can be combined with a half shoe or a device custom made from a prosthetist. That, in combination with the user's support in walking, should give the patient almost full mobility and yet drop the healing time significantly.

It is even more important, that the controller is equipped with optimal gait patterns for different stride lengths and walking speeds. Therefore, even if the patient developed an abnormal gait behavior due to his foot's condition, the device takes care of teaching him the correct pattern again. Therefore the risk of long term damage can be minimzed.

In this chapter of the thesis the actual device is going to be explained. For the purpose of having a clear outline, there are four subchapters:

- Kinematics, Kinetics and Motor Layout
- Modeling
- Electronics
- Controls

However, a general overview of the final device should be of help for better understanding:

The physical device in general can be split up in a mechanical and an electrical part. The mechanical components can be split up according to the assemblies within the CAD software into foot, actuator, slider and main assembly. The different assemblies are displayed in figure 3.1.

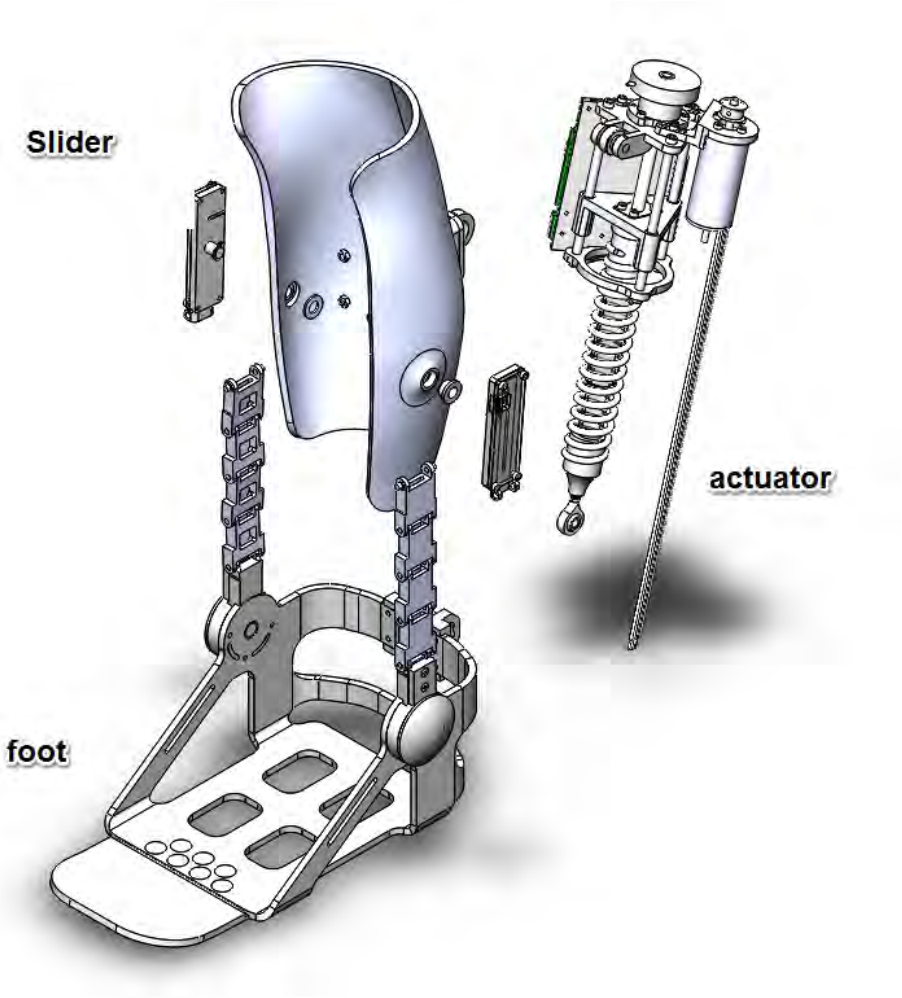

Figure 3.1: Main assembly, displaying slider, foot, and actuator assembly

As one can see from the figure, the actuator is using a spring to connect to the foot. The use of the spring allows us to break down the input power of the system by a faction, because it acts like a power storage device during the gait cycle. Also it adds some flexibility to the device, making it less rigid and therefore also more comfortable to wear.

The sliders are inserted into the calf shell and then connected to the chain elements

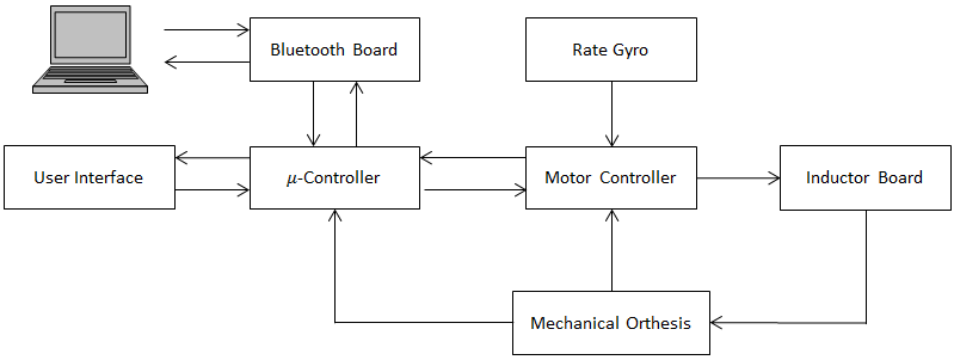

Figure 3.2: Electronics Schematic

coming up from the sides of the foot assembly. The chain elements enable the user to invert and evert his foot, giving him more flexibility. However, because these chain elements are set off from the middle of the foot, creating a leverarm, they will move up and down during inversion and eversion. This linear up and down movement is compensated by the use of the sliders.

Furthermore, big attention was paid to the overall weight. Making the device more lightweight and small, the comfort for the user increases. Adding additional weight always influences the gait behavior and at a certain point the device's weight itself has to be factored into the power calculation. One major factor influencing the weight of the device is the motor. However, because of the use of a spring, storing power during the cycle requiring less active input power, as well as a high transmission ratio, a low powered and lightweight motor can be used.

The electrical side of the PAFO can be split into motor controller, μ-controller, bluetooth board, inductor board, rate gyro and user interface. A schema of how they interact with each other is shown in figure 3.2.

3.1 Kinematics, Kinetics and Motor Layout

In order to verify that the device is capable of supporting normal gait behavior to the patient, as well as supporting the patient's weight and the requirement of 50% support, which is depending on the patient's weight, the kinematics, nut pattern and the motor have to be dimensioned accordingly. Different stages of the gait cycle were already explained in chapter 2.3.2, therefore the different stages and terms are not repeated in this chapter.

However, prior to start laying out the motor and other components of the device, a

kinematic model, representing the device's movements, has to be established in order to proceed. The following graphics display the kinematics of the device, consisting of the ankle joint, a lever arm connected to a spring, mounted on a ball screw which is then driven by the motor.

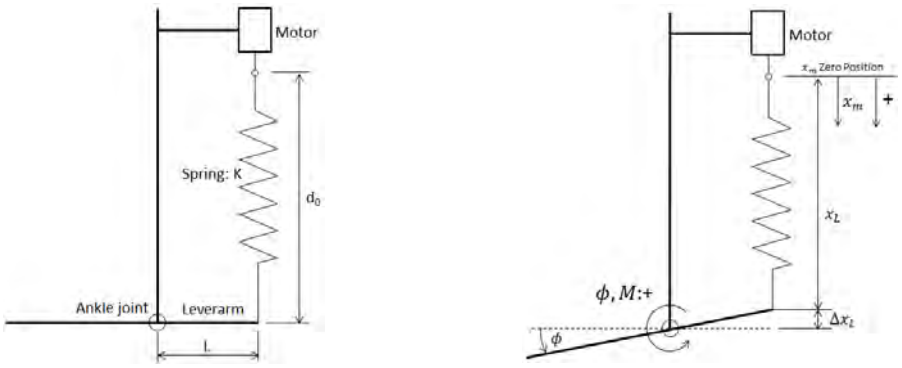

(a) Ankle in zero position (b) Ankle deflected by angle ϕ

Figure 3.3: Kinematic model of the PAFO, both in zero and deflected position, where Δx_L represents the deviation of the leverarm position and x_m the motornut position.

In order to understand the kinematics accordingly, one has to understand the way the device will act throughout the gait cycle. Figure 3.4 shows the PAFO in six different positions during one gait cycle, which are of interest to us for the calculations of the kinematics.

Picture 1 shows the PAFO at heel strike. The motor will move into positive direction to further compress the spring as soon as heel strike occurs to support the user. This has the result, that the front of the foot does not slap down on the ground but experiences some resistance, causing it to touch the ground more gently. At point 2, the foot has established full contact with the ground. The nut is still in a positive position, compressing the spring, making it easier for the user to start moving forward, rolling over the ankle joint. Point 3 shows the foot leg perpendicular to the ground. Here the angle of the foot switches from dorsiflexion to plantarflexion. The user still moves forward causing the spring to be stretched. In order to store even more energy in the spring, the motor moves the nut into a negative direction, stretching the spring even further. At point 4 the spring is stretched to its maximum and the heel starts to lift off the ground. At 5, maximum plantarflexion is reached and the push off occurs. The toes lose contact with the ground. At 6, the foot enters swing phase.

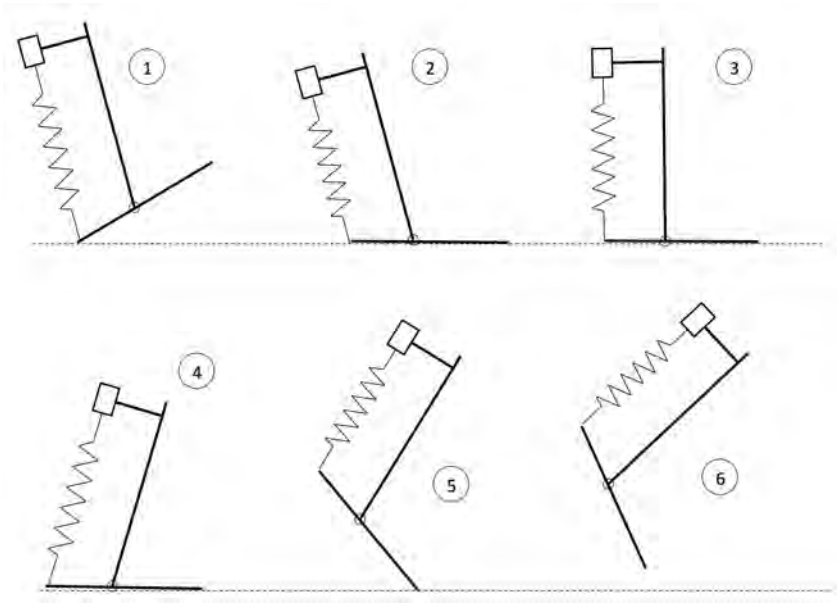

Figure 3.4: PAFO orientations

3.1.1 Nut Pattern

The model is used to derive the equation for the necessary nut pattern, the ball screw has to follow, in order to provide the user with support. As input variables the ankle moment and the ankle angle are provided. The data is obtained from Whittle Whittle, 2007. The following graphs represent the ankle moment (figure 3.6) and the ankle angle (figure 3.5) during one gait cycle.

Compared with figure 3.3b, the angle of the ankle must reach its maximum negative value during the push off phase. However, the maximum moment occurs when the heel starts to rise after maximum dorsiflexion. Comparison to figures 3.5 and 3.6 confirms that.

The graphs displayed and the kinematic model of the ankle, enable us to follow the kinematic chain of the device from the ankle to the necessary nut pattern of the ball screw. The symbols used in the following equations are described in table 3.1

Knowing the ankle angle, we are able to calculate the displacement of the attachment point of the spring on the leverarm. Assuming that the attachment point of the spring is at coordinates (0,0) the displacement in x respectively in y-direction is calculated as:

$$\Delta x_L = L \cdot sin(\phi) \tag{3.1}$$

$$\Delta y_L = (L - (L \cdot cos(\phi)) \tag{3.2}$$

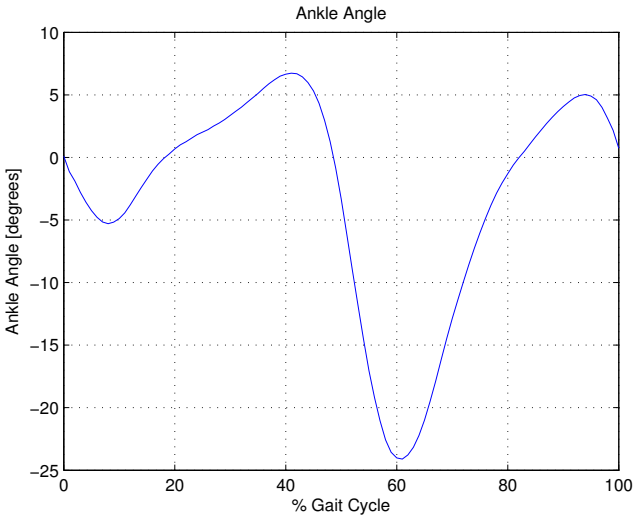

Figure 3.5: Ankle angle

Symbol	Meaning
M	Ankle moment
ϕ	Ankle angle
L	Leverarm length
K	Spring stiffness
d_0	Undeflected spring length
x_L	Length of deflected spring
Δx_L	Deflection of spring
x_m	Nut position

Table 3.1: Symbols of fig. 3.3

In the following process, in order to get the optimal Stiffness K and Leverarm L for the respective bodyweight, equations have to be derivated. To ensure the best accuracy, the calculations were performed with all the sin and cos terms. However, to speed up calculation time the assumption of $cos(\phi) \approx 1$ and $sin(\phi) \approx \phi$ were made.

The ankle angles vary from a maximum of 6.7° to a minimum of -24.1°. Obviously there will be a slight error due to the assumption of small angles. The errors in x and y-direction are:

$$err_x = \frac{0.4206rad - sin(0.4206rad)}{0.4206rad} = 2.9\% \tag{3.3a}$$

$$err_y = \frac{1 - cos(0.4206rad)}{1} = 8.7\% \tag{3.3b}$$

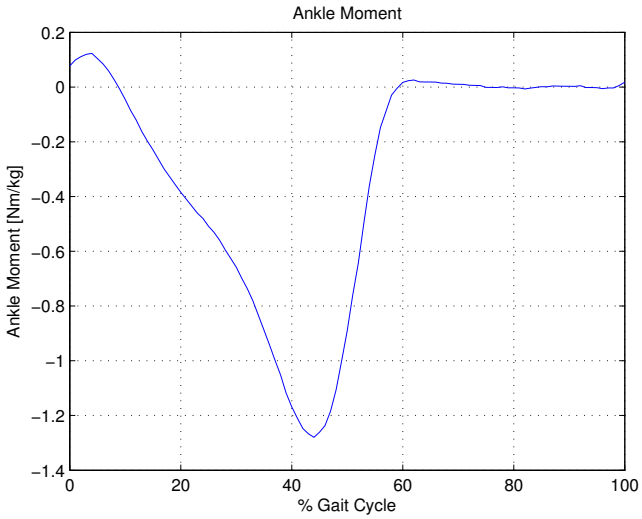

Figure 3.6: Ankle moment

In coordination with the responsible superiors, these errors are acceptable. Therefore, using the ankle moment and the leverarm length, the force needed can be calculated:

$$F = \frac{M}{L \cdot cos(\phi)} \approx \frac{M}{L} \tag{3.4}$$

While the force is provided by the spring, we can calculate the force of the spring with

$$F = K \cdot \Delta d \tag{3.5}$$

where Δd represents the deviation of the spring

$$\Delta d = -\Delta x_L - x_m \tag{3.6}$$

Δd represents a positive value, if the spring is stretched. x_m represents the movement of the nut attached to the spring, responsible for stretching and compressing the spring if Δx_L is held constant. Also, knowing that Δx_L is dependent on the leverarm length L and the angle ϕ, we can combine equations 3.1, 3.5, 3.4 and 3.6 with the assumptions of small angles made, to get the equation for the nut pattern.

$$x_m = L \cdot \phi - \frac{M}{K \cdot L} \tag{3.7}$$

Due to the time dependency of the ankle angle and the ankle moment, the equation

changes to the following:

$$x_m(\phi, M) = L \cdot \phi(t) - \frac{M(t)}{K \cdot L} \tag{3.8}$$

Equation 3.8 provides the necessary information to compute the needed nut position at every time interval during the gait cycle. For calculation, the values shown in table 3.2 are used. The weight is set to $150kg$,a safety factor of 1.2 and patient's support of 50% was applied, according to the objective described in chapter 1.3. Figure 3.7 shows the calculated nut pattern and the leverarm position during one gait cycle.

Parameter	**Value**
Weight	$150kg$
K	$20000N/m$
L	$0.12m$

Table 3.2: table:simulation values for figure 3.3

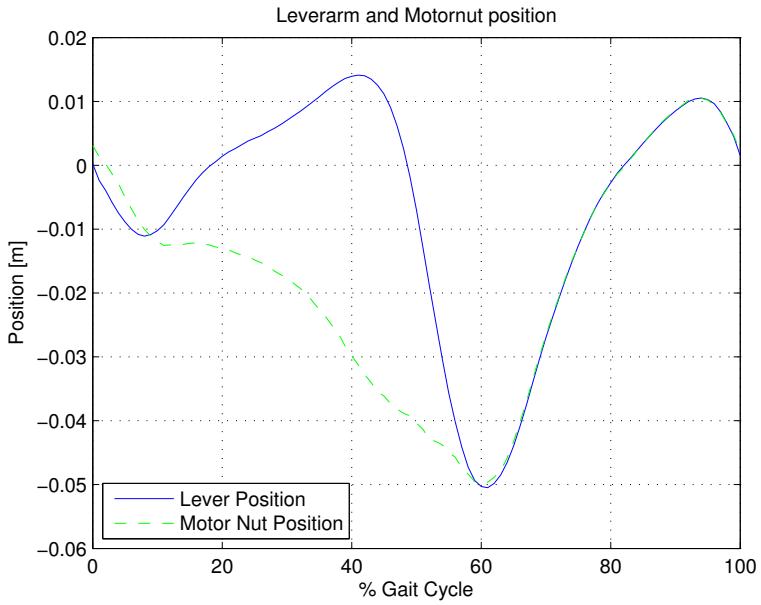

Figure 3.7: Nut and leverarm position throughout the gait cycle, based on table 3.2 and figure 3.3. For calculations, the approximated equations were used.

3.1.2 Power and Energy Consumption

Power consumption is always an important topic when it comes to mobile devices. Assuming that the necessary moment would be introduced directly to the ankle to fully support the patient, a motor with peak power of approximately 500W would be needed. A possible motor would be the Maxon EC 60 weighing around 2.5kg which only provides 400W, therefore requiring a gearbox. By using suitable transmissions, the size of the motor can possibly be decreased, but the weight of the gearbox will be added. All this additional weight has to be mounted on the patient's foot increasing the pressure and stress to the area affected by ulceration. Therefore, directly powering the ankle or even a transmission-motor combination alone is out of question.

By introducing a spring to the system, acting as a power storage device, we are able to decrease the necessary power provided from the battery dramatically. This is very helpful in two different ways. First of all, the motor size and weight can be reduced to a fraction of what would be necessary for direct powering and second, the batteries power will not drain as fast, ensuring a longer operation time.

To link that knowledge to the ankle, we are going to calculate the power necessary based on the already derived nut pattern of equation 3.8. The power in general is the moment multiplied by the angular velocity, or if converted to linear movements, a force times a velocity.

$$P = M \cdot \omega = F \cdot \dot{x} \tag{3.9}$$

To get the required power for the motor, we can combine equations 3.9 and 3.8. Also because power is going to be added to the system and not drained from it, all values have to be positive. Therefore we end up with

$$P_m = \left| L \cdot F \cdot \dot{\phi} - \frac{F \cdot \dot{F}}{K} \right| \tag{3.10}$$

Both of the two factors in this equation L and K can be varied. Therefore it makes sense to try to optimize the peak power by varying these parameters to find the lowest value. The formula used to find the perfect K and L values is

$$P_{m,peak} = max \left| L \cdot F \cdot \dot{\phi} - \frac{F \cdot \dot{F}}{K} \right| \tag{3.11}$$

First the spring constant K was varied and plotted against the power consumption shown in figure 3.8. The graph represents the spring motor peak power depending on the spring

stiffness at a chosen leverarm length.

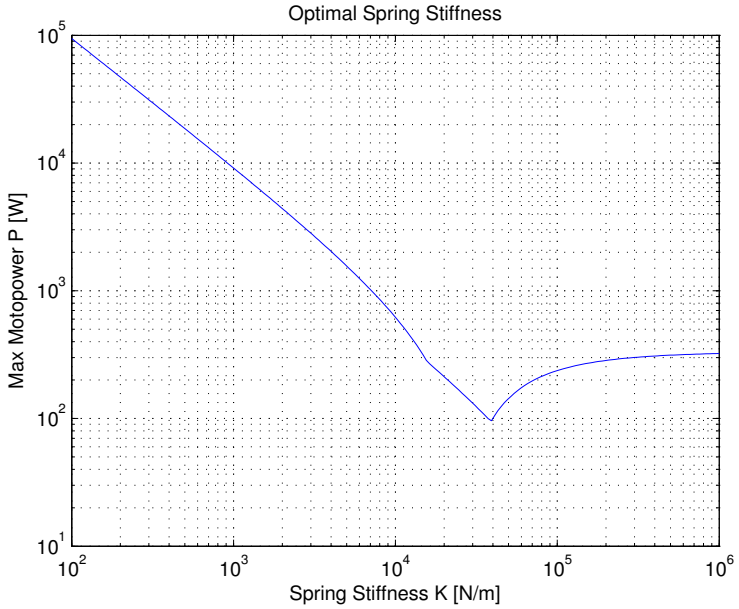

Figure 3.8: Motor peak power depending on the stiffness of the spring.

The stiffness was varied between values of $100N/m$ and $10^6N/m$. As apparent from the graph, a stiffness value exists, resulting in a minimum power consumption. Because of the normalized ankle moment used as an input to the equation, one can assume, that there will be an optimal spring stiffness for every person's bodyweight.

As mentioned already, the leverarm length was varied too. However because of the human anatomy and our approach to minimize the the device's size, the length of the arm was limited from $0.04m$ to $0.12m$. Figure3.9 shows the peak power consumption as a function of the leverarm length.

As shown in the figure, there is a minimum power consumption apparent in the graph resulting in an optimal leverarm length for the device. Again, the equation contains the ankle moment being dependent on the patient's weight. Therefore it can be assumed that there is an optimal leverarm length for every patient as well.

Having that knowledge, an overall minimum power consumption is obtained by searching the minimum of equation 3.11, which is being changed according to the following:

$$P_{m,peak}(K, L) = max \left| L \cdot F \cdot \dot{\phi} - \frac{F \cdot \dot{F}}{K} \right| \tag{3.12}$$

The new function therefore is represented in 3D space because of $P(K, L)$ resulting

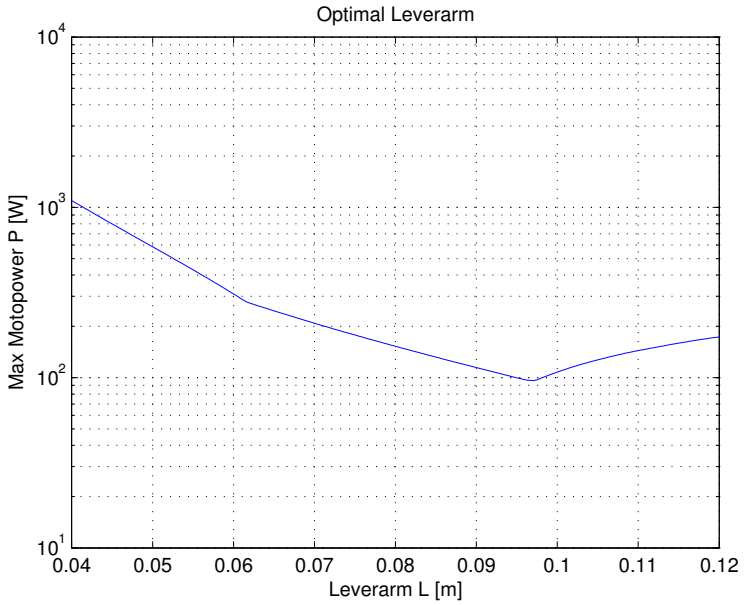

Figure 3.9: Peak power consumption as a function of the leverarm length of the robot.

in a graph displayed in figure 3.10.

From those calculations, the following optimal Values for K and L and from them respectively the lowest peak Power P were retrieved:

- $K_{optimal} = 41027N/m$
- $L_{optimal} = 0.0886m$
- $P_{optimal} = 95.8W$

However, because of modeling and transmission ratio restrictions as well as because the leveram was not intended to be varied for every person, the leverarm was changed to a value of $L = 0.093m$. By running the calculations again, the following values were the results and used for further calculations and the motor layout:

- $K_{optimal} = 37399N/m$
- $L_{optimal} = 0.093m$
- $P_{optimal} = 96.5W$

Due to that change, the device is not at optimal efficiency. The following equation calculates the deviation from optimal efficiency.

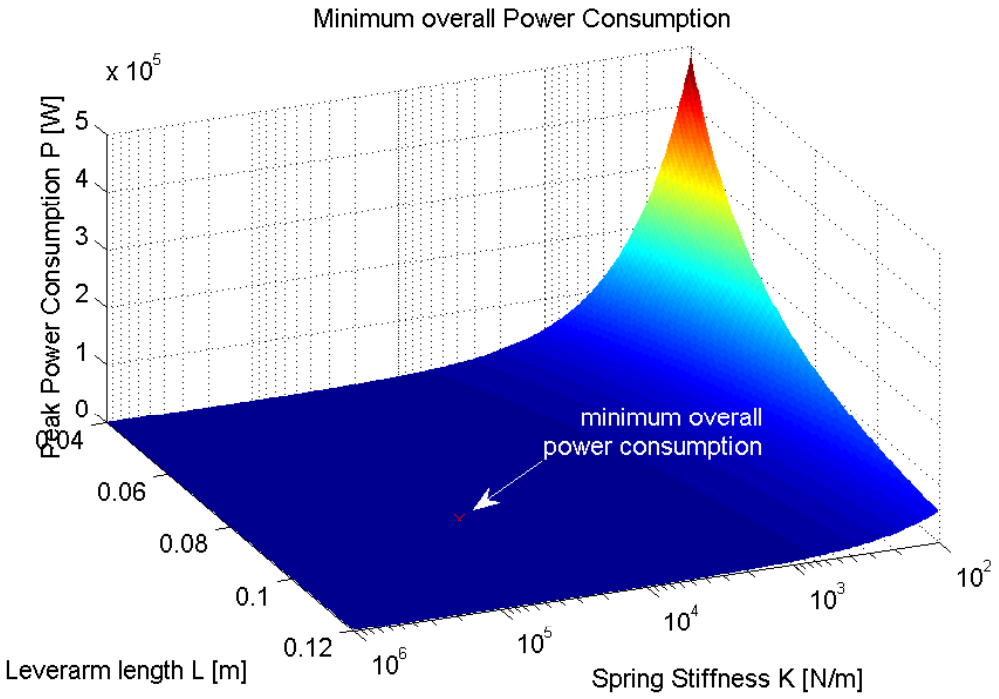

Figure 3.10: Peak power consumption as a function of K and L.

$$err_P = \left| \frac{96.5W - 95.8W}{95.8W} \cdot 100\% \right| = 1.04\% \tag{3.13}$$

The deviation caused by the adjustments of the leverarm are easily within acceptable limitation.

As already mentioned, by introducing a spring as a power storage device into the actuator system, the necessary power can be cut down to a fraction. Figure 3.11 displays the power needed by the leverarm to provide a 150kg person with an additional safety factor of 1.2 on the weight with 50% support throughout the gait cycle. Due to the spring, the peak power drops from $332W$ down to $96.5W$, enabling us to use a smaller motor and ensuring a longer operational time by using the same battery as a power supply.

Taking into account the optimized spring constant as well as the chosen leverarm length, a new nut pattern was simulated. The results displayed in figure 3.12 are fairly similar to the original plot shown in figure 3.7.

Also figure 3.12 directly shows the stretching of the spring. The deviation the spring will experience throughout the gait cycle is simply the difference between the lever position and the motor nut position. As we can see, the spring will be stretched between

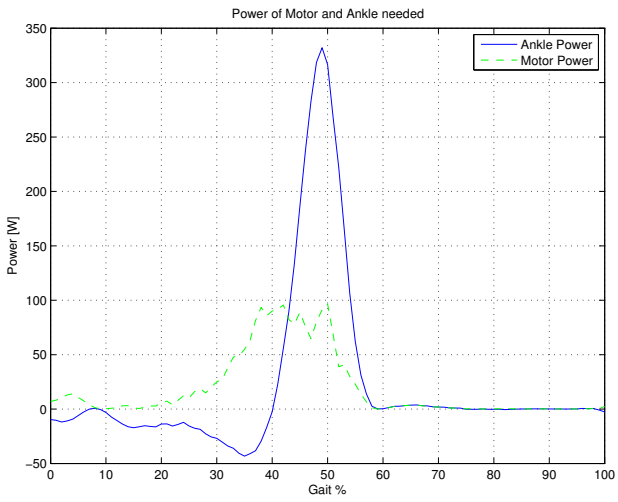

Figure 3.11: Power needed by the motor and the ankle to provide 50% support for a 150kg person with a safety factor of 1.2 throughout the gait cycle

15% and 60% of the gait cycle, where energy is stored in order to get ready for push off. On the other side, in the beginning of the graph we can see, that the spring will be compressed, in order to support the user at heel strike, as mentioned earlier.

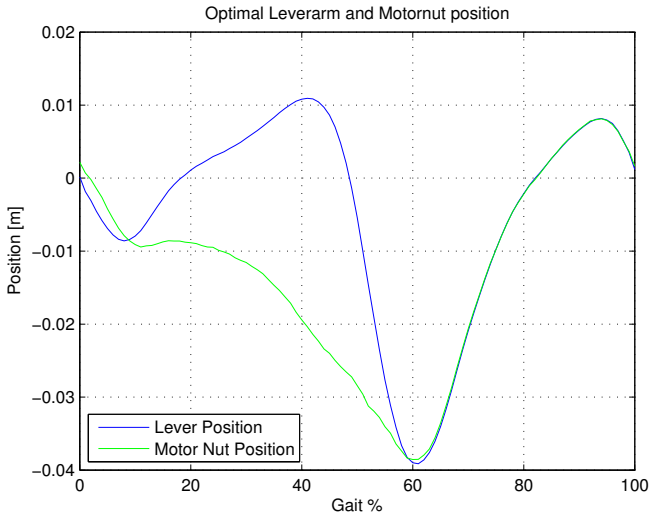

Figure 3.12: Optimal leverarm and motornut position

3.1.3 Motor Layout

In order to compress and stretch the spring, a motor has to introduce a linear movement to the spring itself, according to the desired nut pattern. For that purpose, finished linear motion systems could be bought. However, because we have limited space, to keep the weight as low as possible and need only small movements, such systems would not be the best choice. Therefore a combination of motor, pullies and a ball screw is used to move the spring. A ball screw was preferred over a regular lead screw, due to its higher efficiency. A regular lead screw would be much cheaper and easier to make, but due to the friction between the components, the efficiency would drop dramatically, causing a higher power drain from the battery. Typical ballscrews operate at around 90% efficiency, while regular lead screws vary between 20% and 40%. [ThomsonLinear_2, 2014]

To convert translational to rotational movement, some kind of transmission is necessary. At that point we do not pay attention on how the final transmission can be realized and assume there is a transmission ratio U available. U has no physical limits and can be whatever value necessary. Also, we assume that each, the transmission and the motor, have an efficiency of 90% ending up in a total efficiency of $\eta = 81\%$.

Taking these assumptions into account, we can calculate the necessary motor moment and speed by using the previously calculated force F and nut velocity $\dot{x}_m$:

$$M = \frac{F}{U \cdot \eta} \tag{3.14}$$

$$\omega = U \cdot \dot{x_m} \tag{3.15}$$

Having these values, the mechanical power from the motor can be calculated based on equation 3.9.
Besides that the electrical power has to be taken into consideration as well. Figure 3.13 represents the electrical circuit of a DC Motor, while the used symbols are described in table 3.3.

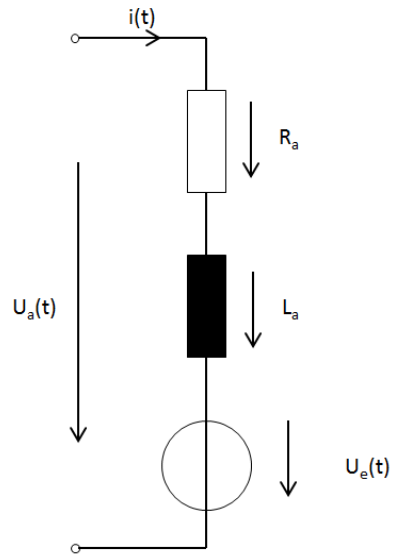

Figure 3.13: Circuit diagram representing a DC Motor

Symbol	Meaning
$i(t)$	armature current
U_a	armature voltage
R_a	Resistance within the motor
L_a	motor inductance
$U_e(t)$	Back EMF voltage

Table 3.3: Motor circuit symbols

Applying Kirchoff's law to figure 3.13 results in

$$-U_a(t) + i_a(t) \cdot R_a + L_a \cdot \frac{di}{dt} + U_e(t) = 0 \tag{3.16}$$

Because of $L << 1$, this term will be neglected, resulting in our final equation:

$$U_a(t) = i_a(t) \cdot R_a + U_e(t) \tag{3.17}$$

The armature current and the back EMF voltage can be easily calculated by using the motor's torque respectively the motors speed constant:

$$i_a = \frac{M}{K_m} \tag{3.18a}$$

$$U_e = \frac{RPM}{K_v} \tag{3.18b}$$

Using equations 3.17, 3.18a and 3.18b the electrical power consumption can be calculated

$$P_e = U_a(t) \cdot i_a(t) \tag{3.19}$$

enabling us to get the overall efficiency at every point in time.

$$\eta_{abs}(t) = \frac{P_{mechanical}(t)}{P_{electrical}(t)} \tag{3.20}$$

However, we might not find the overall perfect transmission ratio due to our hardware limitations regarding current and voltage provided. The maximum voltage and current available are:

- Max. voltage: $28V$
- Max. current: $40A$

Therefore two separate calculations were made to find the limits for the transmission ratio depending on the limitations of the voltage respectively the current. Figure 3.14 shows the limitations in transmission for the device.

As one can observe from figures 3.14a and 3.14b, the lower transmission limit is given by the max current available, while the upper limit is set by the battery voltage. Now to find the overall best transmission ratio, the energy used is calculated by integrating the power consumption (eq. 3.19) in between the former calculated transmission limits. The energy was chosen in order to optimize not only for one peak moment as performed during the layout of K and L, but to optimize the consumption over the full course of one gait cycle.

$$J = \int P_e \cdot dt \tag{3.21}$$

Therefore the final chosen transmission ratio is the one with the lowest energy consumption during one gait cycle as shown in 3.15.

Figure 3.15 shows that the overall best transmission ratio is the same as the one for max. voltage available.

Also the current ripple of the motor has to be taken into account. The maximum allowed ripple was set to 20% of the nominal motor current i_n. The motor controller uses a 3 level scheme and a maximum switching frequency of $f_s = 50kHz$. Therefore

the additional necessary inductance is calculated as following

$$L_{additional} = \frac{U_a}{4 \cdot 0.2 \cdot i_n \cdot f_s} - L_{motor} \tag{3.22}$$

If an additional inductance is necessary, one with a very low direct current resistance is preferred to affect the efficiency as little as possible. The DCR of the inductance is then added to the circuit diagram, reevaluating the calculations.

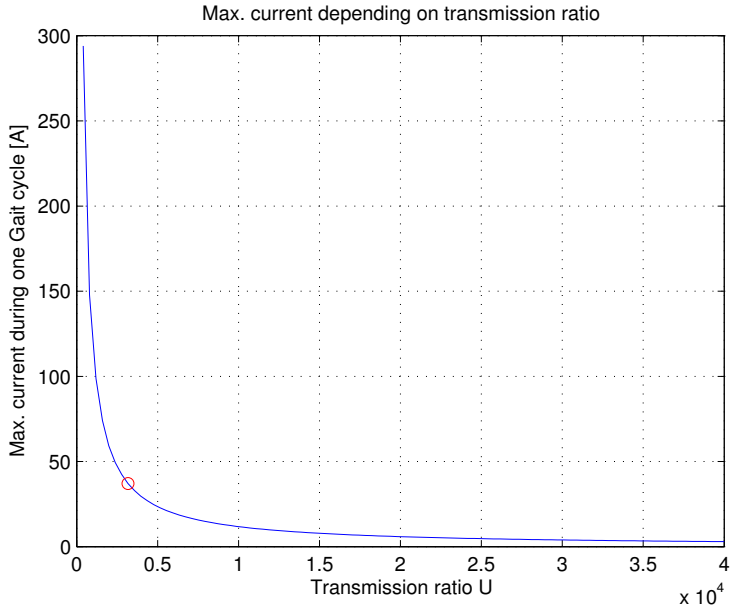

(a) Max. current per gait cycle necessary depending on transmission ratio

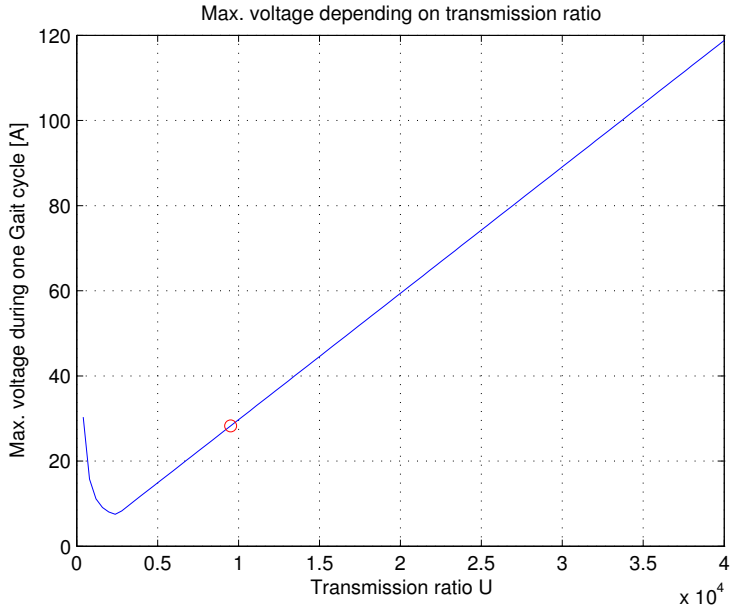

(b) Max. voltage per gait cycle necessary depending on transmission

Figure 3.14: Transmission limitations

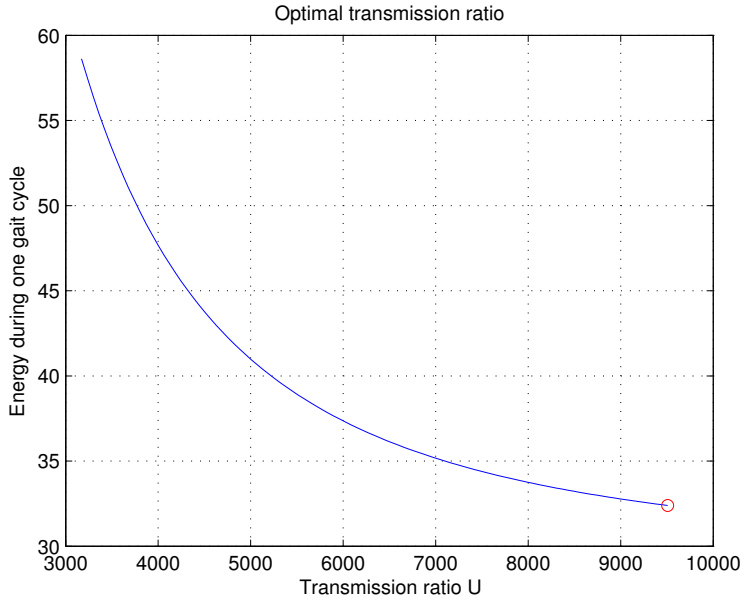

Figure 3.15: Lowest energy consumption as a function of the transmission during one gait cycle

3.1.4 Motor Evaluation

Having gathered all the necessary motor information, one has to verify, that theoretical operational values are within the motor's range. Therefore the following key parameters were checked:

- Maximum moment needed is smaller than maximum moment available
- Maximum RPM needed is smaller than maximum RPM available
- Maximum i_{RMS} is smaller than i_{RMS} allowed

To verify that all operational points of the motor during one gait cycle are within the limits, a $M - \omega Diagram$ is plotted, taking into account our limitations in moment (current) and speed (voltage) of the motor controller. To find the motor fitting our needs best, 14 different Maxon Motors were simulated. In the end, three different motors fulfilled the requirements.

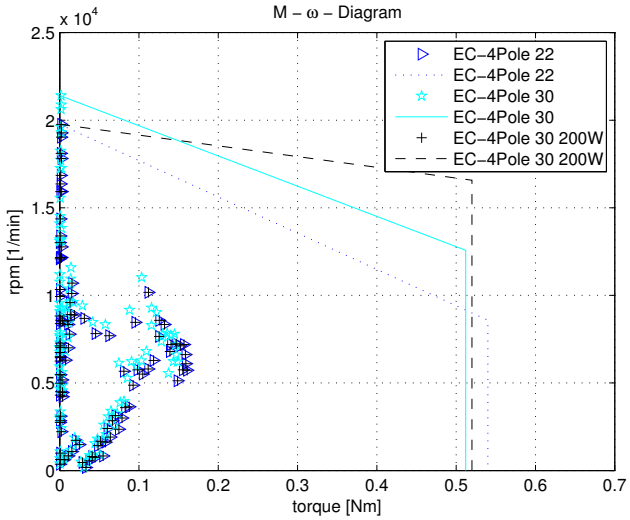

Figure 3.16: M-ω-diagram of motors fulfilling the requirements

The optimal choice in our case would be the EC-4Pole 22. This motor weighs only 170gm, which is a huge drop to the previously mentioned directly attached motor of approximately 2.5kg. Table 3.4 displays the calculated values as well as the values of the motor from its datasheet. However, because of very long lead times for this motor, the EC-4Pole 30 200W motor was chosen. This motor was already in house and could be accessed immediately. Its values are presented in table 3.5.

Symbol	Description	Value
M_h	Stall torque	$0.954Nm$
i_n	Nominal current	$4.95A$
K_m	Torque constant	$0.135Nm/A$
K_v	Speed constant	$705rpm/V$
L_a	Terminal inductance	$30.8\mu H$
R_a	Terminal resistance	0.341Ω
U	Transmission ratio	9508
$rpm_{max,av}$	Maximum speed available	$19856rpm$
rpm_{max}	Maximum speed necessary	19765
$M_{max,av}$	Maximum torque available	$0.54Nm$
M_{max}	Maximum torque necessary	$0.1608Nm$
$i_{RMS,OK}$	Maximum allowed continuous current	4.95
i_{RMS}	Maximum continuous current necessary	$4.8639A$
L_z	Additional inductance necessary	$110.6\mu H$

Table 3.4: Final motor, values

Symbol	Description	Value
M_h	Stall torque	$3.22Nm$
i_n	Nominal current	$10.5A$
K_m	Torque constant	$0.013Nm/A$
K_v	Speed constant	$700rpm/V$
L_a	Terminal inductance	$16.3mH$
R_a	Terminal resistance	0.102Ω
U	Transmission ratio	9508
$rpm_{max,av}$	Maximum speed available	$19780rpm$
rpm_{max}	Maximum speed necessary	19765
$M_{max,av}$	Maximum torque available	$0.52Nm$
M_{max}	Maximum torque necessary	$0.1608Nm$
$i_{RMS,OK}$	Maximum allowed continuous current	$10.5A$
i_{RMS}	Maximum continuous current necessary	$5.05A$
L_z	Additional inductance necessary	$50\mu H$

Table 3.5: Chosen motor, values

3.2 Modeling

Prior to start modeling in the CAD software, different concepts were generated to get an idea, how the key parts of the device could look like. The different concepts then were grouped together in a morphological box, to choose the most promising ones. After modeling the device in SolidWorks, the most critical parts were chosen and run through a Finite Element Analysis (FEA).

3.2.1 Concepts

The concepts presented in the following were developed, with the knowledge in mind, that the device is designed for long term usage. However, because of this device being a prototype, some of the concepts might have been altered or ended up not being used for the prototype, to make the device as easy as possible in the first place in order to just verify the desired output. The concepts can be easily adopted for other ongoing projects and are saved for later usage if not used yet. The final concepts where all chosen in collaboration with the supervisor and several instructors.

3.2.1.1 Sole

The device is designed for multiple patients use. Therefore it might be necessary to change the sole of the device after a certain time of usage. The following concepts aim to make the sole interchangeable.

This approach uses T-Slots to make the sole easily exchangeable. On the one side the slots are closed, while on the other side a slider prevents the sole from falling out by itself.

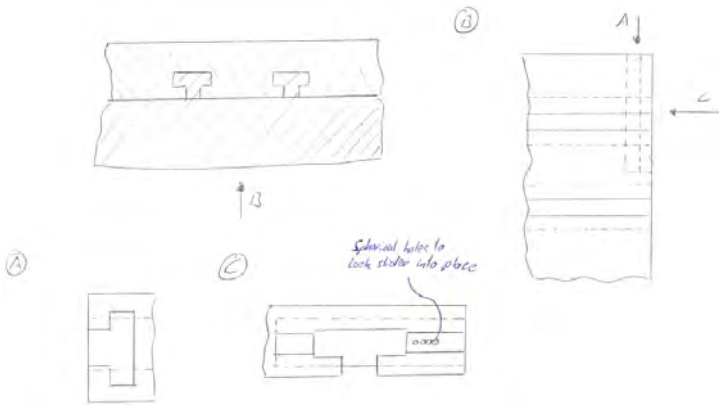

Figure 3.17: Sole concept 1

Figure 3.18 shows the sole fixed on the device by using screws. This approach is not as fast as the one shown above, but definitely the easiest one.

The approach in figure 3.19 is similar to the one before, but the screws are attached

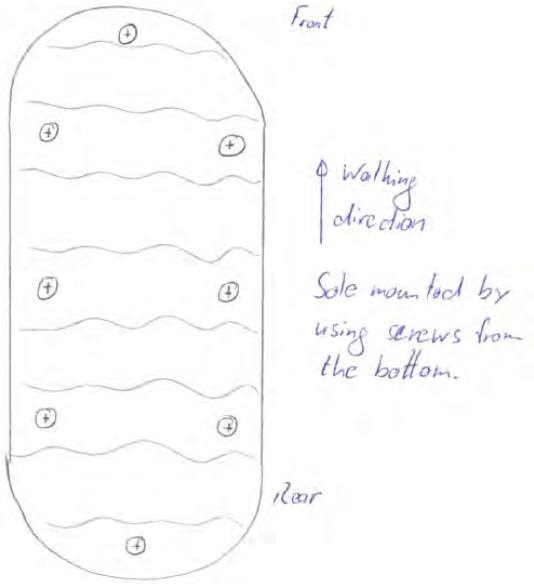

Figure 3.18: Sole concept 2

from above. Therefore thread inserts have to be used and placed into the sole. A big advantage is, that the bottom of the sole is completely closed in contrast to the previous concept.

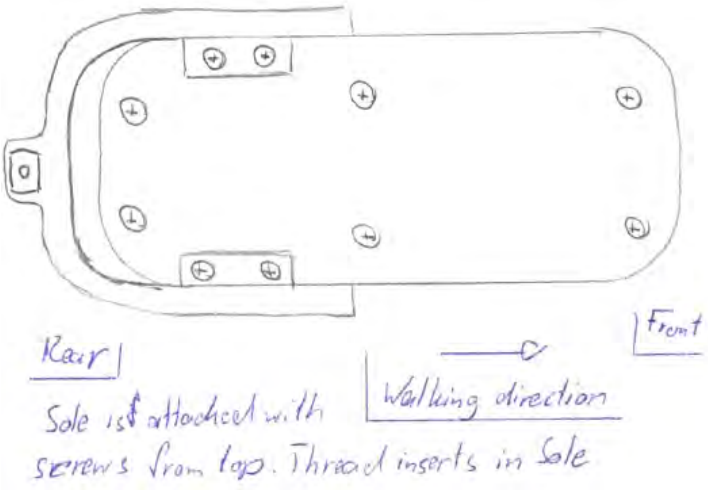

Figure 3.19: Sole concept 3

This approach is probably the most complicated one, using slots and pockets to hold the plate in place. A snap lock is used to secure the sole in its position.

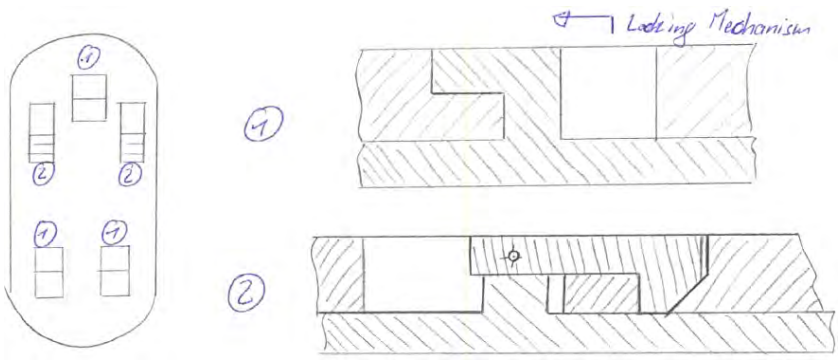

Figure 3.20: Sole concept 4

Despite all the concepts, it was decided to simply glue the sole onto the device of the prototype. Should the testing of the prototype reveal a fully functioning system, this part of the device needs to be reevaluated.

3.2.1.2 Ankle Joint

The ankle joint is one of the key features of the whole device, enabling the user to dorsiflex and plantarflex his foot. It is important to mention, that the joint itself should align as well as possible with the patient's ankle to make the movement most comfortable. Because the ankle position varies slightly from user to user it cannot be predicted. However, because the device is supposed to be used in combination with a custom fitted half shoe, the shoe can compensate for some of the variances.

Also the safety aspect has to be taken into account. High torques at the ankle joint make it necessary to not only have software safety measures, but also mechanical ones. From our reference gait cycle data it was obtained, that the maximum dorsiflexion is at 6.7° and the maximum plantarflexion at 24°. That knowledge was taken into account by creating these concepts.

This concept was adapted from an existing product. The two set screws, screwed in from the top into the designated tapped holes to the left and right, limit the angular movement of the ankle. The angular movement depends on how far the set screws are screwed into the material, acting as a stop for the flat surfaces of the rod (left and right side). As mentioned, this is a precaution preventing the patient's foot to over-bend in case of a malfunction.

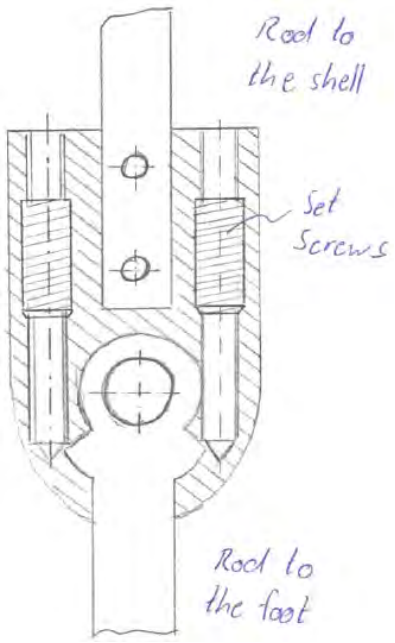

Figure 3.21: Ankle joint concept 1

The concept shown in fig 3.22 uses an approach where one piece of the joint is directly attached to the frame of the foot (stationary part). On the inside there is a modified bushing reducing friction between the stationary part and the rod. The cover prevents the rod from falling out and holds the sensor to monitor the rod's angular position.

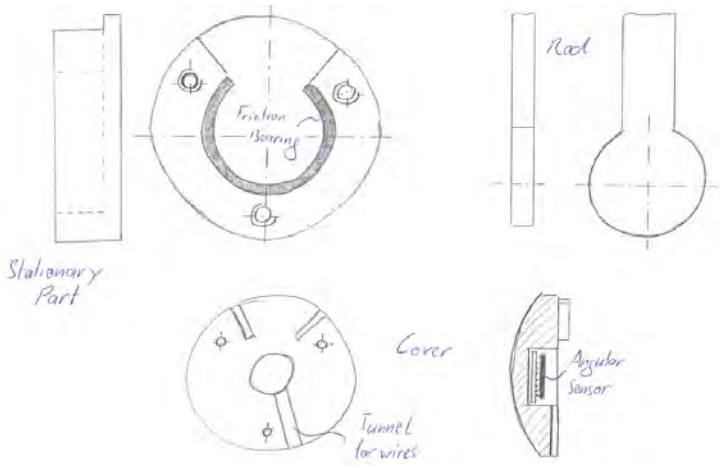

Figure 3.22: Ankle joint concept 2

This concept uses a similar approach as the one before. However, the friction bearing has a flange and the rod an extrusion fitting in the bearing. Again, the cover serves as a holder for the sensor and prevents the rod from falling out.

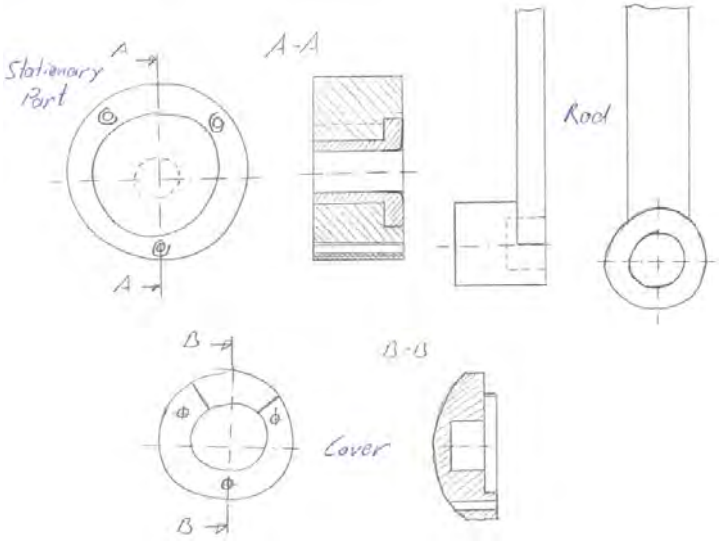

Figure 3.23: Ankle joint concept 3

Finally figure 3.24 shows an approach where the rod sits on a bolt, supported on two sides. The cover's only purpose is to hold the sensor. The stationary part is mounted on the foot frame again. Another alternative is to machine off one mounting point of the stationary part and use the frame as the second support structure.

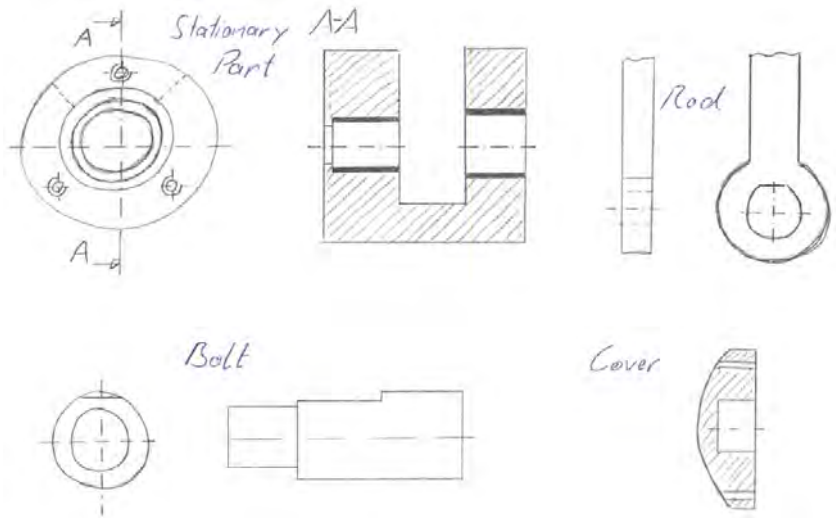

Figure 3.24: Ankle joint concept 4

The final choice was made in favor for concept 4 presented in fig 3.24. The reason for choosing this concept was, that the bolt, used to connect to the rod, is supported on both sides and therefore is not influenced by bending. However, for the final prototype, this concept was slightly adjusted as will be mentioned in chapter 3.2.2.1

3.2.1.3 Actuator

The concepts can easily be divided into two different groups. First, the ones where the spring is compressed to apply the force on the leverarm and second, the ones where the spring is stretched. The concepts in here do not only focus on one specific part, but are always modeled as an assembly to get a better overview of how the components interact with each other. The connection to the leverarm as well as to the interface at the human's calf, both are intended to be realized to support movement in any direction. Therefore the joints at these points are represented by ball joints, ensuring maximum movement for the user.

The following concept shows a double supported ball screw with two arms attached to a slider guided by the surrounding enclosure. Attached to these arms are rods going

all the way down to the leverarm of the ankle. The spring is between the nut and the slider. due to the arms coming from the slider, moments are introduced to the system.

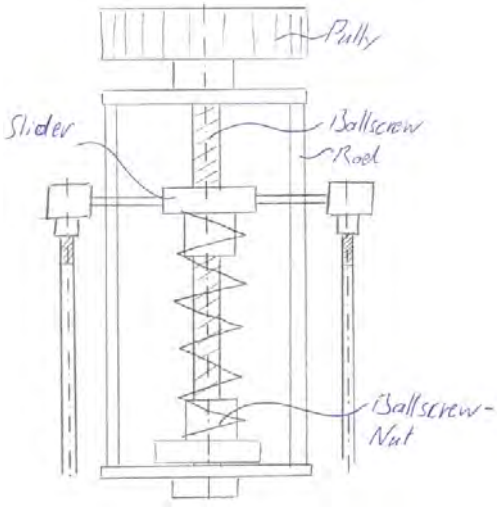

Figure 3.25: Actuator concept 1

Figure 3.26 shows a similiar concept to the previous one. The ball screw is double supported as well, but the springs are outside of the enclosure. The springs are connected to the nut via the arms. Also plastic rods have to be added inside of the spring to prevent buckling during compression. Due to the two attachment points at the leverarm, again moments may be introduced to the system.

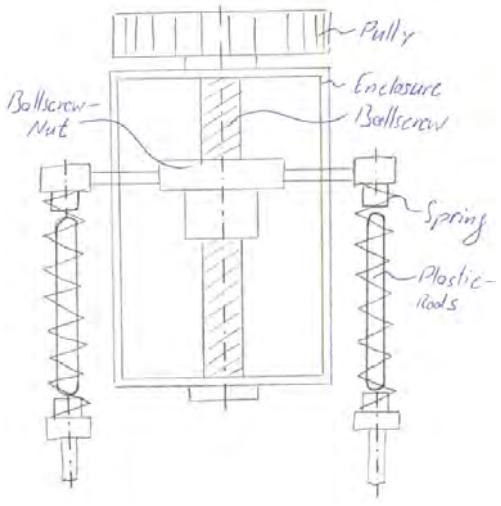

Figure 3.26: Actuator concept 2

This concept puts all elements into one single axis. To do so, a hole at the bottom of the enclosure is necessary, eliminating the possibility of double supporting the ball screw. The ballnut is prevented from rotation by restraining it to the enclosure.

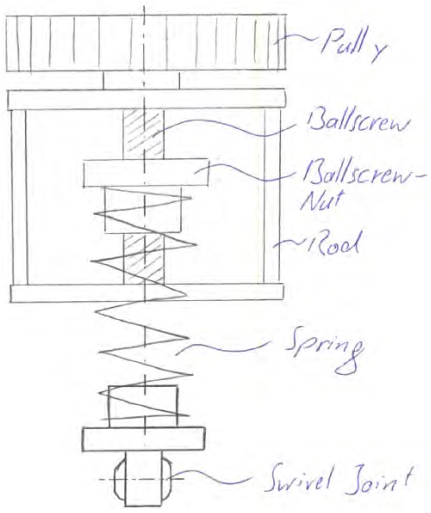

Figure 3.27: Actuator concept 3

This idea was triggered by the thought of getting away from a ball screw approach. The rack is driven by a gearbox combining a harmonic drive and a planetary gear to get the necessary transmission.

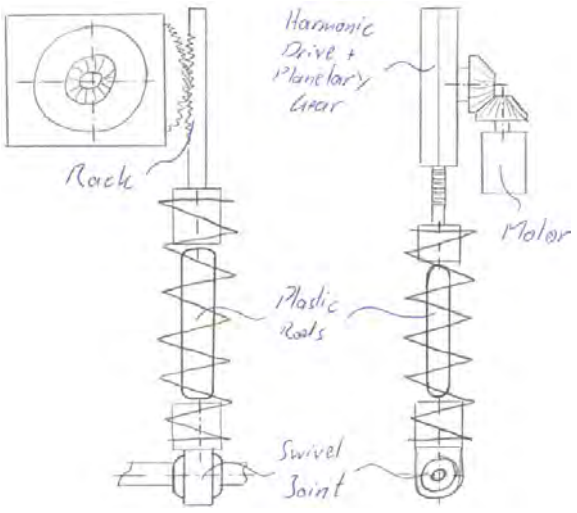

Figure 3.28: Actuator concept 4

The last concept shown in figure 3.29 intends to use a different material than a spring. To be more specific a composite material or spring like plastic material was in mind when this idea was generated. The ball screw nut is directly attached to the leverarm, while the other end of the ball screw is mounted on top and connected to the motor.

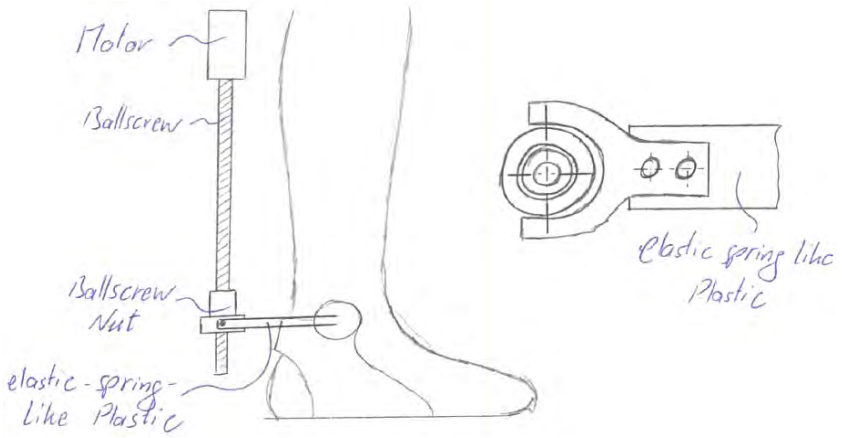

Figure 3.29: Actuator concept 5

The last figure (see figure 3.30) is not directly a concept for the actuator, but another possibility to prevent the spring from buckling while being compressed.

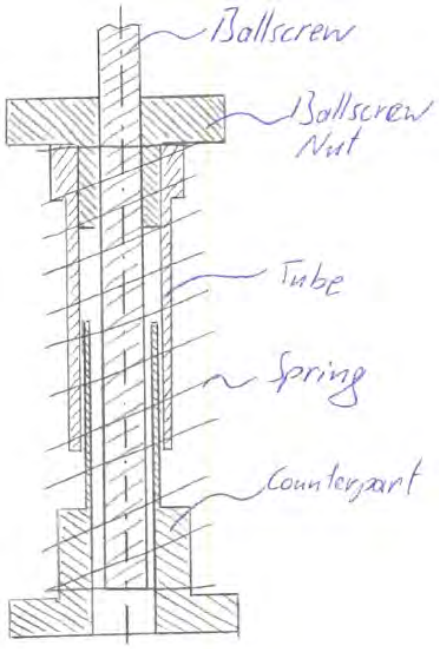

Figure 3.30: Actuator concept 6

The final choice was made in favor of concept 3 shown in fig 3.27. The reason was merely because there is no possibility of introducing bending moments on the nut and the rod, extending the lifetime of this part. Concept 4 would be of the same type in general, however the usage of such a complex gearbox would increase weight and the risk of early failure and fatigue, especially on the part of the harmonic drive.

3.2.1.4 Interface Leg - Calf Shell

This part is probably one of the most critical ones while yet the least complicated one when it comes to implemented functions. Its only purpose is to serve as an attachment for the actuator and even more important as the interface between the device and the patient's leg. Also it holds the straps responsible for tightening the shell to the foot. However, it is important to ensure a fit as perfect as possible. Due to the reduced vascular blood flow, already mentioned in earlier chapters, the regenerative capabilities of the patient's skin are decreased. Due to the force applied to the leverarm, the shell always shifts up and down on the patient's foot. To prevent sliding between the leg and the shell, inlays are inserted to get a better fit.

The first concept displayed in figure 3.31 shows an interface with two parts. One surrounds most of the calf and mounts the actuator, while the other plastic shell sits on the front of the tibia. Both are covered with soft material providing more comfort. The front shell is kept in place with a velcro strap tightening the leg in the shell, to avoid movement between skin and shell.

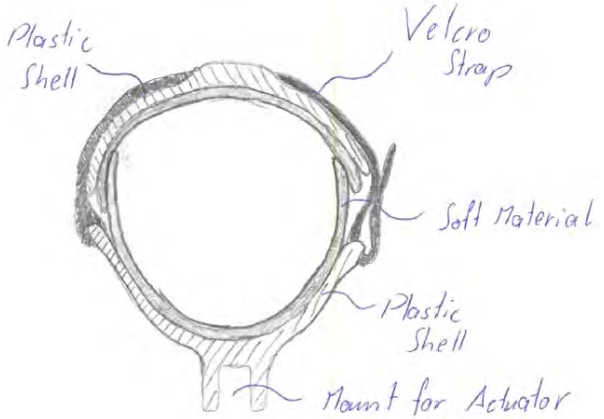

Figure 3.31: Calf shell concept 1

This concept has only one plastic shell. The soft material is extended so that the ends can overlap, providing double padding on the shin bone. A velcro straps holds the leg in place.

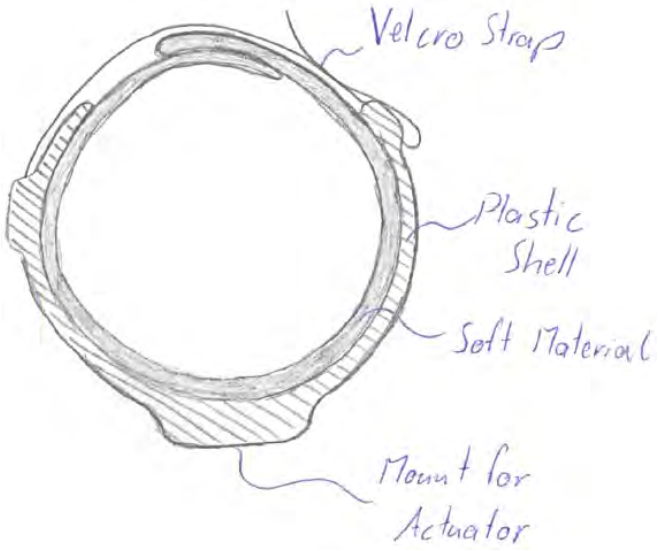

Figure 3.32: Calf shell concept 2

The concept of figure 3.33 is similar to the one before. Only one side of the padding is extended going all the way to the other side of the shell. Again, a velcro stap secures the leg in its position. Due to only one layer of padding the pressure on certain areas on the leg should be evened out.

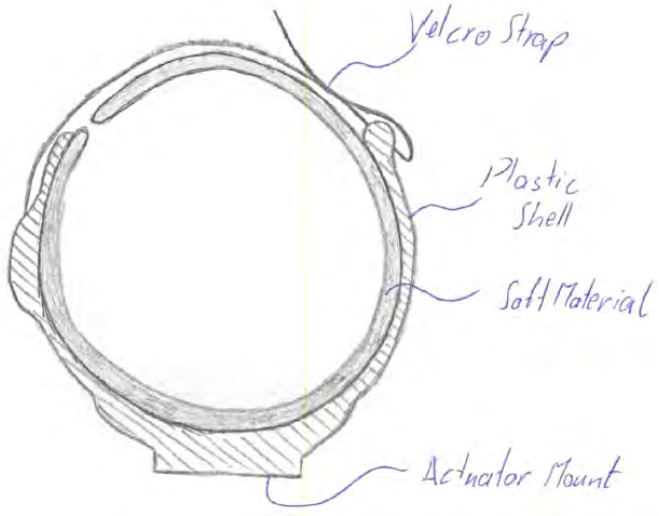

Figure 3.33: Calf shell concept 3

The last concept is very similar to the first one in 3.31. The padding is extended again. However it does not overlap and therefore leaves an open space where the shin bone is. The front plastic shell is used to even out the load applied by the velcro by tightening. Furthermore, there is a slot in the front shell at the shin bone's position, to avoid load on that area at all and redistribute it on the sides, making the user more comfortable to wear the device.

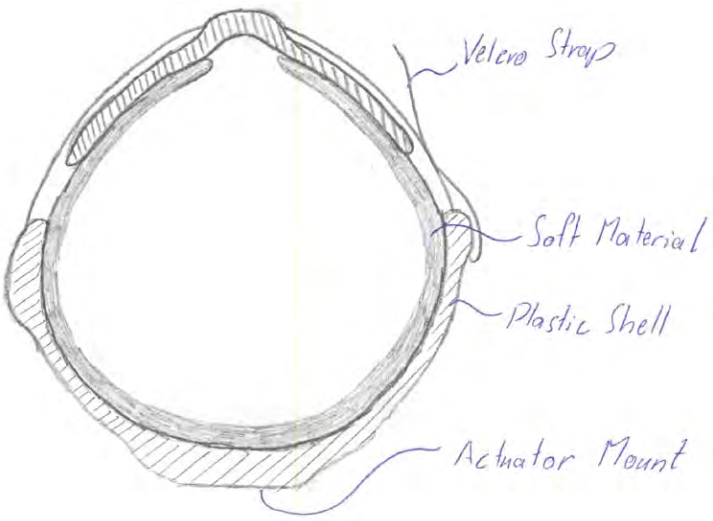

Figure 3.34: Calf shell concept 4

From personal experience our shin or tibia is sensitive to pressure acting from up front. Therefore for the final product the shell is intended to be designed in a way, where the shinbone is not directly exposed to the straps but covered by either extended inlays or another shell piece. However, because of this device being a prototype, the used shell does not necessarily coincide with the ones sketched.

For the prototype none of these concepts were chosen. It was decided to just use a 3D printer to come up with a shell which fits on the test subject's foot. If used commercially another in depth conversation with a prosthetist must be held to get the final specifics in order to fit the patient's needs the best.

3.2.1.5 Eversion/Inversion

As mentioned earlier, this device intends to give its user maximum motion range, also including eversion and inversion of the foot (see chapter 2.3.1). Therefore another degree of freedom has to be added to the device. An appropriate place to do so, is the connection from the ankle to the calf shell. Most of the concepts are heading towards conventional joint approaches while one is inspired by a different product, which then was adopted to our needs.

The first concept shows an approach where a flat steel bar is inserted to the joint. Two of the parts together form the link enabling eversion and inversion.

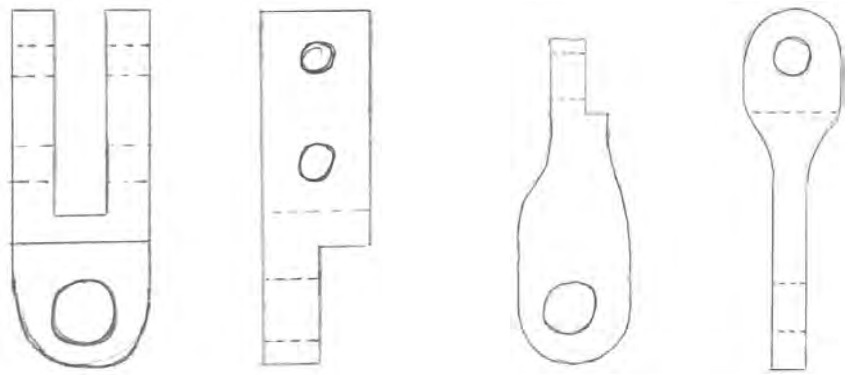

(a) Concept joint 1a (b) Concept joint 1b

Figure 3.35: Concept joint 1

In this concept, the connectors between the foot and the shell are in cylindrical shape. They can be screwed on the joints, allowing height adjustment specific to the user.

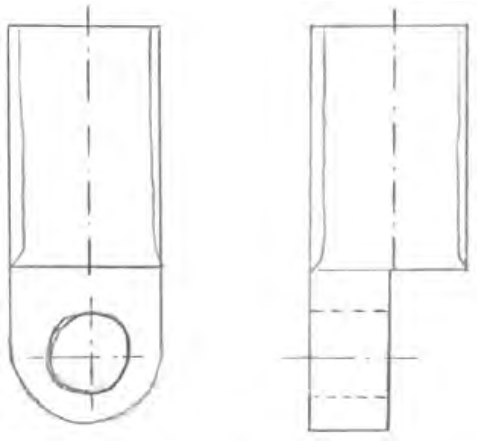

Figure 3.36: Concept joint 2

The concept of figure 3.36 does not add material to the existing rod. The parts will fit into each other and then be secured in place by a bolt.

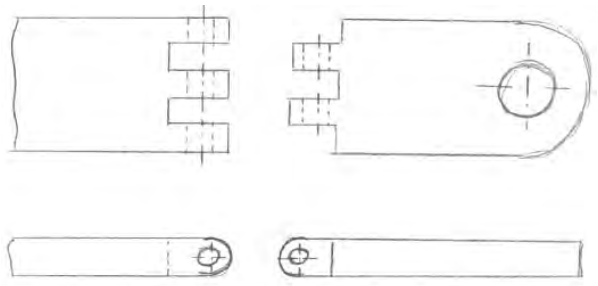

Figure 3.37: Concept joint 3

Here a sheet metal bending approach was used. The connectors are bent into shape, so that they fit on top of each other. A bolt is used to finish the joint.

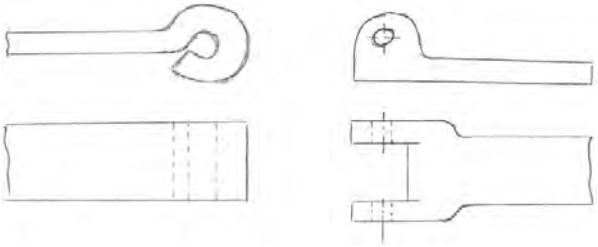

Figure 3.38: Concept joint 4

In this concept, the ankle joint and the joint responsible for eversion and inversion are at the same place. This means that one part is going to be more difficult, but the overall design would benefit from this solution.

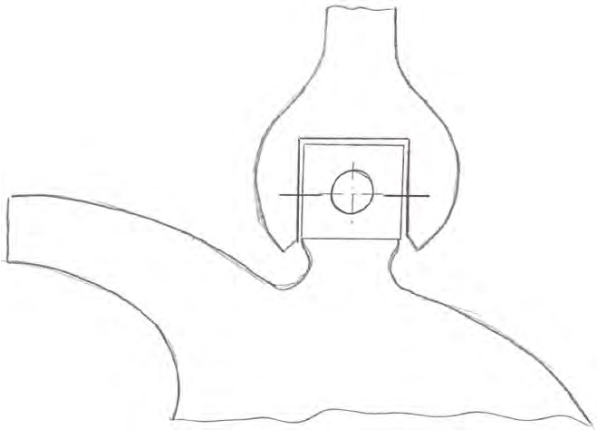

Figure 3.39: Concept joint 5

The last concept takes a different approach, which was inspired by a different product. This concepts uses several chain elements which are connected with small bolts to each other. A sheet metal spring is going through the parts, providing it with some rigidity to avoid it from collapsing. Out of these concepts, number 6 was chosen. It provides the

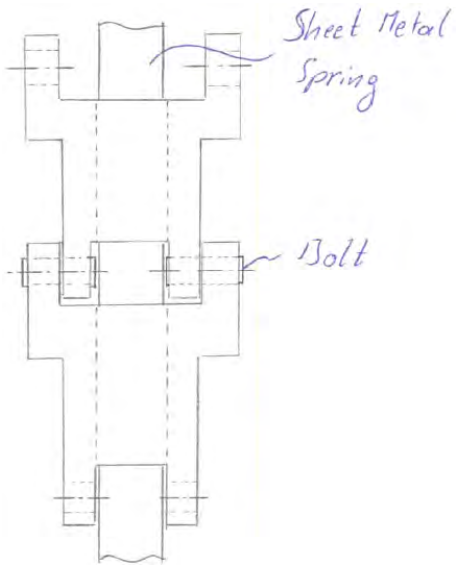

Figure 3.40: Concept joint 6

user with the most flexibility and therefore seems to fulfill the requirements the best. However due to the higher number of parts for this solution, it has to be kept in mind that the risk of failure will increase.

3.2.1.6 Connection Rods

The rods connecting the foot part and the calf shell are not in line with the vertical axis of the foot. Therefore there is a leverarm and the rod is moving up and down during inversion and eversion. So a joint alone, as described in the previous concepts, is not sufficient to compensate for the linear movement.

Furthermore it must be possible to lock the linear movement of these rods. As described in the objective of the study in chapter 1.3, a "pumping" mode has to be implemented into the device. To not stress the patient's foot by the ankle movements, the sliders will also have a locking mechanism, ensuring that the device stays in place. Possible solutions are presented in the following figures.

The following two figures both are concepts for a flat steel connection from foot to bottom. In figure 3.42a a leverarm is used which will be held in place by the spring

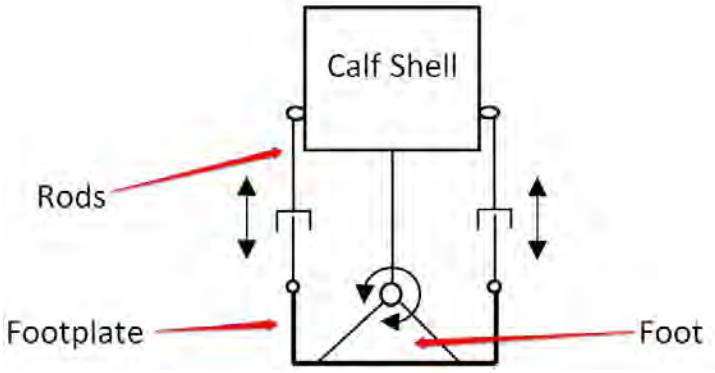

Figure 3.41: Connection rod schematic

loaded ball. In figure 3.42b the locking mechanism is realized by using a slider. Again the spring loaded ball secures it in its position.

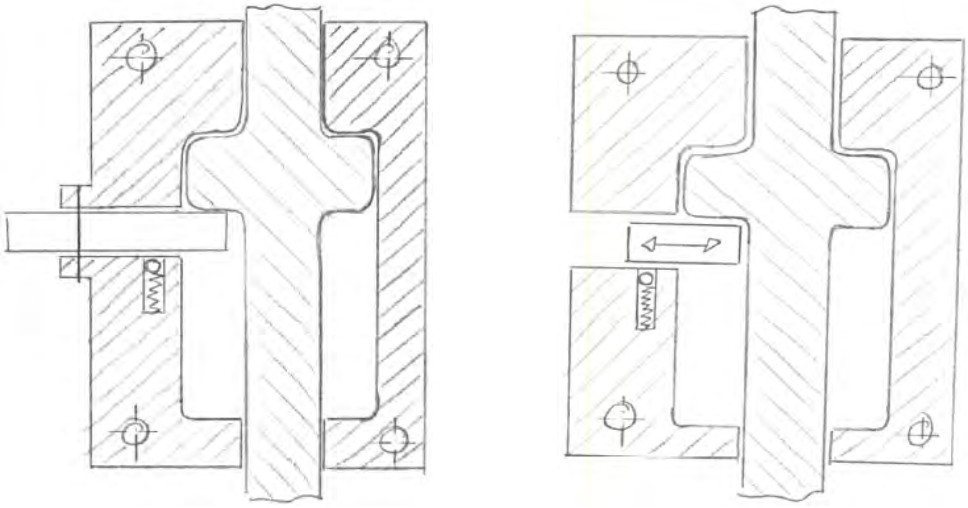

(a) Concept slider 1a (b) Concept slider 1b

Figure 3.42: Concept slider 1

This concept (see figure 3.43) shows a mechanism used for a cylindrical rod used as a connection. A ring with slots placed appropriately can lock the rod in its place. The lower rod is guided in a tube connected to the calf shell.

It was decided that concept of figure 3.42b will be chosen for the final product as well as for the prototype. The lack of the leverarm extending outside of the case decreases the risk of accidentally locking or unlocking the mechanism. Also the usage of flat elements over tubes decreases the overall perceived size of the device which is beneficial for the final product.

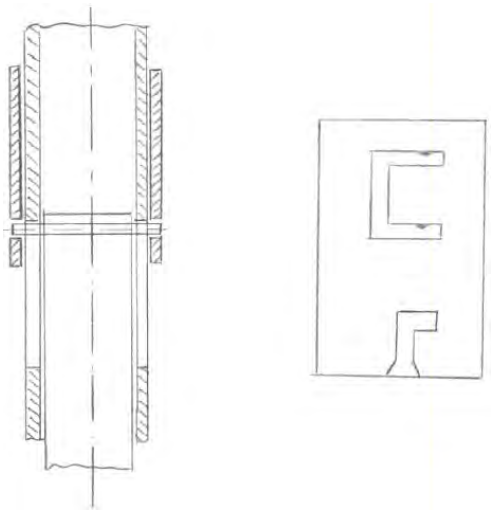

Figure 3.43: Concept slider 3

3.2.1.7 Morphological Box

The morphological box is used to group the different concepts which evolved during the brain storming process in different categories. The goal is, to choose one concept of each category which is then used for further consideration in order to model the parts in SolidWorks.

Sometimes it is also used, to generate multiple combinations of solutions which are then compared to each other in another evaluation process, taking into account certain selection criteria.

This method is especially interesting if the final product can be split into different modules which can be combined freely. However in these concepts some of the connection rods can only be used in combination with the proper eversion / inversion concepts. The final morphological box along the finally chosen concepts is presented in figure 3.44.

Figure 3.44: Morphological Box

3.2.2 CAD

After the concepts were chosen, the modeling in SolidWorks began. The version used is SolidWorks Premium x64 Edition. It would not make sense to go into every little detail of the assembly, therefore only the most important elements will be mentioned. To keep an overview where the different features are located within the device, this chapter will be split up according to the assembly into the following parts:

- Foot
- Actuator
- Slider
- Main Assembly

3.2.2.1 Foot

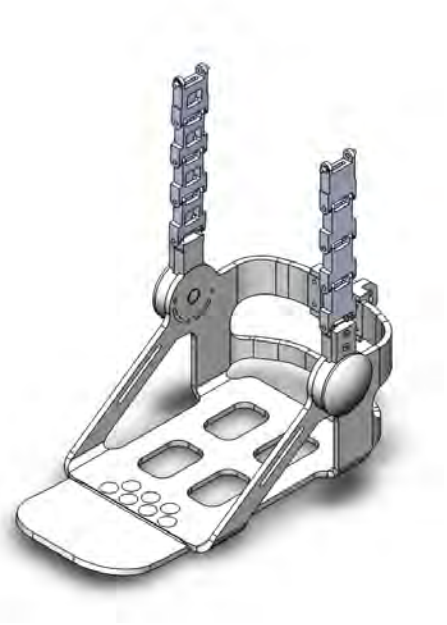

Figure 3.45: Foot assembly

The foot assembly consists of the foot plate itself as well as of a 3D printed flexible part attached to its front. On the left and right each there is an ankle joint connected to one of the previously mentioned chain elements connecting the foot and the calf shell. In the back, a connector is attached to the footplate serving as a connection point for

the actuator.

Footplate

The footplate is the main part of the foot assembly, where all the other parts are mounted. It is designed as a sheet metal part which can be cut out by using either Waterjet or Laser manufacturing methods. After getting the cut out parts, one pocket had to be machined and the holes tapped as well as the sides bent into place. The lower extensions on the backside are welded together, while the upper ones serve as mounting point for the actuator connector. On the left and the right side, the ankle joints are attached to the plate. The cut outs at the bottom only serve the purpose of saving weight. The material used is Aluminum.

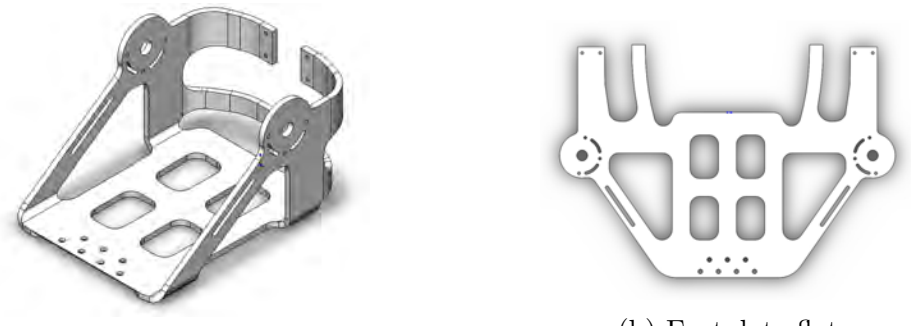

(a) Footplate isometric

(b) Footplate flat

Figure 3.46: Footplate

Flexible Footplate

We are used to have a flat foot or sole we are able to walk on. Also our natural gait includes bending our toes while preparing for push off. A straight plate all the way up to the front of the patients shoe would fulfill the requirement of a flat surface, however the patient would not be able to bend his toes, ending up in a not satisfying feeling during the walk. Therefore a flexible front plate was attached. It starts a few centimeters before the joints of the toes and has the same height as the actual foot plate. During roll over the plate bends and moves back into its original position after push off. It is attached to the foot plate using several rivets (figure 3.47)

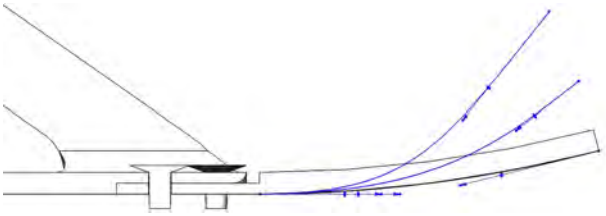

Figure 3.47: Flexible front of foot plate. Bending prior and during push off, ensuring normal gait feeling.

Ankle Joint

The ankle joint is built in the same way as described in figure 3.24. The foot plate serves as one of the support structures for the bolt. Another part attached to the foot plate acts as the second support for the bolt. In between, there is the ankle joint connector staying aligned with the patient's tibia, connecting the chain elements with the foot plate, while the footplate is tilting.

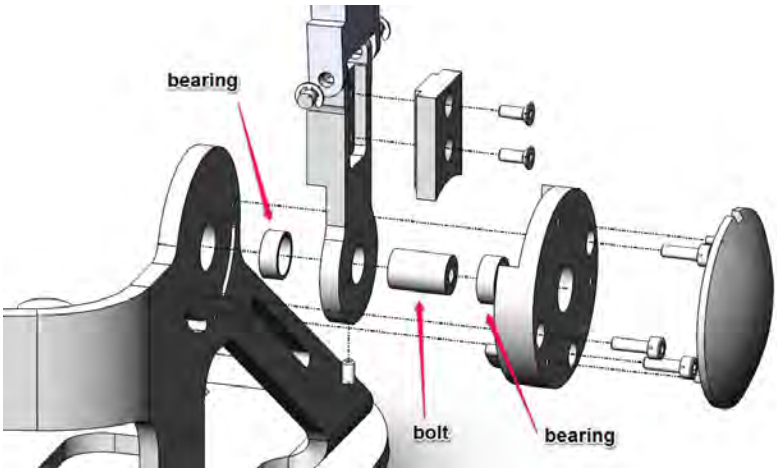

Figure 3.48: Ankle joint exploded view

The bearings fit into the foot plate and the ankle plate, supporting the bolt on both sides. They are press fitted, to ensure that they stay in place. Also they are PTFE coated on the inside to further reduce friction. The ankle plate (second from the right) fits onto the foot plate and is supported by two slotted holes, while three M3 screws lock it into place. The set screw fits into the ankle joint connector and finally sits on the bolt's flattened surface preventing it from falling out. The cover, on the far right side in the figure, holds up the ankle sensor.

Chain Elements

The chain elements are responsible for the connection between calf shell and foot, but also for enabling the patient to evert and invert. The following figure displays how they are connected to each other.

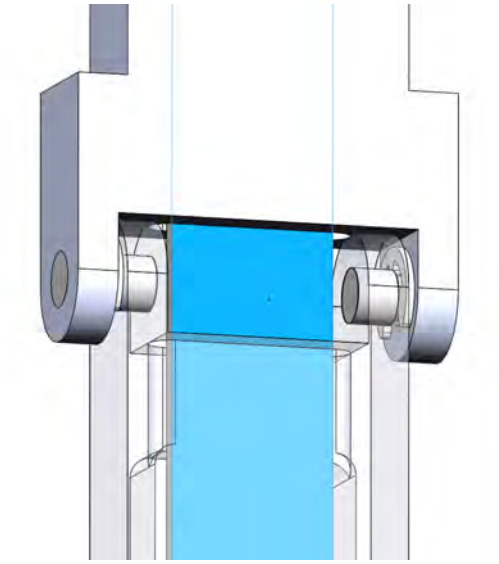

Figure 3.49: Chain connection

The bolts on the left and the right serve as connectors/joints for the chain elements to rotate on. Two separate bolts are used because there is a sheet metal spring passing through the chain elements in the middle, making it impossible to use one bolt going through. The bolts are kept in place by retaining rings which sit in between the two flanks of the chain elements. This is a rather unusual approach, but because there is not much movement on these parts, it should not cause any long term problems. The sheet metal spring is mounted in the ankle joint connector with a form fit ensuring that it stays in place even if the patient bends a lot. It goes through all the chain elements and ends where the last element is connected to the slider.

Actuator Connector

The actuator connector serves as an attachment point for the actuator on the foot. The distance from the point of attachment to the ankle joint represents the leverarm length used in the motor layout calculation in chapter 3.1.2. It is mounted on the footplate and is locked into place by four M4 screws. A bolt going through the part is the attachment point for the ball rod end screw of the actuator. The bolt is kept in place and prevented

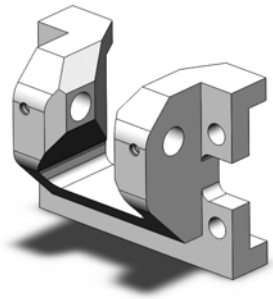

Figure 3.50: Actuator connector

from rotating by two M3 setscrews on the left and the right backside of the connector. To ensure that the rod end stays in the middle of the connector, two spacers were used.

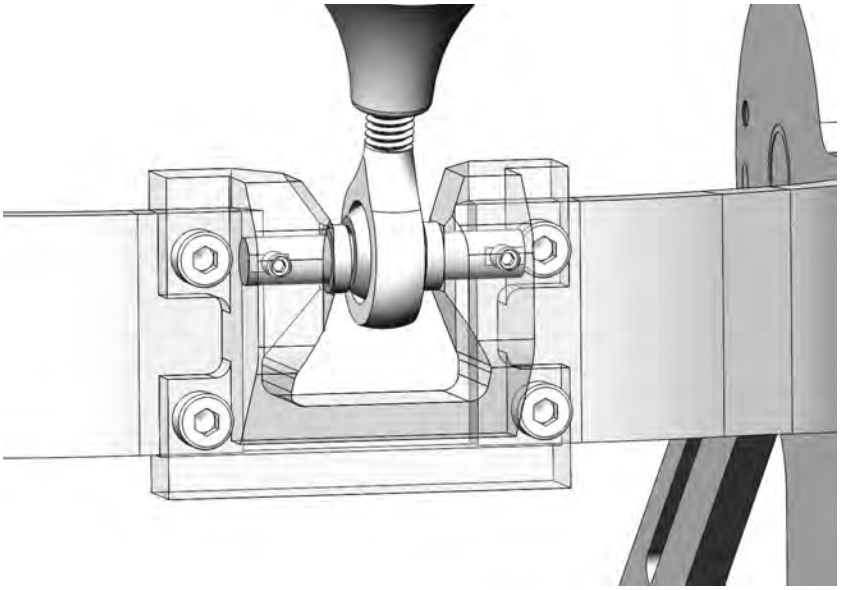

Figure 3.51: Actuator connector in assembly

This is important to prevent the rod from hitting the chamfered sides of the connector if eversion or inversion occurs. The notch on the lower end of the connector was machined out to save weight and give the rod freedom to tilt. The connector has a tight fit around the extensions of the footplate, not relying solely on the friction between the parts introduced by the normal forces of the screws.

3.2.2.2 Actuator

The actuator is the so called heart of the assembly providing the user with the necessary power to support his gait. It consists of a motor connected with pullies to a ball screw. Its nut compresses respectively stretches the spring which is then connected to a rod end, introducing its force to the actuator connector of the foot assembly.

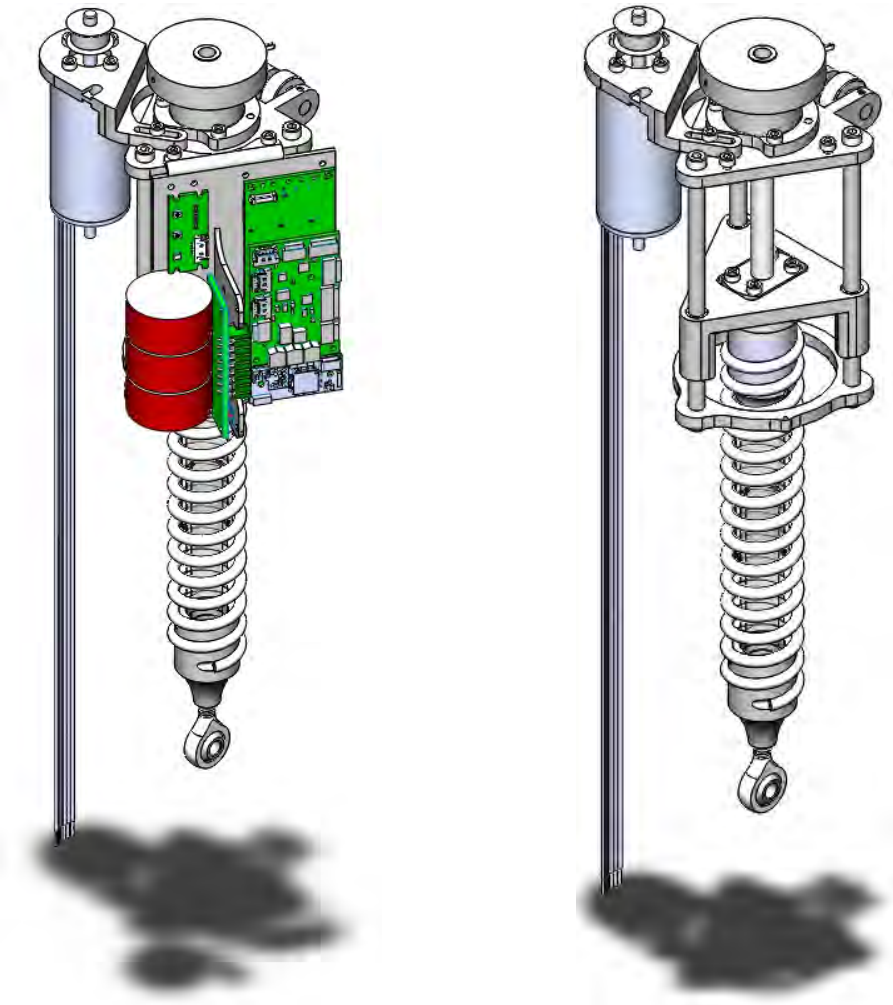

(a) Actuator assembly all (b) Actuator assembly without electronics

Figure 3.52: Actuator assemblies

As mentioned initially, the device is supposed to support users up to 150kg. However also users down to 70kg should be supported. It is not possible to support this bandwidth with just one spring setting while keeping all other variables as optimized as possible. Therefore the range from 70 to 150kg was split up in 20kg intervals. For each of the intervals a different spring was chosen. To find the optimal one, 17 different springs were

entered into Matlab. However, because the spring in this application is used in tension as well as in compression, regular springs could not be used, because most of them are closed and grounded at the ends. To get a spring, which can be held as shown in the assembly, the top and bottom of the spring must be machined off which affects the spring rate. Therefore the final spring ratio after altering the spring has to be recalculated.

To do so, first the number of coils of the original spring had to be calculated. The formula for calculation varies with the way the ends of the spring are formed. For closed and grounded springs (all of the 17 entered springs are of this type) the total number of coils can be calculated as

$$N_t = \frac{L_s}{d} \tag{3.23}$$

where L_s represents the solid length of the spring and d the wire diameter. Because of the closed and grounded ends, two coils are subtracted in order to get the number of active coils N_a for the original spring. By knowing the number of active coils the shear modulus can be calculated

$$G = k \cdot 8 \cdot \frac{D^3}{d^4} \tag{3.24}$$

where k represents the spring rate D the mean diameter and d the wire diameter. Because we want to grab the spring on both ends to be able to use it in tension, a total of another three coils were subtracted from the active number of coils. 1.5 coils are used for holding the spring on each side. By now knowing the final number of active coils $N_{a,fin}$ of each spring as well as the shear modulus, the new spring rate can be calculated.

$$k_{fin} = G \cdot \frac{d^4}{8 \cdot D^3 \cdot N_a} \tag{3.25}$$

Another set of active coils was calculated which represents the exact number needed to get the desired k value. Therefore equation 3.25 was reevaluated to compute $N_{a,need}$. If the number of actual available active coils N_a, minus the 3 coils used for grabbing the spring, is higher than the number of coils used to reach the desired stiffness, the spring is taken into further consideration.

Also the length of the spring is a major factor because of limited space of the orthosis. Therefore the pitch of the original spring had to be calculated which also depends on the way the ends of the springs are shaped. For closed and grounded ones, the pitch is calculated as

$$P = \frac{L_f - 2 \cdot d}{Na} \tag{3.26}$$

where L_f represents the free length of the spring and N_a the total number of active

coils of the original spring (not including the 3 coils for grabbing the spring). Then the new free length of both springs, with maximum length and $N_{a,fin}$ as well as the finally needed one to satisfy the spring rate with the number of coils $N_{a,need}$, can be calculated with

$$L_{f,fin} = P \cdot (N_{a,fin} + 3) + d \tag{3.27a}$$

$$L_{f,need} = P \cdot (N_{a,need} + 3) + d \tag{3.27b}$$

Finally for each weight interval the one spring was chosen, where the delta between the final and needed value of both the length and the number of coils was the smallest. The following table shows which spring was chosen for which weight and which changes were applied.

Interval	**Spring**	**Δ Coils**	**Final Length**
70kg	Lee Spring LHL1250A 12	-1.8	$155.2mm$
90kg	Century Spring Corp 4393	-1.13	$159.5mm$
110kg	Century Spring Corp 10393	-0.7	$170.25mm$
130kg	Century Spring Corp 10393	-2.8	$147.89mm$
150kg	Century Spring Corp 3417	-0.4	$178.25mm$

Table 3.6: Springs for 20kg intervals

To adjust the actuator assembly for a certain patient, only the fitting spring and the appropriate sockets have to be exchanged. The rod end connecting to the foot assembly allows some minor adjustments in length, to get the right initial position.

To adjust the device to a different weight category, the nut socket has to be unscrewed from the sliding plate and the foot spring socket from the rod end. The two tubes which are located inside the spring, prevent it from buckling while being compressed and can be used in all weight categories. They are kept in place with 2 set screws coming in from the sides of the sockets. The different parts are named in figure 3.53.

The nut socket mounts on the sliding place with a tight fit to ensure that all the parts are aligned. In the sliding plate, there is a pocket where the ball screw nut fits in. Further, the ball screw nut has a tight fit in the nut socket, again to ensure alignment. All three parts are connected to each other with four screws. A cross section of the sliding plate is shown in figure 3.54.

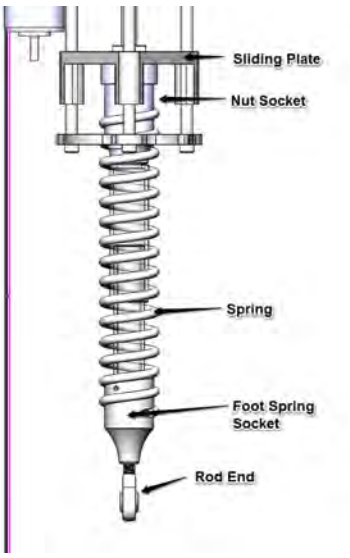

Figure 3.53: Actuator assembly bottom

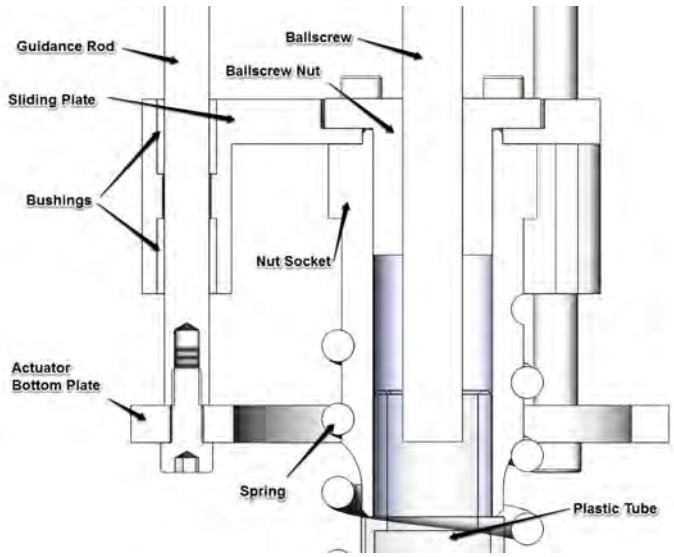

Figure 3.54: Actuator spring connector cross section

In general, it is recommended to have the ball screw supported on each end. However, because of using one spring which is on the same axis as the ball screw, double support for the ball screw is not possible. In order not to leave one end completely unsupported, the ball screw nut acts as a moving support. It is guided by the sliding plate which is kept in place by three guidance rods. To minimize friction, six bushings with PTFE coating are press fitted into the sliding plate. The rods running on those bushings are out of steel. The rods are mounted on the actuator bottom plate as well as on the actuator top plate. They are set on the flat surface and not in predefined positions, to have some room for adjustments to ensure smooth sliding. After adjusting the rods to the perfect distances to each other, they are tied down with six M4 screws, three on the top and three on the bottom.

Ball Screw Lifetime Calculation

The ball screw is one of the most affected parts when it comes to wear of the device. Therefore a lifetime calculation was performed, to ensure that it fulfills the requirements. The minimum time the screw has to withstand, is 8 weeks while used 7 days a week with 2000 steps per day. This results in a total of 112,000 steps. To convert this into the revolutions the ball screw has to make, we have to know the pitch and the total travel distance per step.

The ball screw chosen for this device has the part number PRM0802 from Thomson Linear. It has a pitch of 2mm and is 8mm in diameter. Now, we have to calculate the total travel distance of the nut from the nut profile displayed in figure 3.12 on page 46. From the calculation we obtain the information, that the ball screw nut travels a distance of $95mm$ per step. Therefore the rotational life of a ball screw with a pitch of 2mm is calculated as:

$$L = 8Weeks \cdot 7\frac{days}{week} \cdot 2000\frac{steps}{day} \cdot 47.5\frac{rev}{step} = 5.32 \cdot 10^6 rev \tag{3.28}$$

By knowing the dynamic load capacity of the ball screw which is $2.4kN$ and the absolute average load of $311N$ applied on the screw during one gait cycle, the actual lifetime of the ball screw can be calculated [ThomsonLinear_1, 2014, Page 203]:

$$L = \left(\frac{C_{dyn}}{F_m}\right)^3 \cdot 10^6 = 4.595 \cdot 10^8 \tag{3.29}$$

Assuming the same per day and week usage of the device, the ball screw would last as

long as 13.3 years before it has to be exchanged, which easily fulfills the requirements.

Also, the critical speed for the ball screw had to be taken into account. From the product's catalog, the highest allowed DN value of 140,000 was obtained. This value is calculated as

$$DN = d \cdot n_0 \tag{3.30}$$

where d represents the rod's diameter and n_0 the nominal speed of the ball screw. Even if n_0 is chosen with the highest rpm value occuring during one gait cycle, which is $8450\frac{U}{min}$, the value for DN is only 67592, which is way within tolerance limitations.

In figure 3.55, a cross section of the top of the actuator is displayed. This is the part where the ball screw is actually mounted to the surrounding structure. The ball screw connects to the screw mount with a regular M3 screw. The torque coming from the motor is propagated from the screw mount to the ball screw by a hexagon interface, relying again on a tight form fit. To prevent the M3 screw, holding the ball screw, from loosening up due to the sudden directional changes throughout the gait cycles of the motor, a set screw is applied on the side of the screw head.

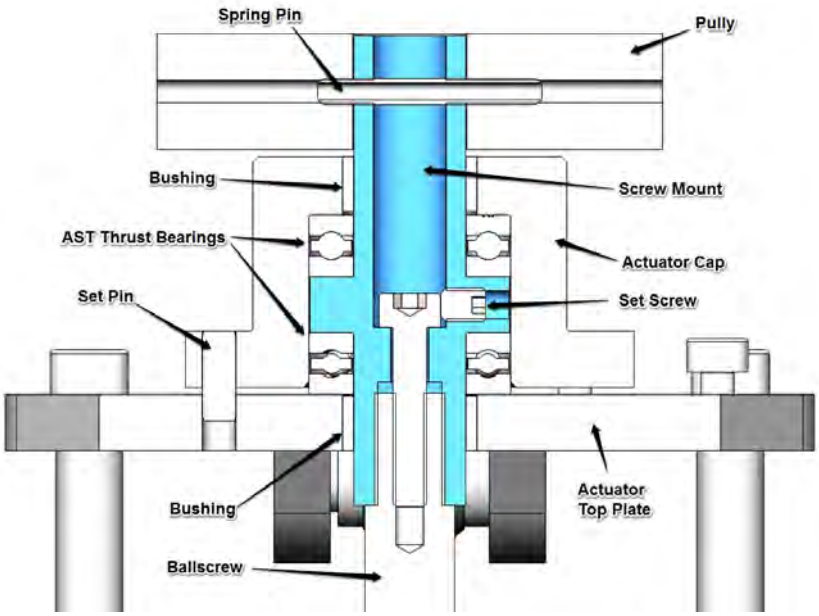

Figure 3.55: Actuator top cross section

On the top of the screw mount, the pulley is located. A spring pin ensures that it is kept in place and the moment is transferred accordingly to the screw mount. To make

sure that all of these parts are aligned properly, the actuator cap is positioned by 2 set pins with tight tolerances and then fixed in position with three screws.

However, the pulley diameter depends on the transmission ratio. As displayed in table 3.4 on page 54, the overall transmission ratio needed is 9508. Now we know that a ball screw with a pitch of 2mm was chosen and therefore its transmission ratio can be calculated as follows:

$$U_{ballscrew} = \frac{2000 \cdot \pi}{P} = 3141 \tag{3.31}$$

Taking this transmission ratio into account, the ratio which has to be covered by the pulley is calculated as:

$$U_{pully} = \frac{9508}{3141} = 3.02 \tag{3.32}$$

A ratio of approximately three can easily be achieved with pulleys. To simplify the choice for the right pulley pair, a software provided by Gates was used to choose the appropriate parts. The closest possible pulley ratio was 3.0 with the following parts:

- Pulley Screw - 3MR-48S-06
- Pulley Motor - 3MR-16S-06
- Belt - 201-3MGT-06

To support the axial loads, the screw mount is supported by two AST grooved ball bearings. All these elements are enclosed within the actuator cap, which also serves the purpose of preloading the thrust bearings. This is accomplished by applying layers of shims between the actuator top plate and the actuator cap. Also there are PTFE bushings pressed into the actuator cap and the actuator top plate. These are only used as a safety measure. During normal operation, if the parts are assembled and machined properly, there should not be any radial forces on the screw mount, besides the ones from the pulley, which are almost negligible. However, just to be sure the bushings were applied to reduce, in case of radial forces, the friction between the interfering parts.

Thrust Bearing Lifetime Calculation

The AST ball bearings experience just as much wear as the ball screw. Therefore a life calculation for the bearings is recommended as well. The necessary formulas to do so are provided by the manufacturers website.[AST, 2014]

In order to calculate the lifetime, the average rpm of the bearings has to be known. This value can be calculated by using the motor speed calculated in chapter 3.1.3 and

taking the pulley ratio into account. Therefore the average rpm of the thrust bearings is $n = 2322\frac{U}{min}$. The used average load for the calculation is the same as for the life calculation of the ball screw and therefore is $F = 311N$. From the bearing's data sheet the dynamic load capacity of $C_{dyn} = 2470N$ was obtained. Now, the expected lifetime can be calculated as:

$$L_{10h} = \frac{16,666}{n} \cdot \left(\frac{C_{dyn}}{F}\right)^3 = 3298h \tag{3.33}$$

To confirm that the life time is within the requirements, the time for one gait cycle has to be known. This data can be obtained from the initial data provided by Whittle, telling us, that a normal gait cycle takes $t = 1.25s$. The minimum total hour count the product has to last is:

$$L_{min} = 8Weeks \cdot 7\frac{days}{week} \cdot 2000\frac{steps}{day} \cdot 1.25\frac{s}{step} \cdot \frac{1}{3600}\frac{h}{s} = 37.3h \tag{3.34}$$

From this calculation it is obvious that the lifetime of the bearing exceeds the requirements by far. As a matter of fact, given the use of 2000 steps a day the bearing would last 13 years.

From the optimal curve of the ball screw nut as presented in fig 3.12 one can see, that one of the bearings is almost constantly loaded, while the other one is only loaded in the beginning and the end of each gait cycle. Taking this into account, two different bearings could be chosen in order to optimize weight, size and costs of the actuator. However, for the prototype it was assumed, that one bearing is constantly loaded during the gait cycle. Based on that, the life calculation was performed. For the second bearing the same type was chosen as the first one for reasons of simplicity.

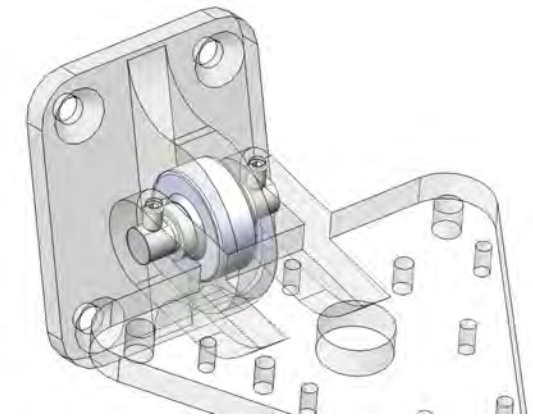

Figure 3.56: Actuator top connector

The connection from the actuator to the calf shell is basically the same as from the foot assembly to the actuator (see figure3.56). The ball joint is pressed into the mounting plate which is fixed to the calf shell. The actuator top plate reaches around the joint and connects to it with a bolt. Spacers on the left and the right ensure that the mounting plate stays centered between the two arms of the actuator plate. Two set screws pointing on the bolt's flat surfaces prevent it from moving and rotating.

Finally, the motor is attached to the actuator plate via the motorplate. Because pulleys are used within the assembly, the motor must be mounted in a way to move linearly to tense the belt once it is applied. Therefore two slotted holes were introduced

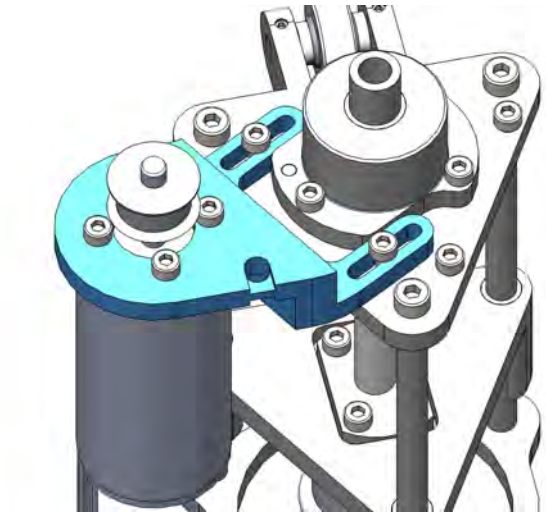

Figure 3.57: Actuator motorplate

to the motorplate allowing the motor to move linearly. To ensure that the plate can only move in one direction, it is guided by the actuator cap. After applying the necessary pretension on the belt, the motorplate is fixed in position by two M3 screws. The motor is positioned to the motorplate by the hole which provides a tight form fit and is locked in place by four M3 screws. The pulley on the motorshaft uses a setscrew to stay in position and transfer the moments. A hole on the side of the motorplate serves as a mounting point for tie wraps to safely position the wires from the motor and its sensor.

3.2.2.3 Slider

As mentioned in earlier chapters, because of the leverarm from the human ankle to the actual ankle joint of the device, a linear motion of the chain elements during eversion and inversion movements is anticipated. To compensate for this movement, the slider assembly, mounted on the calf shell, was introduced.

(a) Slider assembly

(b) Slider assembly without cover

Figure 3.58: Slider

The distance from the ankle to the device's ankle joint is $73.5mm$, if the ankle is centered in the device. By assuming that both, inversion and eversion is 30° maximum, we can calculate the linear vertical movement with

$$x = 73.5 \cdot tan(30°) = 42.4mm \tag{3.35}$$

Just to be on the safe side, a travel distance of $45mm$ was chosen. As displayed in figure 3.59, the slider is guided in the slider case. The slider's slot is occupied with the case stopper from the case, making sure that the slider cannot fall out by itself. The stopper on the left side in the picture represents the earlier mentioned locking mechanism, when the device is switched to pumping mode. To lock the movement, the slider has to be in its high end position, so that the stopper can be moved into the slider's pocket. A combination of spring and ball ensures, that the stopper stays in its place in both locked and unlocked position. All the parts are prevented from falling out by the cover as shown in fig 3.58a.

For the device, two slider assemblies are necessary, one on the left and one on the right side of the calf shell. The slider case has a cylindrical extrusion on the backside

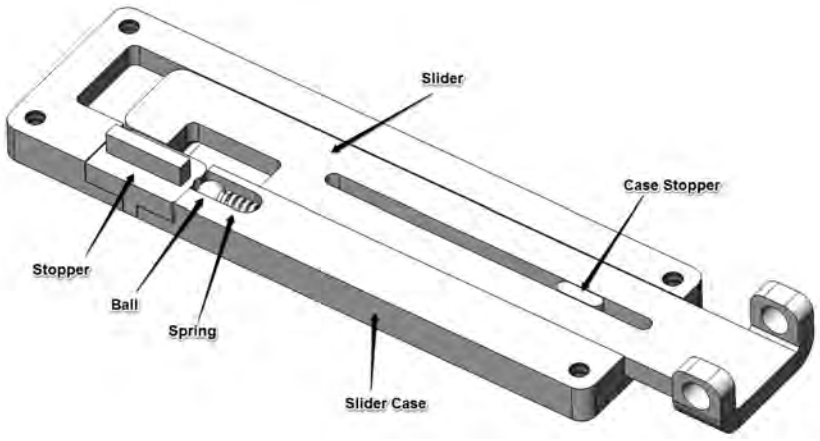

Figure 3.59: Slider markups

with a groove at the end where a retaining ring will be applied. A detailed view of the assembled slider on the calf shell is presented in the next chapter in figure 3.61.

3.2.2.4 Main Assembly

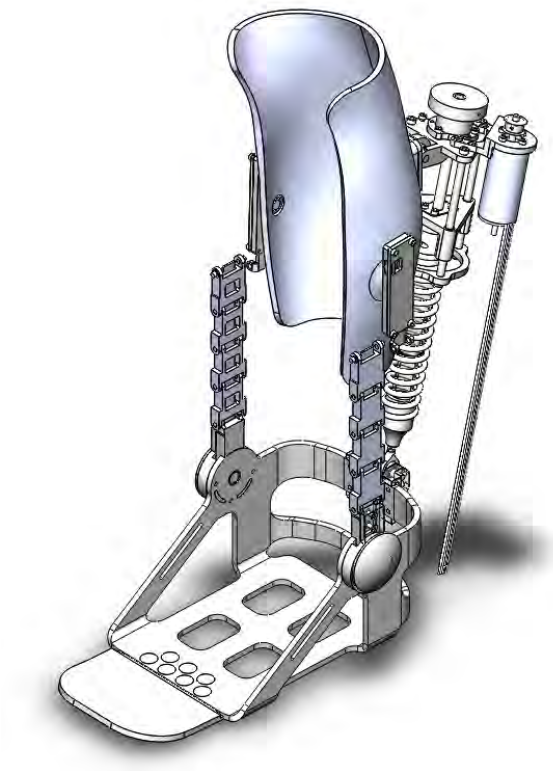

Figure 3.60: Powered Ankle Foot Orthosis

Figure 3.60 represents the finished device. The chain elements should be connected to the sliders on each side. Mounting it this way results in fewer modeling errors due to constraints. The slider assemblies, as mentioned in the previous chapter, are directly attached to the calf shell and held in place from the inside of the calf shell.

From figure 3.61b one can see the calf shell and the mounting point of the slider, which is partly visible behind the calf shell, as well as the end of the chain elements with the sheet metal spring. Figure 3.61a represents a cross section through the mounting of the slider assembly and the calf shell. The blue highlighted parts represent the slider assembly, where the cylindrical extrusion belongs to the slider case and the blue ring on the far left represents the earlier mentioned retaining ring. To reduce the wear of the calf shell, which is made from plastic, a flanged bronze bushing is introduced to the calf shell. To be able to keep the slider assembly and the bearing in place, a washer is used. The washer and the retaining ring have to be applied from the inside and are located in a pocket within the shell to not affect or touch the patient's leg. Also, the pocket is covered by padding.

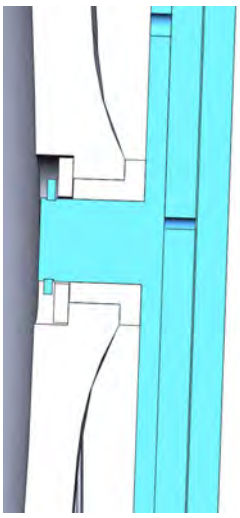

(a) Slider-Calf shell mount cross section

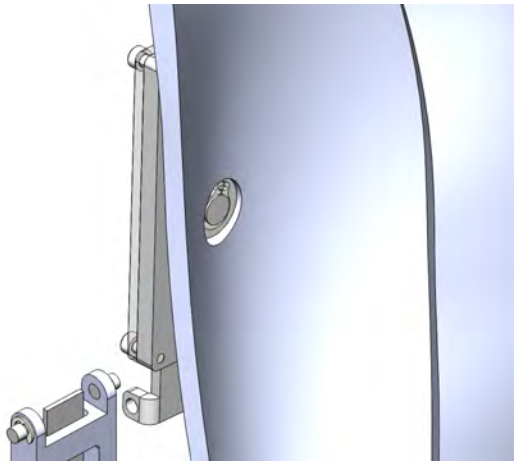

(b) Slider-Calf mounting point

Figure 3.61: Slider mounting

On the backside of the calf shell, the mounting plate for the actuator, displayed in figure 3.56 on page 85, is attached to the shell by the use of four M4 screws. The inside of the calf shell has four hexagon shaped pockets to host the corresponding nuts.

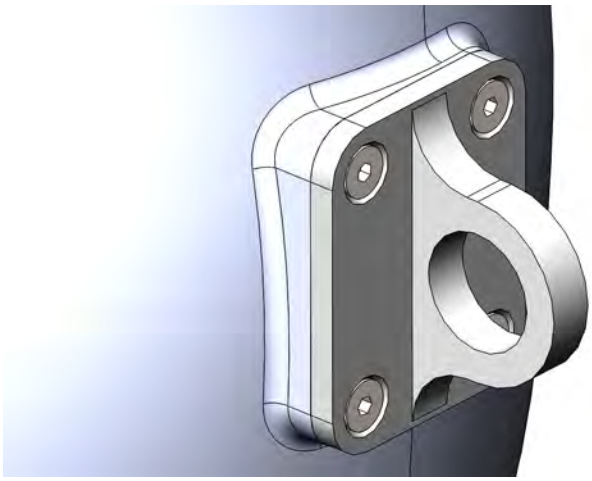

Figure 3.62: Actuator mount

3.2.2.5 Bill of Materials

This chapter should give an overview of how many parts were used, what the total costs are and how many standard parts as well as custom made parts were used.

To start, we have to keep in mind, that most of the parts of the device are consistent throughout the whole covered weight spectrum from 70kg to 150kg. However, as mentioned earlier, a few parts have to be exchanged to adjust the device to the patient's needs. The following table represents the parts which are specific for each weight interval, while all other parts can stay the same.

70kg	**90kg**	**110kg**
nut-socket-70	nut-socket-90	nut-socket-110
foot-spring-socket-70	foot-spring-socket-90	foot-spring-socket-11
70kg-spring	90kg-spring	110kg-spring

130kg	**150kg**
nut-socket-130	nut-socket-150
foot-spring-socket-130	foot-spring-socket-150
130kg-spring	150kg-spring

Table 3.7: Parts to interchange for distinct weight categories

From the table above, it is obvious, that the overall count of parts stays the same throughout the covered weight range. Therefore the following data will refer to only one category, namely 70kg.

In general, the parts used to build the assembly can be split up in standard parts and custom machined ones. However, some of the standard parts had to be modified to fit into the assemblies. It would not make sense to point out every part, therefore the following table gives an overview of the used parts.

Part Type	**Number of Parts**
Custom Made	92
Standard Parts (Total)	115
Standard Parts (untouched)	98
Standard Parts (processed)	17
Total Amount	190

Table 3.8: Number of parts per category

Most of the purchased parts came from standard distributors like McMaster Carr or other major suppliers. However, a few of the used parts had to be purchased from more specialized suppliers in order to fit the requirements. These parts are:

- AST - Thrust Bearing F10-18MH

- Thomson Linear - Ball Screw PRM0802
- Maxon Motors - EC4-Pole 30 200W 24V

In the end, the device is supposed to be used in a commercial way for rehabilitation. Therefore the expenses of the product are of interest. The final costs to manufacture the product, summed up to $11,850 . However, the person hours were not taken into account for that calculation and neither were the parts which were manufactured or 3D printed at the lab. This value only represents the costs caused by external manufacturing and purchasing the necessary parts or raw material. This is an enormous amount of money, considering that the device is supposed to be used to heal a patient's disease, especially when keeping in mind, that it will not be used any more by the patient after his recovery. Therefore it must be thought of as a device which will be rented to several patients. As from the calculations in previous chapters, the estimated lifetime of the device is set to more than 10 years. Assuming that there will be no additional maintenance costs and a total of 50 patients, each patient would end up with costs of $237 in order to just pay off the device. Taking it one step further, only some small parts might be necessary to be exchanged after a 10 years, not influencing the total costs a lot and therefore the overall price might drop even further with extended usage.

The total estimated weight measured in SolidWorks for the PAFO is **2.5kg** for the 70kg weight category. The calf shell is not included in this calculation because it changes in size from patient to patient.

3.2.3 Stress Calculation and Finite Elements Analysis

To verify that the stress applied on the most important parts does not exceed the materials limits, hand calculations, respectively an FE analysis were performed. The program for the FEA was Abaqus CAE in Version 6.12-1. A separate safety factor for the analysis itself is not included. However, for the initial calculations in chapter 3.1, a safety factor of 1.2 was applied to the patient's weight already. Therefore all the calculated values and forces, applied on the models during FEA include a safety factor of 1.2 as well.

If assemblies had to be transferred from SolidWorks to Abaqus, the parts where positioned properly in SolidWorks and then exported separately, so that they align after importing to Abaqus. For exporting, the filetype ACIS (ending on *.sat) was chosen in version 20.0. The standard setting is on version 22.0, however, by choosing the default settings, the file cannot be read by Abaqus. All parts simulated were created in SolidWorks as solid models.

In general, simplifications to parts which are to be analyzed speed up the computation time. More important for the project was to get the most accurate results. Therefore, if not mentioned otherwise, no simplifications were applied on the parts.

The following properties where assigned to each and every part simulated:

- Solid, homogeneous elements
- Mesh: Tetrahedral elements in quadratic geometric order

The solid, homogeneous elements setting allows to simulate solid models. Another opportunity would be, to choose shell elements, but therefore all the parts would have had to be remodeled, if possible at all. The homogeneous setting only describes that a material is assumed with a constant density throughout the body.

As long as the parts are of quadratic shape, hexahedral elements could be used, allowing faster computational time. Unfortunately, most of the parts used are not of quadratic shape and therefore the tetrahedral elements had to be used to build up the mesh. The second order, or quadratic geometric order, was chosen, to simulate bending moments appropriately. Linear elements only have nodes on the corners and therefore the edges can only represent straight lines between the corners if the shape of the cube is altered. On the other hand, quadratic elements have additional nodes on the edges in the middle between the corners. So if bending occurs and the shape of the element is altered, the corners are not connected with a linear edge, but with a quadratic one,

making the calculations much more comparable to the real world. Examples for linear and quadratic elements can be found in figure 3.63.

(a) FEA linear elements

(b) FEA quadratic elements

Figure 3.63: FEA linear and quadratic elements [Comsol, 2014]

3.2.3.1 Footplate

The footplate is used as support structure for multiple other parts. Also the patient is standing with his weight on this part. Especially critical are the arms on the backside, where the actuator connector is located. Furthermore, the area of the ankle joint and the front, where the flexible footplate is attached is of interest.

To simulate the stresses appropriately, an assembly consisting of the footplate, the ankle plates and the actuator connector was created. Furthermore, this assembly was simulated in two different positions. In the first one, the assumption was made, that the actuator is pulling at the actuator connector with its maximum force, while the ankle joints carry the patient's whole bodyweight. In the second scenario, the assembly is simulated while the maximum moment from the ankle acts on its parts. Again, the actuator pulls up at the actuator connector while the ankle joints carry the patients bodyweight. Furthermore the reaction forces from the ground, due to the ankle moment are acting on the front of the footplate. Figure 3.64 represents the assembly imported to Abaqus

The simulated assembly consisted of the following elements:

- footplate
- actuator connector
- ankle plate (left)
- ankle plate (right)

All the mentioned parts are made of the same material, hence they are all assigned with the same material parameters:

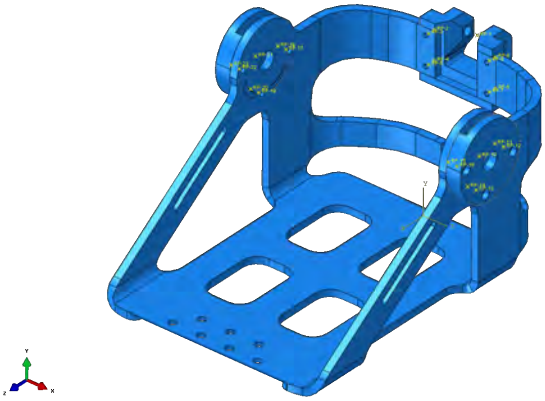

Figure 3.64: FAE footplate assembly

- Density: $\rho = 2.7 \cdot 10^{-6} \frac{kg}{mm^3}$
- E-Modulus: $E = 69,000 \frac{N}{mm^2}$
- Poisson ratio $\nu = 0.34$

The parts where constrained to each other by using the holes designated for the screws. To do so, reference points were created in the middle of each hole and then constrained with rigid beam elements to the surrounding hole surface. The connection between the holes was realized by the usage of the Connector Builder applying a connector of type hinge between the reference points. This connector, which represents the screw connecting the parts to each other, was assumed to be rigid as well. A graphical representation of the beams and the hinge is shown in figure 3.65. Contact areas between the parts used for form fits, e.g. between ankle plate and footplate, were taken into account as well. All contact areas are assumed to be frictionless.

Loads for scenario one where applied in vertical direction along the y-axis. From calculations in chapter 3.1 we know, that the maximum force acting on the bolt of the actuator connector is $1238N$ for a 150kg person with safety factor 1.2 included. The ankle joints should be loaded with the patient's weight which results in $883N$ on each joint. Again, the forces were applied by using reference points, constricted to the designated surfaces. For the boundary condition, the lower surface of the footplate, heading towards the ground, was pinned, restricting linear movement in x,y and z-direction.

After meshing the parts with the initially mentioned properties, the simulation was performed. The results for scenario one, are presented in figure 3.66

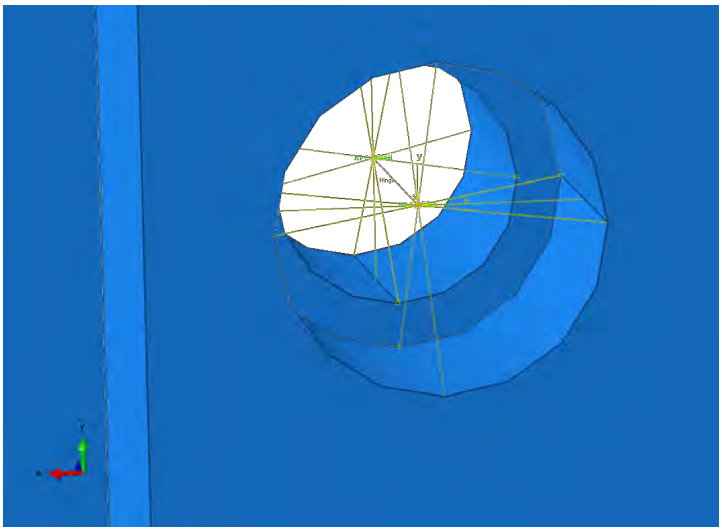

Figure 3.65: FAE constraints and connectors

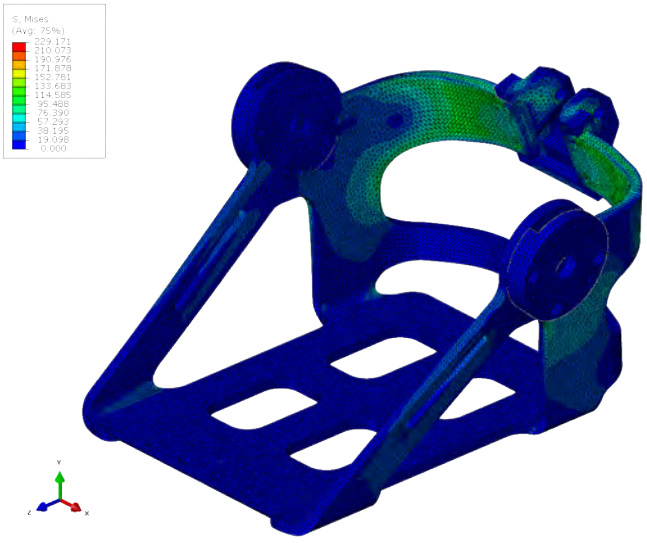

Figure 3.66: FAE footplate stress analysis

The simulation shows no highlights or peak stress areas. In general, the stresses acting on the part do not exceed $221 \frac{N}{mm^2}$.

For the second scenario simulated, the time index of maximum moment had to be calculated to find the device's angle at that time. One might suspect, that maximum moment occurs during maximum plantarflexion prior to take off. However, figure 3.67 shows, that the maximum moment acts in a dorsiflexed position, where the foot still has full ground contact.

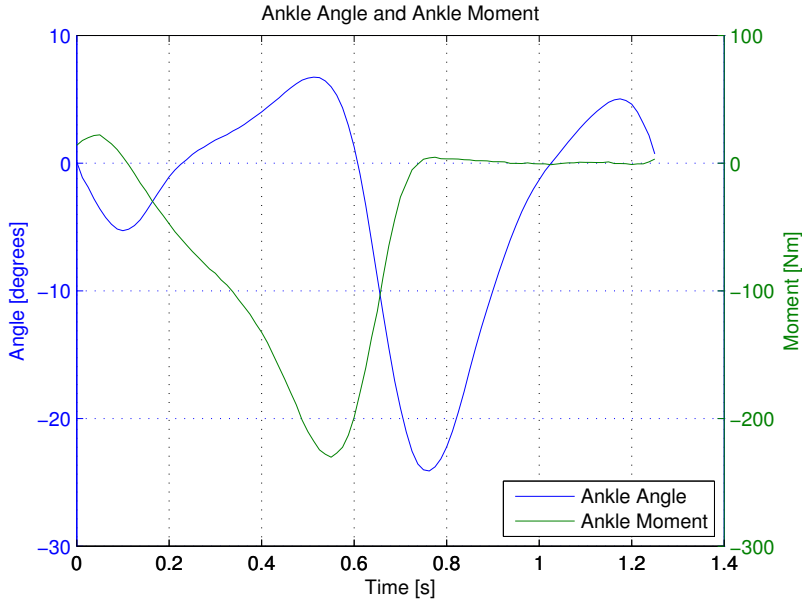

Figure 3.67: Ankle angle and moment as a function of time

The ankle angle at maximum moment indicates an angle of 6° in dorsiflexed position. For convenience the forces acting on the ankle joints as well as on the actuator connector were both assumed to be 6° tilted as well. However, the magnitude of the forces stay the same. The working point of the ground reaction forces due to the moment was assumed to be between the two rows of holes designated for the rivets. The normal distance from this point to the ankle joint is $150.5mm$ resulting in a force perpendicular to the leverarm of $F = 1530N$. Measuring the angle of the leverarm to the ground results in 35.9°. Applying the laws of sine and cosine results in the ground forces of $F_y = 1239.36N$ and $F_z = 897.15N$ according to the coordinate system of Abaqus.

For boundary condition, only the back of the footplate was pinned (see figure 3.68).This gives the front of the footplate the flexibility to deform accordingly to get closer to the real stress distribution.

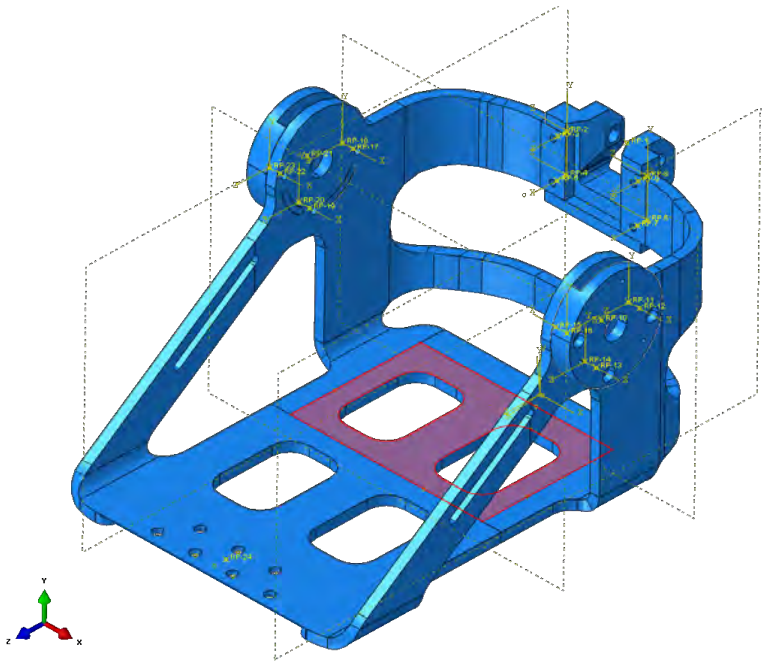

Figure 3.68: FAE footplate assembly boundary condition during maximum ankle moment

Again the patient's weight of 150kg with a safety factor of 1.2 was distributed onto the two ankle joints and the maximum force of $1238N$ was applied to the actuator connector. Both were tilted by 6° to simulate dorsiflexed position. The previously calculated ground reaction forces are applied in the middle of the footplate between the two rows of holes designated for the rivets. Reference points and rigid beam elements were used to apply the forces.

The results displayed in figure 3.69 show no significant changes to the previous simulations. Peak stresses with a magnitude of $483\frac{N}{mm^2}$ occur in the corner of the pocket where the flexible footplate is attached to the footplate. However, these values are more likely results of inaccuracy due to the mesh size, than valid values, because they are localized in a very small area with almost no surrounding stress. Also, and probably even more important is the fact, that the force was attached with rigid beam elements, causing the pocket to be perfectly rigid. In reality, this force would apply differently, depending on a variety of factors, like the material of the front plate, weight distribution of the patient, ground conditions, etc. Therefore, these values most likely do not represent the actual stresses acting during use. However, the forces had to be applied to monitor the influence on the surrounding structure.

Conclusively it can be reported, by taking a look at the structure except the pocket,

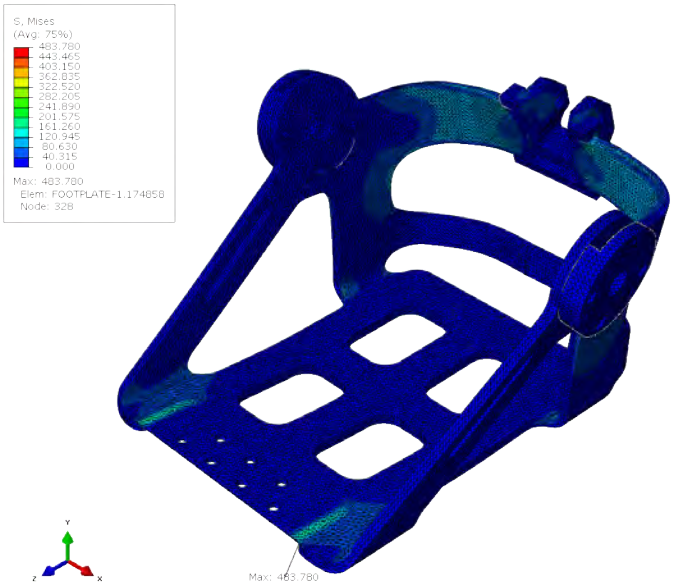

Figure 3.69: FAE footplate assembly stresses during maximum moment

that the stresses are within the material's stress limits of $\sigma = 317\frac{N}{mm^2}$ for a 4032 T6 Aluminum.

3.2.3.2 Foot - Actuator Bolt

The actuator bolt connects the actuator connector and the balljoint rod end of the actuator assembly, transferring the force from one assembly to the other. Therefore this is one of the most important parts of the assembly. The flat surfaces of the bolt where the setscrews are applied on, were not taken into account, ending up with just a cylinder. The bolt was then split into 5 different segments representing the different stress affected areas of the bolt (compare to figure 3.70).

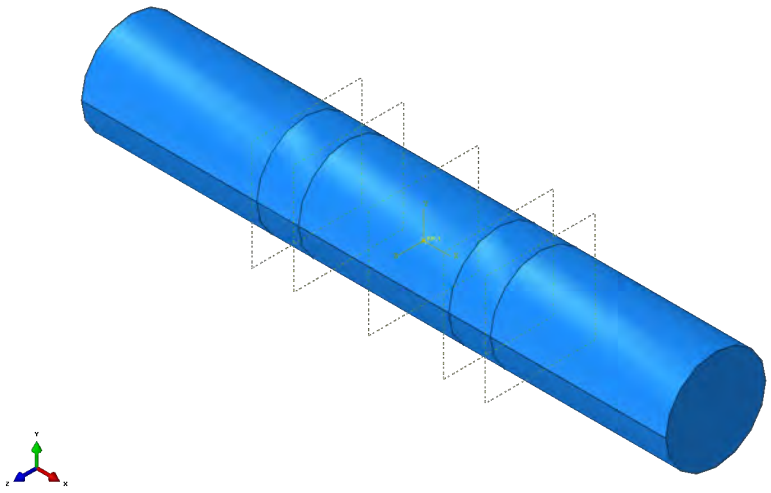

Figure 3.70: FAE footplate balljoint

As material an AISI 1055 steel with a yield strength of $\sigma = 560\frac{N}{mm^2}$ was chosen. The following properties were assigned to the model :

- Density: $\rho = 7.85 \cdot 10^{-6}\frac{kg}{mm^3}$
- E-Modulus: $E = 210,000\frac{N}{mm^2}$
- Poisson ratio $\nu = 0.3$

Hand Calculation

Prior to the FEA, a hand calculation was performed to be able to validate the simulations results. Figure 3.71 shows how the model can be approximated for handcalculation.

The actuator connector can take up moments as well as forces in radial direction. By applying the set screws on the flat surfaces of the bolt, we can assume that movement in axial direction is restricted as well. Hence, by knowing the free length $l = 14mm$, the

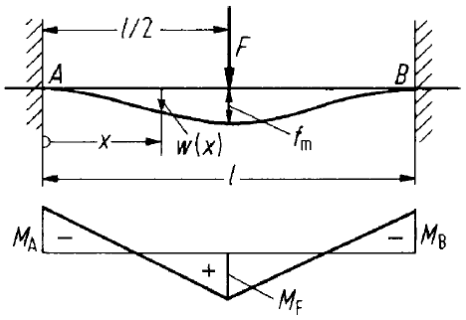

Figure 3.71: Foot - Actuator Bolt handcalculation [Grote and Feldhusen, 2011]

bolt's diameter $d = 6mm$ as well as the force $F = 1238N$ the moment can be calculated as:

$$M_a = \frac{M \cdot l}{8} = 2166Nmm \tag{3.36}$$

Furthermore the bolt's section modulus is:

$$W_b = \frac{d^3 \cdot \pi}{32} = 21.2mm^3 \tag{3.37}$$

Finally the acting stress on the part is:

$$\sigma_b = \frac{M_b}{W_b} = 102.2\frac{N}{mm^2} \tag{3.38}$$

Simulation

The left and right ends of the bolt are held by the actuator connector and locked in place with the set screws. Therefore we assume, that these sections of the bolt do not move at all. Boundary conditions were applied to these parts restricting them in linear movement in x,y, and z-direction. In the middle of the bolt, the rod end is located. Although the rod end has a tight fit around the bolt, there is still the possibility of movement and therefore this area will not be completely restricted in its deformation. The load of the actuator was applied as a pressure on the lower half of the bolt. The actuator's load of $1238N$ is divided by the bolt's projected area of $54mm^2$ ending up in $22.93\frac{N}{mm^2}$. This is not quite accurate, because only a part of the lower half has actual contact with the rod end. Nevertheless this deviation is accepted for this simulation.

The final results of the simulation as described are shown in figure 3.72. As one can observe, the highest stresses occur at the edge of where the actuator connector surrounds the bolt. The highest stress on this part is $\sigma_b = 195\frac{N}{mm^2}$ which is easily within the material's yield stress limits.

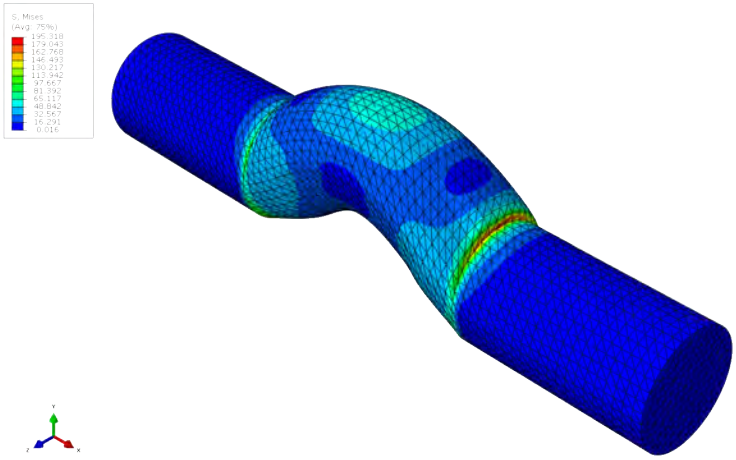

Figure 3.72: FAE foot balljoint bolt stresses

The values of the hand calculation and the simulation are off and cannot be compared to each other. However, because of the boundary conditions in the simulation the stresses at that edge are probably much higher than they would be. Therefore it is quite safe to say, that first, these peak stresses will not occur like that in real life and second, that the part will without doubt withstand the stresses. If necessary an even weaker material could be used. However, it cannot be determined yet, what influence the repeatedly sudden force impacts during heal strike will have on the bolt. Also, as noticed from tests prior to this thesis on other products similar to this one, sometimes patients tend to counteract the device when they use it the first time, increasing the stresses on the parts. Hence, the long term effects have yet to be figured out.

3.2.3.3 Chain Element

These elements represent the connection of the foot itself with the calf shell. This connection is designed as chain elements to give the patient more freedom in his movements throughout the day, allowing eversion and inversion of the foot. They are connected to each other with the so called chain bolts. However these bolts do not connect one side of the element to the other, but there is one bolt on each side. Modeling the parts in this way was necessary, because a sheet metal spring runs through all of these elements.

The elements themselves are made of 7075 T6 Aluminum having a yield strength of $\sigma = 462\frac{N}{mm^2}$. The following properties where assigned to the model:

- Density: $\rho = 2.81 \cdot 10^{-6}\frac{kg}{mm^3}$
- E-Modulus: $E = 74,700\frac{N}{mm^2}$
- Poisson ratio $\nu = 0.33$

The part was imported to Abaqus and assigned with the properties. A reference point was set and constrained to the holes on one side of the part as displayed in figure 3.73.

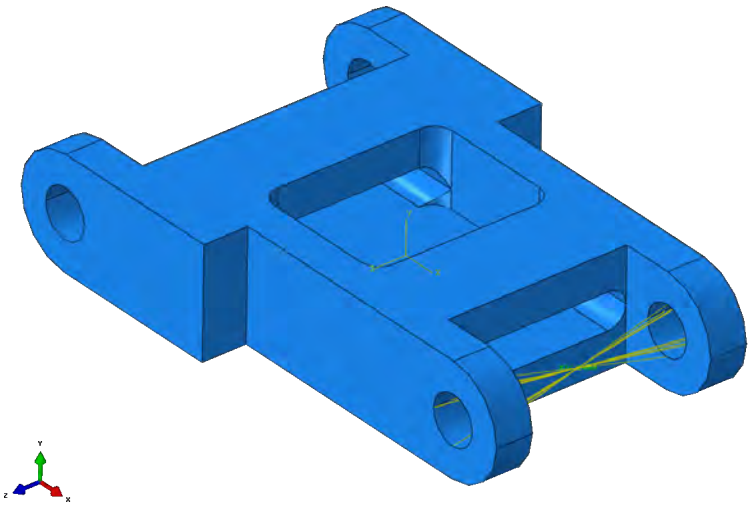

Figure 3.73: FAE chain element

It was assumed, that the chain elements are constrained to each other in a way so that they cannot rotate. Also, for the simulation the assumption was made, that the patient's full body weight is supported by the device. Hence, half of his bodyweight is carried by one chain element. The load applied is a concentrated force of $F = 882N$ in x-direction representing the weight of 150kg and a safety factor of 1.2.

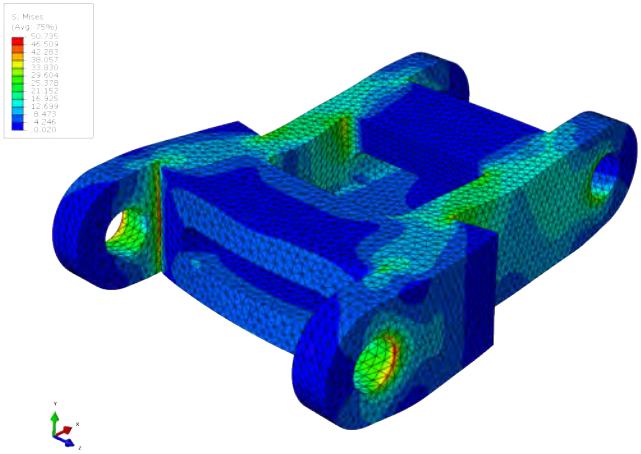

Figure 3.74: FAE chain element - stress

As expected, the highest stresses occur at the joints. However, the maximum stress does not exceed $51\frac{N}{mm^2}$. At this point it should be mentioned, that the initial approach was to model the chain elements as sheet metal parts. The material chosen for this approach was a high yield strength steel. Still, the thickness of the sheet metal itself had to be at least $3mm$ in order to withstand the stresses. During the ordering process of these parts it turned out that no machine shop was able to manufacture the parts. Hence, the parts where remodeled as close to the original ones as possible.

As the simulation shows, the new parts can be modeled much smaller and still withstand the forces acting on them. This has to be kept in mind for upcoming further improvements of the device.

3.2.3.4 Chain Bolts

The chain bolts connect the previously simulated chain elements to each other and act as a hinge at the same time. The smaller these elements can be made the better, because it directly influences the size of the chain elements as well. To connect two chain elements to each other two bolts are necessary. The bolts are kept in place with a retaining ring located in between the chain elements. Therefore a little groove is added to the bolt, affecting its stability.

The material chosen for these bolts is an AISI 1055 steel with a yield strength of $\sigma = 560\frac{N}{mm^2}$. This material was used for the Foot - Actuator Bolt already. The material properties assigned are:

- Density: $\rho = 7.85 \cdot 10^{-6}\frac{kg}{mm^3}$
- E-Modulus: $E = 210,000\frac{N}{mm^2}$
- Poisson ratio $\nu = 0.3$

For the simulation of this part the assumption was made, that the chain elements surrounding this part are completely rigid. Hence one side of the bolt was constrained with boundary condition and prevented from moving in linear x,y or z-direction. For the other end, a reference point was created in the middle between the bolts end and the groove. The surrounding surfaces were constrained to that point by the use of beam elements.

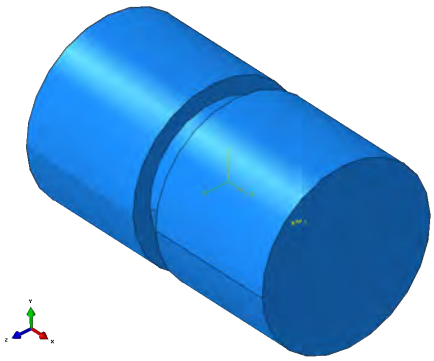

Figure 3.75: FAE chain bolt

Also, it is assumed for the course of this simulation, that the device supports the patient's full bodyweight. Hence the concentrated force on one bolt is $F = 441N$ applied in y-direction. This represents a quarter of a patient's bodyweight of 150kg including

a safety factor of 1.2 because there are chain elements on both sides of the patient's leg, each having two bolts per element. The final results of the simulation as presented in figure 3.76 show high stress concentrations at the edges of the groove as expected. Although the bolt's groove diameter is only $3.2mm$, there is still some tolerance up until the yield stress limits of the material. Keeping in mind that for this simulation the whole patient's bodyweight was applied on the device, the bolts could probably be modeled in an even smaller way. Also it is important to remember, that the bolts are connecting chain elements which are able to move if loaded. Therefore it is valid to assume, that this scenario will never apply in a real testing environment like it applies during simulation. However, for the purpose of the prototype it was more important to ensure to build a fully functional device, rather than an already size and weight optimized one.

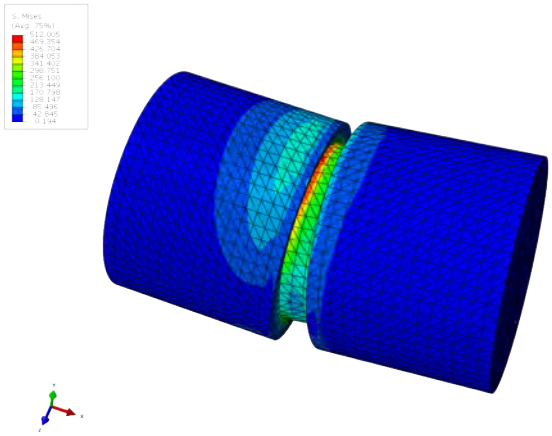

Figure 3.76: FAE chain bolts - stresses

3.2.3.5 Screw for Ball Screw - Screwmount Connection

The moments from the screw mount to the ball screw are transmitted by a tight fit of a hexagon connection, but for transmitting the axial forces, only one M3 screw connects those two parts to each other. A hand calculation was performed to find out what strength category of the screw is necessary to withstand the forces. By knowing the applied maximum load of $F = 1238N$ and the screw's core diameter of $d = 2.39mm$ the stress can be calculated.

$$\sigma = \frac{F}{A} = 275.9\frac{N}{mm^2} \tag{3.39}$$

Therefore a screw with at least ISO strength category 4.8 is necessary. Compared to the inch based system that would represent an ASTM A 307, grade A. Research revealed, that a simple carbon based steel is chosen for this kind of strength category [Keller-Kalmbach, 2014].

3.2.3.6 Ball Screw

The ball screw carries all the load transferred from the spring to the nut. Its weakest part is on the top where the hexagon shape and the screw hole is tapped into the rod. Therefore, this section has to be analyzed in detail.

Because of the lack of detailed knowledge about the used material of the ball screw, the following standard steel values were applied:

- Density: $\rho = 7.85 \cdot 10^{-6}\frac{kg}{mm^3}$
- E-Modulus: $E = 210000\frac{N}{mm^2}$
- Poisson ratio $\nu = 0.3$

Due to the screw fitting into the top of the tapped hole, the hexagon shaped part was split into two distinct parts. The inner surface of the tapped hole heading towards the outside was then restrained while the force of $F = 1238N$ was applied. Figure 3.78 presents a cross section of the simulated ball screw indicating a maximum stress value of $\sigma = 271\frac{N}{mm^2}$. It is a valid assumption, that for the purpose of a ball screw, a higher graded steel was used which easily surpasses the yield strength of $271\frac{N}{mm^2}$. Therefore we can assume that the calculated value is easily within the steel's stress limits.

Furthermore, from the ball screw's datasheet a static load rating of 4.1kN could be obtained. This value is valid for the non manufactured rod, however, relative to the decrease of the cross sectional area of the hexagon im comparison to the main rod, it is obvious that the ball screw will be able to withstand the applied load.

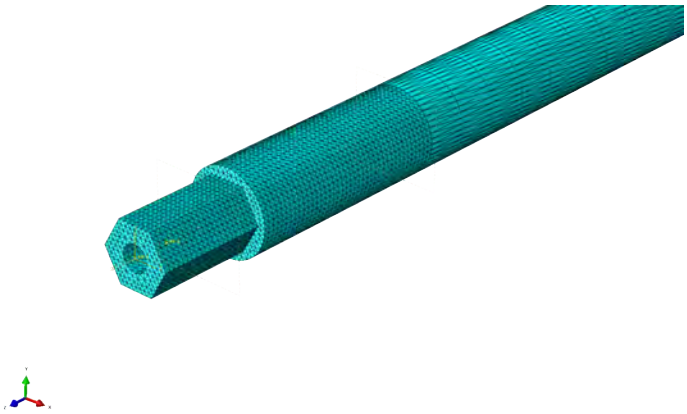

Figure 3.77: FAE mesh ball screw

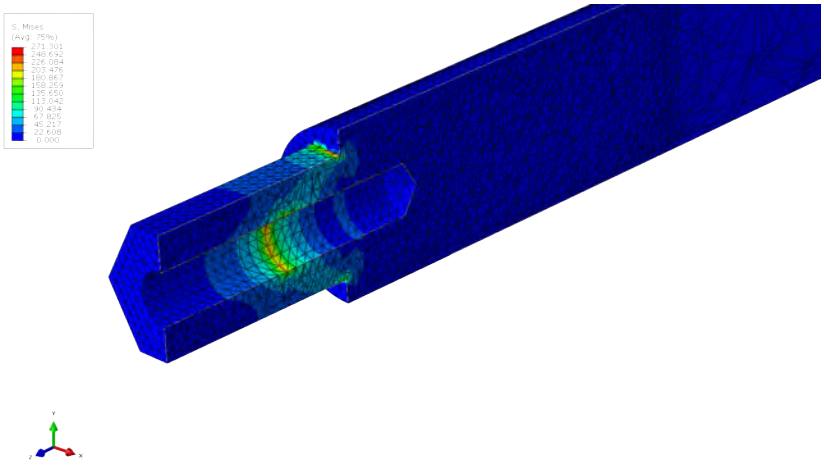

Figure 3.78: FAE ball screw - stresses

3.3 Electronics

The electronics of the device are needed to run the controls, power the motor and provide a data connection via bluetooth to a host pc to monitor the device. All the electronic components, except the ankle sensor, the gyro and the battery, are mounted on the electronic mount plate located within the actuator assembly (see fig 3.79).

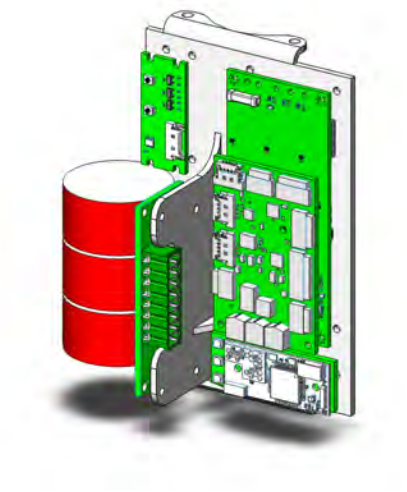

Figure 3.79: Electronics mounted

The following electronic components are in use for the device:

- Motor: Maxon EC4-Pole 30 200W 24V
- Motorcontroller: EPOS2 40/12
- μ - Processor Board: MC710AWA
- Ankle Encoder: RMB20VE
- Bluetooth Board: CB-OBS421I + Interface
- Gyro: LPY550AL
- Inductorboard
- User Interface

3.3.1 Wiring

The following schema represents the way, the components are connected to each other.

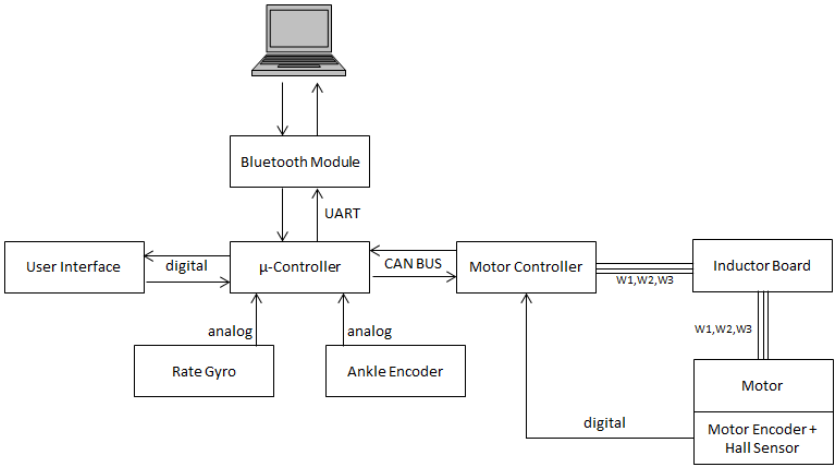

Figure 3.80: Electronics Layout

However this schema can only provide a small overview of the actual wiring between the distinct parts. To get a more in depth view of how the single ports are connected to each other, wire layouts had to be created using OrCAD Capture. Therefore, one main diagram was created, showing the positioning of the pins. The complete layout is shown in figure 3.81.

The power supply from the battery is directly soldered onto the inductor board, as well as the wires coming from the motor controller. All other connections are carried out as plugs. However, there is still a jack between the battery and the inductor board to make sure that the battery is interchangeable.

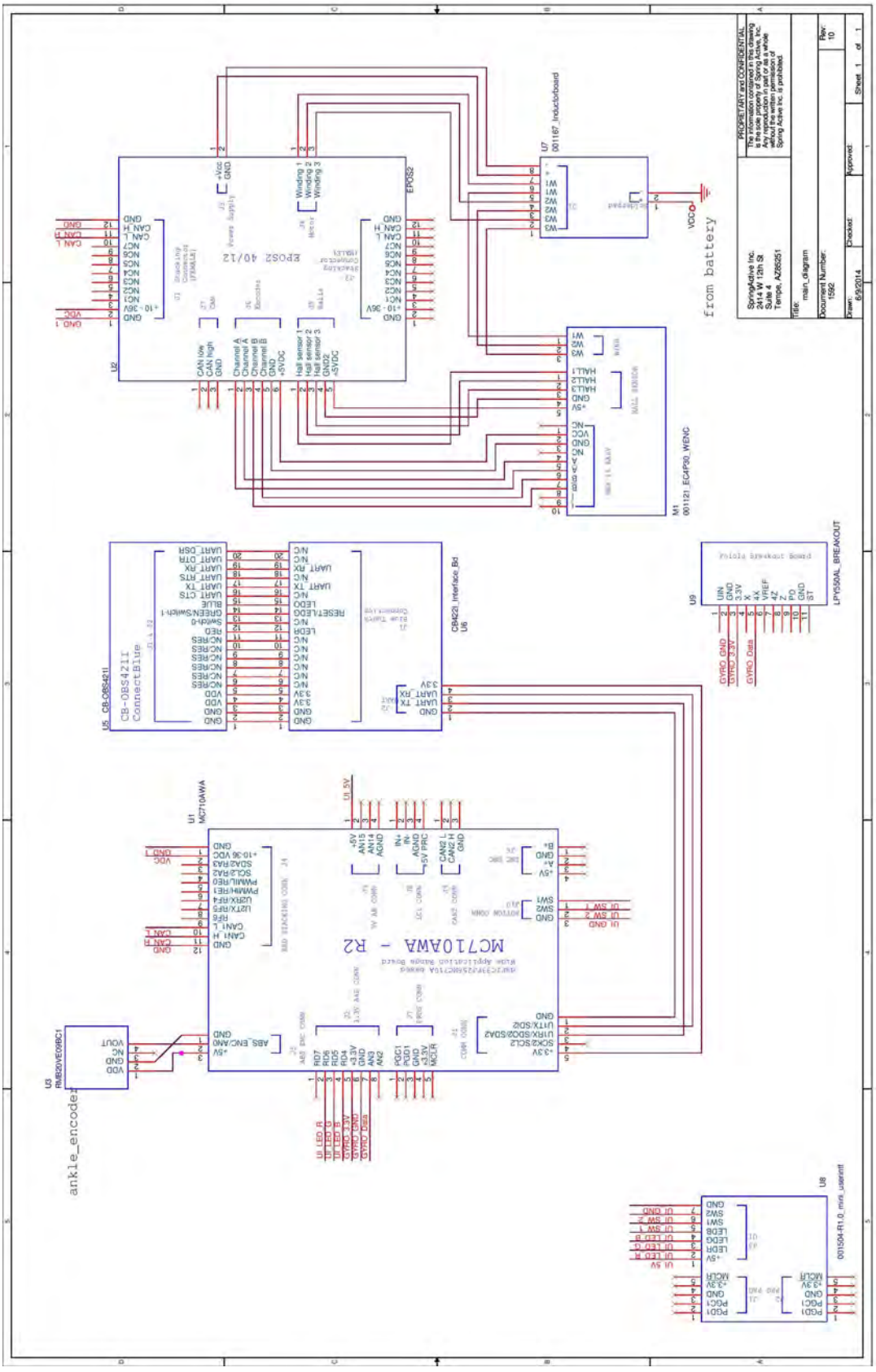

Figure 3.81: Electronics detailed wire layout

3.3.2 Component Specifications

The motor specifications were already presented in chapter 3.1.4, therefore this data will not be presented here again.

MC710AWA

The MC710AWA is a microprocessor board which was specifically designed for the use in robotic applications. Therefore, its size is kept very small, while focusing on the ability to process information specifically for motor controllers, enabling communication through networks and including several ports for direct sensor attachment. The heart of the board is a 16bit digital signal controller, which can be programmed by using Matlab/Simulink. It also enables low profile stacking for up to four controllers of the type EPOS2 40/12, minimizing space occupation as well as offering a communication interface, accessible via on-board connectors.

Its input voltage ranges from 12-36V DC and current input from 100mA to 250mA depending on processor load and input voltage. The on board gyroscope and accelerometer have a range of $\pm 2000°$ per second and $\pm 16g$ interfaced via I2C channel 2. Also an analog temperature sensor is available for emergency shut down preventing overheating of the components in use. A tricolor LED provides the user with direct visual feedback of the board's status.

The on-board power supply is limited to +3.3V and 300mA and +5V and 100mA depending on the port. Its dimensions are given with $35x55mm$.

The board represents the intelligent core of the electronic parts. It is used as the master for the inter-component communication as well as providing the necessary data to the designated boards. Also it holds the code for the tibia controller responsible for the position calculation of the motor nut (see chapter 3.4.3). [Boehler, 2014]

EPOS2 40/12

The EPOS2 40/12 was developed by Maxon Motor Switzerland in cooperation with SpringActive Inc. It is a small-sized, fully digital, smart controller which is capable of driving DC Motors as well as brushless EC Motors with its high efficient power stage. Hall sensors and incremental encoders attached to the motors can be directly connected to the board. The information then can be passed through the CAN bus to the MC710AWA which the controller is stacked onto. It is equipped with position-, velocity- and current control funtionality allowing sophisticated positioning applications.

Its required supply voltage ranges from 10-40V DC while being able to provide $0.9 \cdot V_{CC}$

and up to 40A of peak current output. Its maximum continuous output current is limited with 12A, while the maximum switching frequency is set with 50kHz. As the calculations in chapter 3.1.3 showed, we are still way below the maximum continuous current output.

The board provides connectors for the motor wiring as well as for 3 Hall Sensor inputs and incremental sensor signals. The connection to other devices is realized by using a CAN bus system. The protocol used for transmitting data is CANopen [Maxon, 2013]. This protocol incorporates the following service objects:

- NMT
- SDO
- PDO
- Heartbeat
- Sync
- EMCY

NMT is used to trasmit information regarding the network management and for supervising the other devices connected to, in our case, the master device which is the MC710AWA. SDO (Service Data Objects) is used for transmitting general data like, maximum velocity, position, current, limitations, and other information not necessarily depending on accurate timing. Normally these values do not change in our setup after their first initialization. PDO, called Process Data Objects, are used to transmit real time information. For this application, all the motor nut position data is transferred using these objects to ensure that they arrive with as little delay as possible. The heartbeat signal is sent in fixed time intervals to ensure that the devices are still online and communicating, while the Sync object is used for syncing multiple other components with each other. Syncing is not necessary in our instance, because we only have one component acting as a slave. The EMCY is used to submit error messages. [CANopen, 2014]

Because of the high current output of the board, temperature is a major factor influencing the efficiency and operational range of the board. Continuous current output of 12A is assured up to the temperature of about 58° Celsius. The range can be extended up to about 67° by attaching a heat sink to the coils. From there, the output current decreases linearly down to 85° where the board shuts itself down (see figure 3.82) .

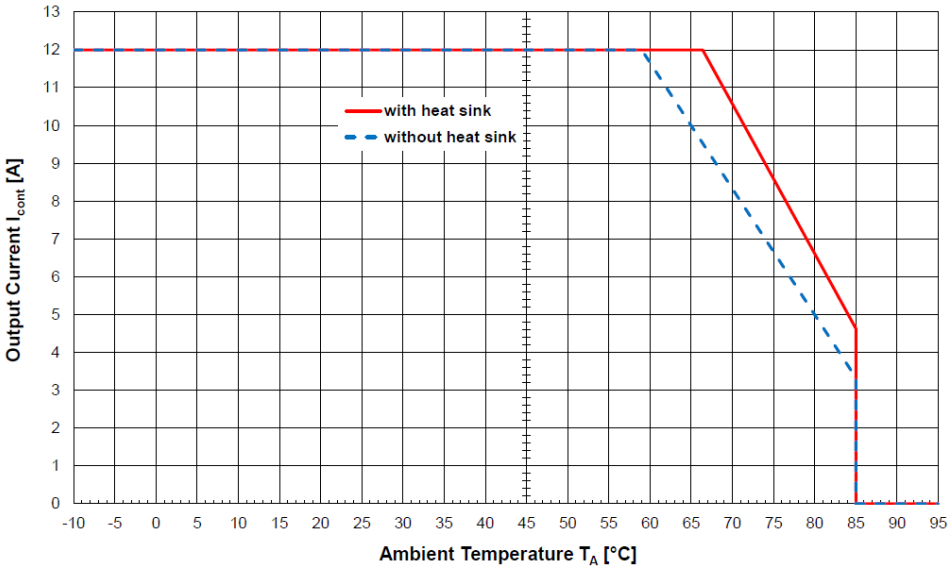

Figure 3.82: Motor controller output current as a function of temperature

The overall dimensions of the device are given by $80mm$ x $35mm$. Optical user feedback is provided by a red and a green status LED, signaling normal operation or ERROR. The motor used in this device includes Hall sensors as well as an incremental sensor. Both are directly attached to the board. The control operation mode used for this product is going to be explained in the following chapter 3.4.2. [Maxon, 2013]

Ankle encoder RMB20VE

The RMB20V used in the ankle joint to track the angular movement is a magnetic encoder module. This version represents the magnet's position in a linear output voltage where the nonlinearity factor is given with 1%. The power supply is specified with $V_{dd} = 5V$ and 26mA typical.

This instance of the sensor has a voltage output range from 0-5V. The range covers 360° of angular rotation in counterclockwise position. The magnet used for tracking the angle is directly implemented into the shaft of the ankle joint. The sensor itself is stored within the 3D printed ankle cover. The magnet and the axis of the sensor have to be concentric to each other within a tolerance of $0.2mm$, while the axis of the magnet has to be perpendicular to the sensor's surface within $0.15mm$. The sensor's PCB has a diameter of $20mm$.

Bluetooth Board CB-OBS421I This bluetooth module is used to monitor the data from the device while walking e.g. the treadmill and making small adjustments while

walking. The module is bluetooth v4.0 capable and communicates with the MC710AWA via a UART interface. Its power supply needs a voltage of 3-6V DC and an average power consumption of 44mA. The overall size is $16x36x3mm$ with a weight of 2g.

LPY550AL - Gyro

The sensor in use on this device is the LPY550AL from ST Microelectronics, offering a sensitivity range from $500°/s$ to $2000°/s$. It can be used on 5V micro controllers due to its integrated 3.3V regulator, while keeping the size still small at $12.5x25.4mm$. By default the output is already two-stage low-pass filtered to reduce high-frequency noise. For retrieving data used to control the orthosis, this sensor is used instead of the on-board gyro of the micro controller. This is because the actuator, where the microprocessor board is mounted on, has multiple degrees of freedom and is able to move sideways while walking. This makes it hard to get accurate, evaluable data. Therefore, this sensor is strapped to the user's foot while testing the prototype.

Inductorboard

The inductorboard holds the coils used to ensure, that our current ripple stays within 20% of the motor's nominal current. Also it is the attachment point of the power source and equipped with a connector to be exchanged easily.

User Interface

The user interface holds two switches for direct interaction with the MC710AWA as well as red, green and blue LEDs to provide the device's user with some optical feedback regarding the status of the orthosis. All inputs and outputs of the userinteface, which is custom made, are digital.

3.4 Controls

This chapter of the thesis describes, what kind of control structures were formerly used in earlier orthosis and prostetics, as well as what kind of modes are used in the EPOS2 motor controller and what kind of inputs are necessary. Finally the tibia controller and its function principle is described as well as how it interacts with the sensor data and the information given by the initial calculations in chapter 3.1

3.4.1 Formerly Used Controllers

This chapter deals with older controllers previously used in prostetics and orthoses. In general, the more simple the controller, the better. However, also the way the device is controlled and what is controlled is of utmost importance.

3.4.1.1 Lever Control

The first and most obvious way to control a device like an orthoses or a prostetic is, to control the leverarm itself, because it is directly responsible for the angle of the foot during the gait cycle as well as for the moment required for walking. Figure 3.83 represents a robotic actuator. Using this control method, L is the controlled value which is the output of the spring. To control, the actual leverarm position, L_a is measured by the use of a potentiometer and subtracted from a reference value r. The following equation represents the control law using a PD-Controller, where u_c represents the control voltage sent to the motor amplifier. [Boehler, 2008]

$$u_c = K_p \cdot (r - L_a) + K_d \cdot (\dot{r} - \dot{L_a}) \tag{3.40}$$

This controller is easy to implement and needs only the input of the potentiometer to

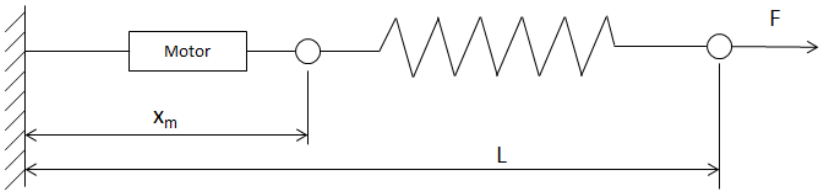

Figure 3.83: Schematic of a robotic actuator

control the position of the leverarm. Also, an automatic zeroing procedure prior to the

use can be initiated. However, because the output side of the spring and therefore the leverarm is controlled, the user is forced to follow the given pattern r. [Boehler, 2008]

3.4.1.2 Basic Nut Control

The Basic Nut Control is basically using the same method as used in the Lever Control, but does not control the spring's output but the spring's input side and therefore the motor nut's position, represented by x_m. The actual position of the nut can be calculated by the use of a motor encoder. Therefore the PD-Controller changes as follows

$$u_c = K_p \cdot (r - x_m) + K_d \cdot (\dot{r} - \dot{x_m}) \tag{3.41}$$

Normally motor encoders are built as incremental encoders. Hence, a manual zeroing procedure is necessary prior to start walking with the device. However, implementing an absolute potentiometer at e.g. the ankle joint could be used to automate this process. Because this controller monitors the nut position on the input side of the spring, the user's comfort during walking is highly increased. Also now the spring can act as a safety device for the user and compensate for small errors in the gait. [Boehler, 2008]

Basic Nut Control is a very safe and robust control method, however, the user is still fixed by its gait pattern. The controller follows the reference input r at any time, predefining the gait pattern and the walking speed. Deviation from that reference on the fly is not possible. Also one has to remember that the reference command might be optimized for walking on even, plain ground, but certainly does not cover walking on ascending or descending slopes nor including stairs. Due to these limitations, all day usage is limited and more sophisticated methods have to be developed. [Boehler, 2008]

3.4.1.3 Nut Control with Time Modulation

The first approach to make the reference input more variable to adopt to different users, was to use time modulation. Therefore the reference pattern was tried to be fitted by using polynomial curves. By changing the durations it was desired to find a mathematical correlation between them. Another approach was to use Fourier series to match the reference pattern and then vary the frequencies of the sine and cosine terms to change the duration and pattern of the curves. However, these approaches only work in a narrow range of walking speeds, because the human kinematics of the ankle motion changes on higher and lower speeds. [Hitt et al., 2007, Oymagil et al., 2007]

3.4.1.4 Impedance Control

This control method was developed to gain more flexibility. Therefore a mass-damper-spring relationship between the input position x and the output force F was established

$$F = m_d\ddot{x} + b_d\dot{x} + K_d x \tag{3.42}$$

where m_d, b_d and K_d represent the virtual inertia, dampening and stiffness coefficients of the system. Using this approach, one can effectively change the dynamics of the system and adapt the response of the device to varying types of grounds. However, still the changes cannot be applied on the fly. Furthermore, in order to make this method work, the reaction force F has to be known. Hence, sensors have to be implemented into the device's sole in order to measure the necessary data, which increases the weight as well as the wiring, influencing the optical appearance in a negative way. Furthermore, most of the time the data from force sensors of that size are of poor quality, introducing problems to design a well functioning feedback loop. This controller was extensively tested by Blaya and Herr at MIT trying zero, constant and variable impedance control strategies. The results of the tests showed, that the constant impedance control eliminated foot slap at slow and self selected speeds and that their variable impedance controller reduced the amount of foot drag due to increased swing dorsiflexion. [Blaya and Herr, 2004]

3.4.1.5 Equilibrium Controlled Stiffness (ECS)

Taking another look at figure 3.83 one can come up with the following formula

$$F = -K_{act} \cdot (L - x_m - d) \tag{3.43}$$

where F is the force acting on the leverarm and d represents the free length of the spring. As shown earlier by T. Sugar [Sugar, 2002], one can use the nut position to influence the device's behavior to imitate any desired stiffness of the spring. Furthermore it can be used to apply a certain preload on the device. The relation between nut position, the stiffness and the force is given by

$$F = -K_{des} \cdot (L - L_0) + F_{des} \tag{3.44}$$

where K_{des} is the desired stiffness value, L_0 the virtual home position and F_{des} the desired preload on the leverarm. By using this equation and substituting it into equation

3.43, one can solve for the nut position y and come up with

$$y = \left(1 - \frac{K_{des}}{K_{act}}\right) \cdot L + \frac{K_{des}}{K_{act}} \cdot L_0 + \frac{f_{des}}{K_{act}} - d \tag{3.45}$$

This equation allows us to control the virtual stiffness of the device. However, because of y being the output, this control method can be combined with any position controller already discussed. This control method for stiffness is rather powerful and can be used in a variety of different ways. Two special cases are presented in the following. [Boehler, 2008]

For simplicity let us assume that the free length of the spring d is equal to zero and that the home position is the same for both cases. Therefore f_{des},L_0 and d are all zero.

Case1: $K_{des} = 0$
By applying this stiffness value to equation 3.43, we end up with $y = L$, meaning that the spring is assumed to be infinitely soft. Hence, the spring follows whatever the lever does. This approach could be used, to measure the gait profile of a patient to gain data about his ankle movements. [Boehler, 2008]

Case2: $K_{des} = K_{act}$)
Applying this case, equation 3.43 becomes $y = 0$. Hence the motor will hold its position, which might be especially of interest for the use of stroke patients regarding foot drop. [Boehler, 2008]

3.4.1.6 Dynamic Pace Controller

As mentioned earlier already, all of the controllers mentioned up to now are only optimized for a narrow range of walking speeds. This is mainly because the dorsi- and plantarflexion of the foot depends on how fast we are walking. The slower our pace, the less dorsi- and plantarflexion and the faster the more flexion respectively. Therefore to adopt to different gait speeds, not only the duration of the nut profile, but also the amplitude has to be modified. [Boehler, 2008]

To get appropriate data concerning the amplitude and length of such a pattern, Sawicki performed tests with people walking on a treadmill at given speeds, but forcing them to take steps with different stride lengths. This data then was used to scale the reference curve up and down respectively. [Boehler, 2008]

The standard gait cycle takes up around 1s. By using the data obtained from the

tests of Sawicki, five different nut profiles were calculated which where then run through a Fourier analysis to obtain a continuous spectrum. Figure 3.84 shows a 3D plot of nut profiles at different strides lengths used for the controller. As one can see from the graph, the nut profiles vary from each other in length as well as in amplitude. [Boehler, 2008]

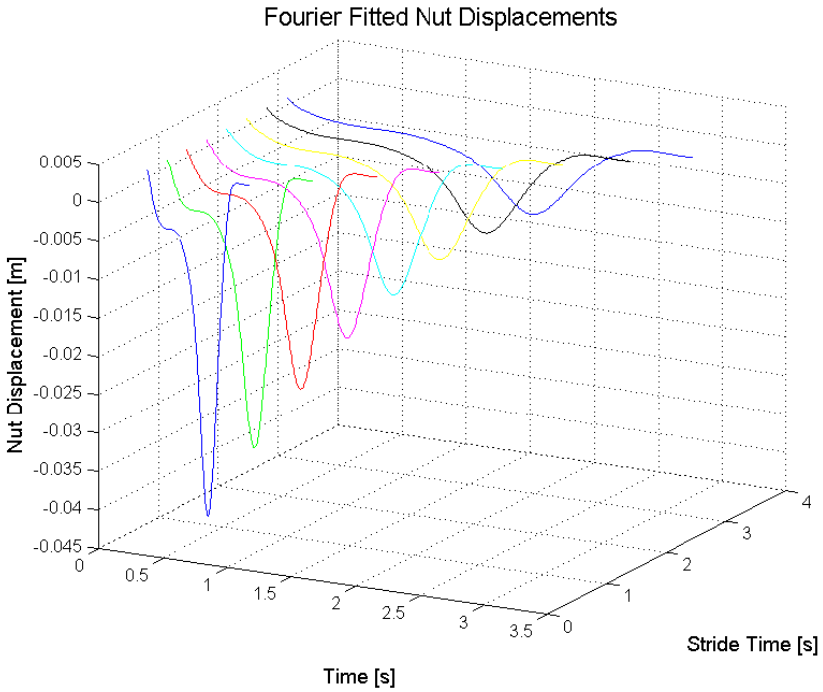

Figure 3.84: Profiles of Dynamic Pace Controller [Boehler, 2008]

By fitting the curves with a spline interpolation, the overall smoothness of the curves are enhanced. The use of splines minimizes unnecessary accelerations of the motor and therefore lowering the overall power consumption and the noise of the motor. However, despite the advantages, some difficulties still remain. For one, the profiles have to be recalculated for every person, because they are dependent on the patient's weight. Furthermore, the curves were recorded on patients walking on a treadmill. Therefore walking on even ground will certainly work as well, but as soon as the environmental conditions change to loose ground, slopes, stairs, etc, the controller will reach its limitations again. Last, the controller will always be one gait cycle too late, because it uses the last cycle to adjust the current profile. [Boehler, 2008]

3.4.1.7 Robust Control

The robust controller uses a combination of two already existing controllers discussed earlier, namely the velocity control and the equilibrium stiffness control. Hollander suggests to split the gait cycle into five distinct parts, each controlled by one of the two mentioned control methods (see figure 3.85) [Hollander and Sugar, 2007]

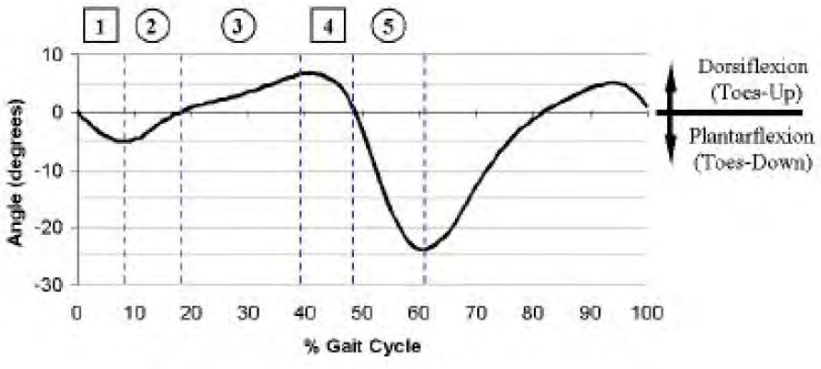

Figure 3.85: Split up of gait cycle for robust control [Hollander and Sugar, 2007]

In this figure, the numbers circled represent the part of the gait cycle controlled by linear stiffness control, while the other ones, represented with squares, incorporate the velocity control method. However, it has to be kept in mind, that the desired stiffness can be calculated using data from the ankle angle, but the actual stiffness is defined by the designer and cannot be altered.

For *zone 1* a velocity controller is in use. It is activated as soon as heel strike occurs and the motor is kept on a constant velocity proportional to the previous gait's velocity.

Zone 2 uses the stiffness control approach to maintain a constant spring stiffness throughout this part of the gait cycle. It starts as soon as the ankles angular velocity passes zero.

Zone 3 uses the stiffness control approach again and starts as soon as flat foot occurs. It occupies most of the loading phase.

Zone 4 is activated when the heel lifts off the ground. Here, the constant velocity is maintained.

Zone 5 starts when the spring is loaded to its maximum, so that the body accelerates forward. In this phase, the motor holds position using the constant stiffness method to release the energy stored in the spring. The end of this part in the gait cycle is marked, when all the energy of the spring is released and the swing phase begins.

By using this method the delay in adopting to the patient's gait, as mentioned in

the previous controller, doesn't occur any more, allowing dynamic adjustments to the walking pattern as the patient walks. Interesting is, that this approach follows a simple *stretch-hold-release* pattern, while the device can still compensate for small errors of the user. However, again, the reference profile was taken for only one specific average walking speed, while the Dynamic Pace Controller allowed the user to change speeds and still adapt to it, but with a delay of one gait cycle.

3.4.2 EPOS2 Controller

As mentioned earlier, the EPOS2 40/12 is a motor controller specifically designed for the use on robots. It was developed in cooperation of SpringActive and Maxon Motors in Switzerland, where SpringActive defined the requirements and the layout and manufacturing as well as the programming was performed by Maxon.

The EPOS2 has a variety of different control modes which can be used. These are:

- Profile Position Mode
- Homing Mode
- Interpolated Position Mode
- Position Mode
- Master Encoder Mode
- Step/Direction Mode
- Profile Velocity Mode
- Velocity Mode
- Current Mode

Despite the vast amount of opportunities of which we can choose from, it still is the simplest way for us to use the position control approach of the Position Mode. This mode requires several inputs to the controller in order to work properly:

- Software Position Limit
- Max. Profile Velocity
- Max. Acceleration

- Position Value

Because the Controller is connected to the Microprocessor Board MC710AWA via a CAN Bus connection, the data is transmitted digitally, minimizing the possibility of getting corrupted signals due to environmental influences.

The desired position value is being checked if it is within the limits given during initialization and then passed forwards as a *position demand value* to the control structure consisting of a PID-Controller. The motor encoder, provides the necessary information for the feedback loop to make certain, that the motor is at its desired position. [Maxon, 2013]

3.4.3 Tibia Controller

The tibia controller is the newest and so far most sophisticated controller used in this field of application. It tries to mathematically link the tibia angle with the ankle movement throughout the gait cycle. Therefore the tibia angles (in world coordinates) were measured for one gait cycle at different stride lengths. Figure 3.86 shows those recordings and as one can see the curves are all close to each other, only scaled by a function of stride length.

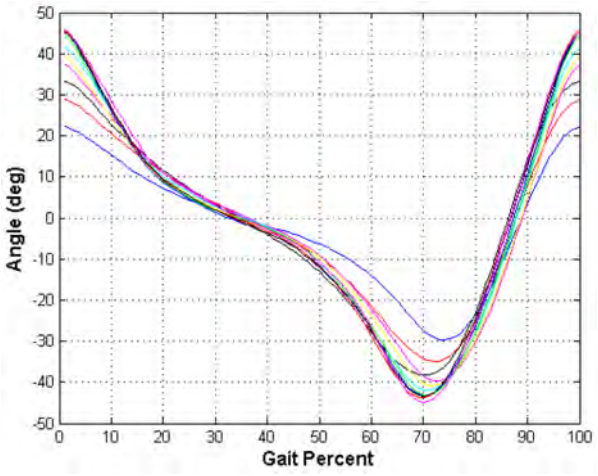

Figure 3.86: Tibia angle during one gait cycle [Holgate et al., 2009]

Also, if the curves are split at 70%, at the minimum, each curve becomes invertible. The slope of the split up curves further distinguish them from each other. The goal of that controller is it, to provide continuous control on the motor by using a gyro and accelerometer sensor only, which both can be placed on the e.g. prosthetics shell around the tibia. Because a function is needed that can be inverted, the tibia angular velocity is

introduced and plotted as a function of the tibia angle. Figure 3.87 shows the function in polar coordinates. [Holgate et al., 2009]

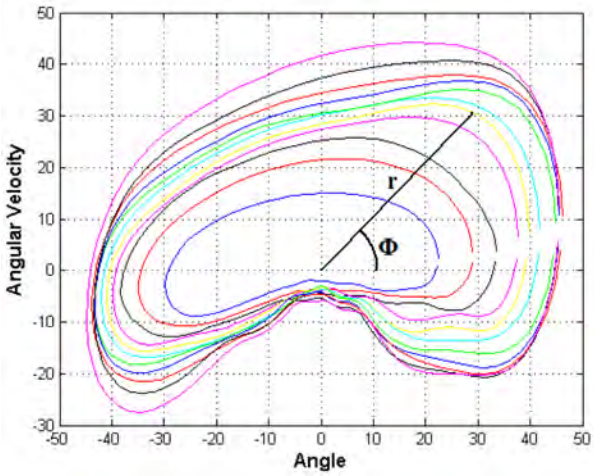

Figure 3.87: Tibia angular velocity as a function of tibia angle [Holgate et al., 2009]

From that graph it is obvious, that there must be a connection to the gait percent. Therefore the polar angle ϕ was plotted against the gait percent as shown in figure 3.88, which is invertible. Hence, the angular velocity and the angle of the tibia can be measured and the polar angle calculated and used as an input to a function relating tibia angle to the gait percent. [Holgate et al., 2009]

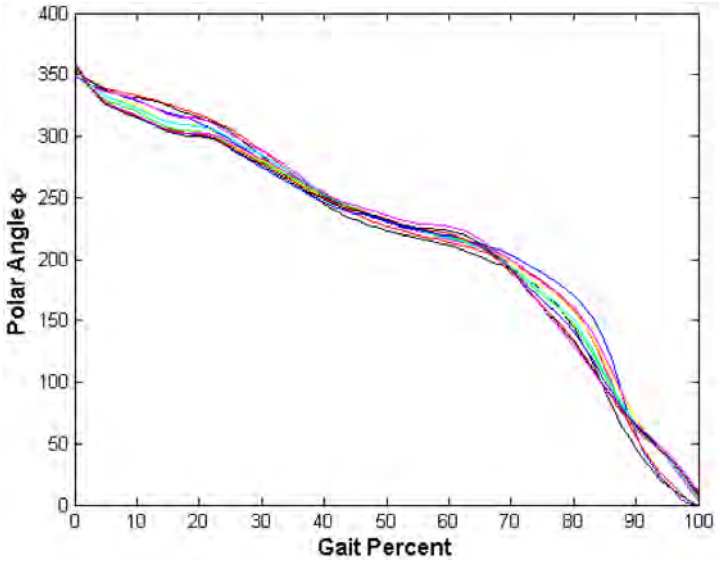

Figure 3.88: Polar angel as function of gait percent [Holgate et al., 2009]

Calculating the gait percent based on the so far mentioned information is straight forward, but the ankle angle is also dependent on the stride length. By taking a closer

look at figure 3.87, it can be seen, that the polar radius depends on the stride length. Therefore the polar radius was plotted as a function of gait percent and stride length, because the function relating the stride length to r is also dependent on the polar angle ϕ. [Holgate et al., 2009]

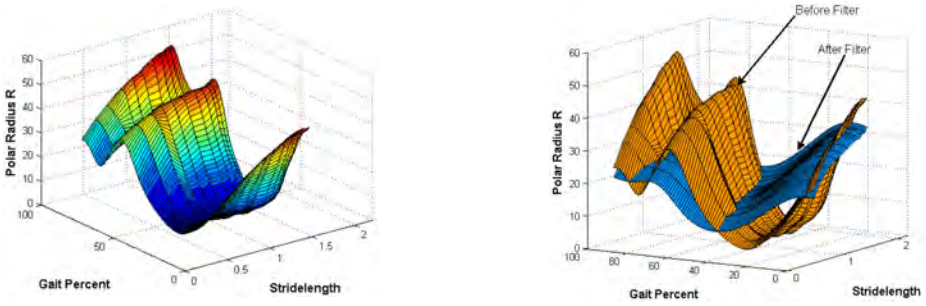

(a) Polar radius as a function of gait percent and stride length [Holgate et al., 2009]

(b) Filtered polar radius as a function of gait percent and stride length[Holgate et al., 2009]

Figure 3.89: Polar radius as function of gait percent and stride length

Taking a look at figure 3.89a, one can see that the surface is almost flat at 25% resulting in an almost vertical plane where one point has multiple solutions, if inverted. This is directly related to the area of angular velocity -5 and angle 0 in figure 3.87. Applying a first order filter on 3.89a results in a much smoother surface which can be inverted, presented in figure 3.89b. Now, that the stride length can be calculated as well, the connection to the ankle angle has to be made. Therefore motion capture data from literature was taken into account and sampled across multiple stride lengths. The data then is plotted as a function of gait percent and stride length, resulting in a surface plot as shown in figure 3.90. [Holgate et al., 2009]

With that knowledge the tibia angle and velocity can be related to the ankle angle of the foot.

With implementing sensors, problems are introduced all the time. In this instance the question is, how accurate the measurements are. In our case we have two gyros to choose from. However, because the one implemented on the micro processor board has multiple degrees of freedom due to the mounting of the actuator, the second gyro, strapped to the foot, is used, in order to get more accurate and evaluable data. It provides us with a voltage proportional to the angular velocity. Therefore the signal has to be integrated to get the angle of the tibia. Because the signal is sampled discretely

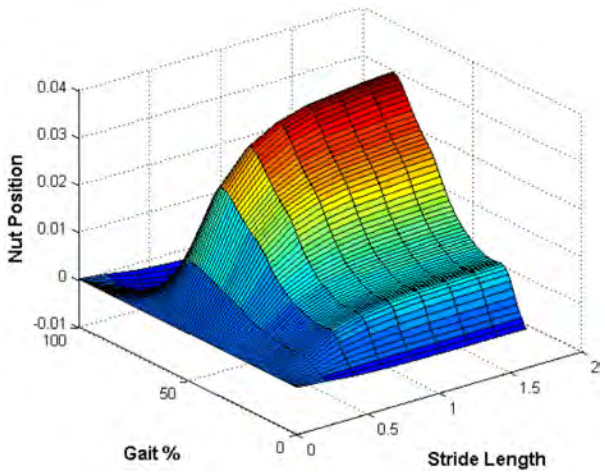

Figure 3.90: Ankle angle as function of gait percent and stride length[Holgate et al., 2009]

and contains noise, the errors sum up due to integration causing the signal to drift away from its true value. Strap down algorithms or Kalman filters are not preferred due to the necessity of introducing another set of sensors, and so a pseudo integration, using a transfer function, was introduced

$$\frac{\tau^2 \cdot s}{(\tau \cdot s + 1)^2} \tag{3.46}$$

As shown in figure 3.91, the transfer function approximates an integrator for frequencies above τ. The magnitudes of the function and the integrator are almost the same above τ, while a phase lag remains. However, depending on the chosen value of τ the lag is not significant anymore. Also, instead of having one pole in the center of the pole-zero diagram, which would make the system marginally stable, the use of the pseudo integrator, introduces two poles which are both fixed in position in the negative area of the imaginary axis. Again depending on the chosen τ value, the controller's speed can be adjusted as well, making the controller more stable, reducing the drift and the initial condition are not as important any more. [Holgate et al., 2009]

Also, the choice of τ has an influence on the phase lag. While some phase lag is accepted, it must not be exaggerated, because the axes in figure 3.87 should stay at 90° to each other. Otherwise the functions become a diagonal and the control strategy will not work any more. [Holgate et al., 2009]

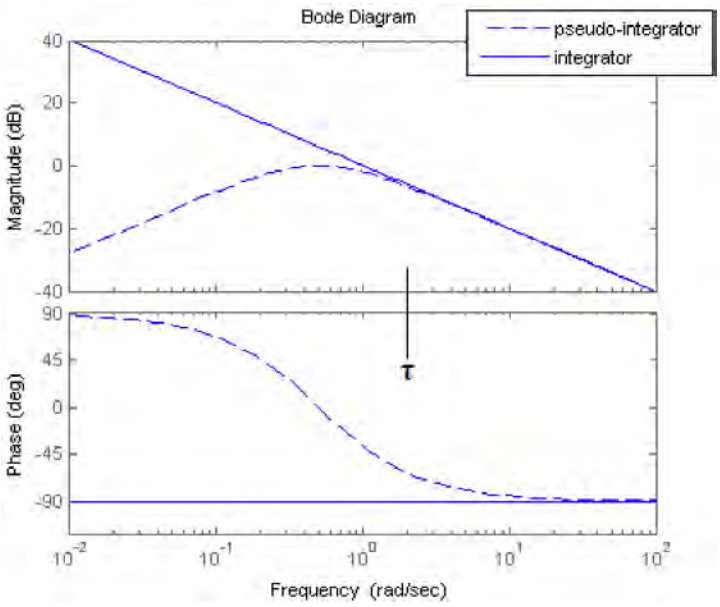

Figure 3.91: Pseudo integrator Bode Diagram [Holgate et al., 2009]

3.4.4 Signal Conditioning

In order to adapt the tibia controller to our needs, the previously calculated nut pattern has to be entered into the system. Experiences in the field of motor controlling showed, that even smooth looking curves sometimes inherit high accelerations, causing the motor and the controller to use more energy than necessary.

In order to optimize the run time of the device even further and make sure to use as little energy as possible, the signal of the nut pattern was given a more in depth observation. Therefore the position signal was differentiated twice to show the accelerations within the signal. Figure 3.92 shows the accelerations of the original nut pattern as the red curve. As one can observe there are lots of spikes, influencing the power drain due to constantly and rapidly changing accelerations. Also they affect the audible noise for the user, the vibrations of the device and the control of the device. In order to circumvent this issue, a Fourier Analysis was performed to replace the original pattern. Because we are dealing with a function which repeats itself and therefore is periodic, it can be replaced by a combination of sine and cosine terms. The analysis was performed by using an already existing function in Matlab to fit the curve. A total of 12 terms was used to gain an accurate fitting function while still significantly reducing the amount of accelerations as one can see in 3.92, where the blue curve represents the accelerations of the fitted function.

Now in order to validate that the original signal can be represented by the new curve

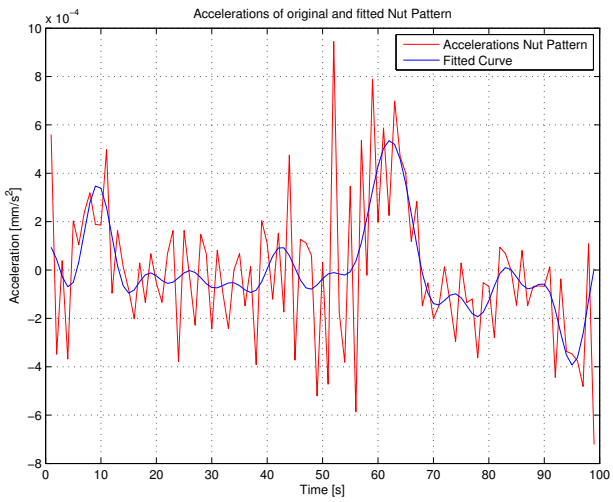

Figure 3.92: Accelerations of original and fitted nut pattern

as well, both of them were plotted on top of each other to verify their shape. As one can see from figure 3.93, there is no misalignment between the curves.

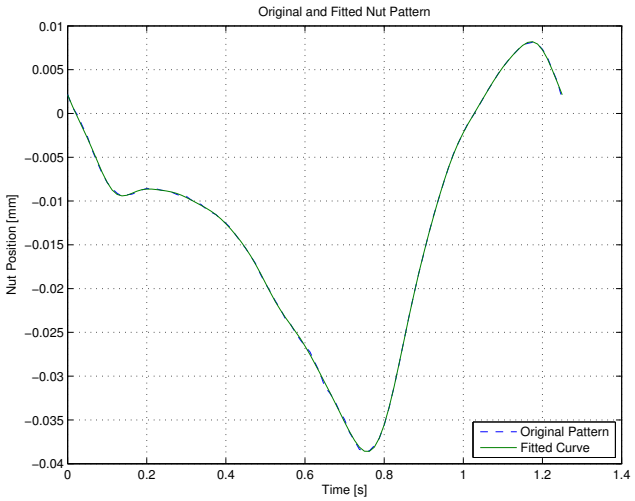

Figure 3.93: Original and fitted nut position

4 Testing and Data Analysis

In order to verify the theory, the device was built and tested on three different subjects, in the range of 75kg to 85kg. While personal opinions were asked from all of them regarding the behavior and the feel of walking with the device strapped onto the leg, data was collected from one subject while walking on the treadmill in various speeds. Each one was given a few minutes to walk around and get used to the device and its behavior to adjust, before the testing was started. Each subject was first asked to walk around in the lab on even ground, to experience how much the device supports the user and how it feels. Afterwards each one was asked to walk on the treadmill for several minutes at various speeds. The final device built and used for testing purposes is presented in figure 4.1.

The feedback of each and everyone exceeded the initial expectations and therefore verified the product. Every subject confirmed that the device is powerful and is certainly capable of supporting the user with at least 50% support. Furthermore it was mentioned by all of them that the device feels very comfortable to wear, because of the multiple degrees of freedom, giving the user the necessary flexibility to not feel restrained at all. Another positively mentioned fact was the weight and the form factor of the device. With only 2.1kg of total weight (battery not included), the PAFO is very lightweight. As reported, the user does not recognize the device at all while walking, except the swing phase, where the device can be felt on the foot. However, while the foot is in contact with the ground, the PAFO has enough power to compensate for its own weight and support the user. Also, the fact that all components necessary are mounted on the device, reducing the amount of stray wires to a minimum, adds to the general positive impression of the device making it easier to be carried and mounted.

Besides the personal opinions, which graded the device positively, data had to be collected and evaluated to qualitatively support the personal opinions. In order to do so, as initially mentioned, one subject was walking the treadmill at different speeds. Prior to recording data via the bluetooth interface, the subject was walking at the determined speed for at least 2 minutes. From all the information recorded, the following were the

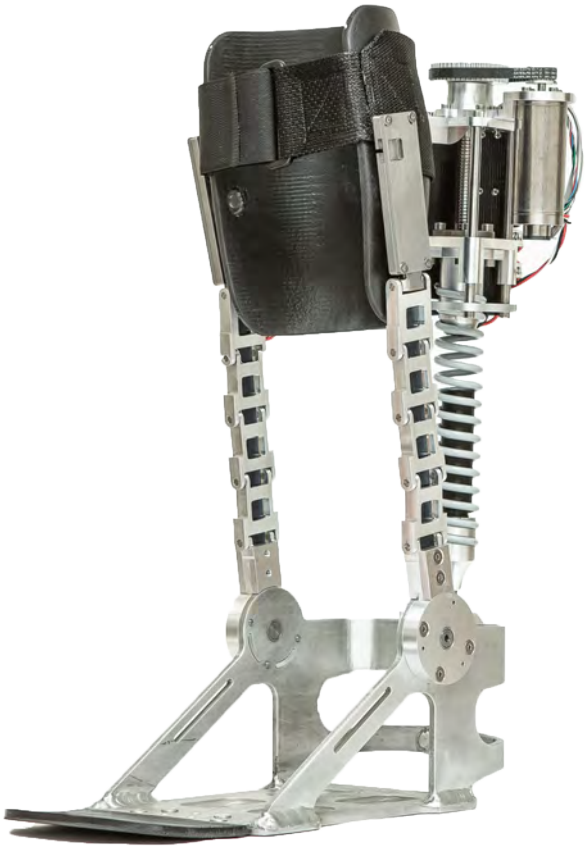

Figure 4.1: PAFO

most important, used for further calculations:

- Motor reference position [rev]
- Motor actual position [rev]
- Motor current [A]
- Ankle joint position [deg]

By now knowing the motor properties as well as the transmission ratio, leverarm and pitch of the ball screw, all necessary information could be derived. First of all it had to be verified, that the motor follows the given reference pattern. As figure 4.2 shows, the motor follows the reference quite accurately with a slight time delay which is acceptable.

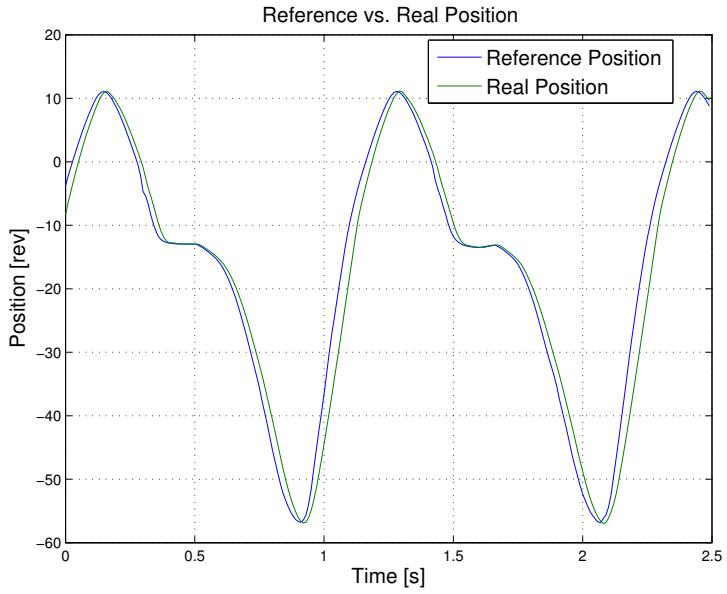

Figure 4.2: Reference vs. real motor position

Figure 4.3 shows three different graphs representing data of the ankle, spring and ball screw nut. From figure 4.3a we can see the nut position, the leverarm and the ankle position. From this graph, it is easy to see that the spring deflection is the difference between the nut position and the leverarm deflection. While the nut is driving towards the highest negative value, the leveram reaches its maximum. The difference between those two curves is represented in figure 4.3b as the spring deflection. Then, the spring deflection can be multiplied with the spring constant and the leverarm of the PAFO to calculate the ankle moment presented in figure 4.3c. As mentioned before, data was recorded at different walking speeds on the treadmill. Figure 4.5 shows a comparison of the ankle moments between a walking speed of $3mph$ and $2mph$. As we see from the figure, there is a slight difference between the speeds, as one would presume, causing the ankle moment to rise from around $50Nm$ to $60Nm$.

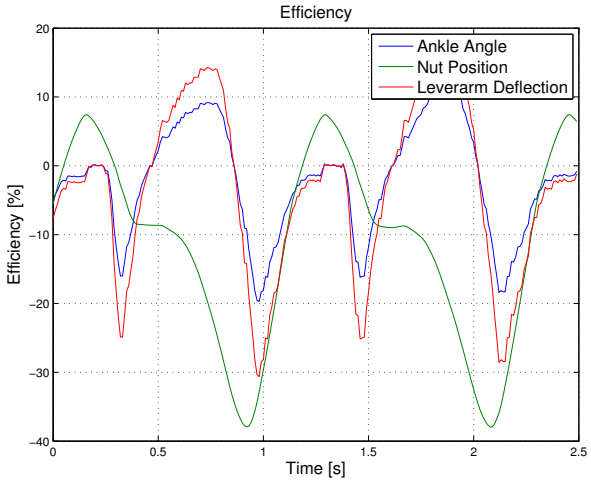

(a) Nut position, ankle angle, leverarm deflection

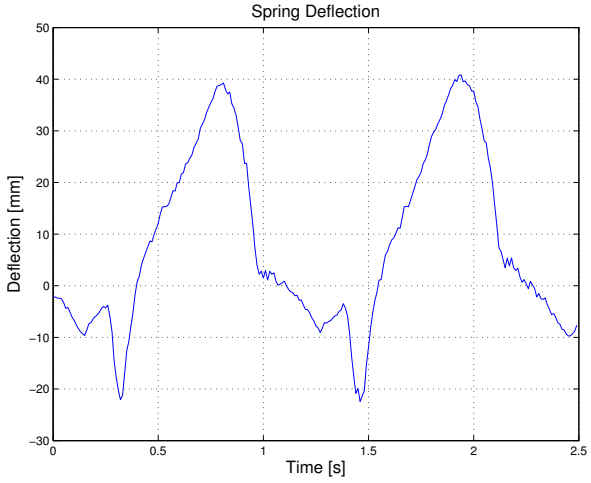

(b) Spring deflection over two consecutive cycles

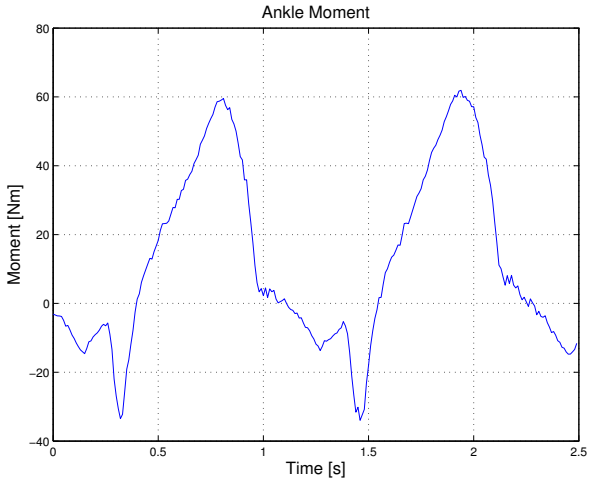

(c) Ankle moment over two consecutive cycles

Figure 4.3: Moments, deflections and positions of the ankle, spring and leverarm at 3mph

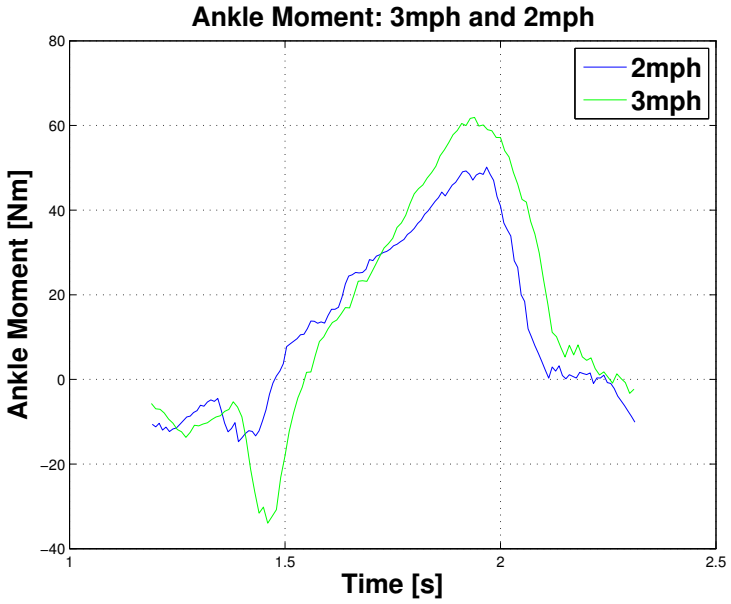

Figure 4.4: Ankle moment comparison 2mph vs 3mph

However, by taking a closer look at the ankle moment and comparing it with the theoretical values calculated during laying out the motor we see, as presented in figure 4.5, that the values do match at the peak of the curve, but are completely off in the beginning and the end. After further investigation, the reason was found and could be referred to the multiple degrees of freedom. In earlier versions of the PAFO, e.g. the version of Alexander Böhler, the connection between the calf shell and the foot assembly was a rigid beam, only having one degree of freedom at the ankle joint. On the calf shell, the rod was fixed in position and could not translate or rotate. Therefore all the movement of the ankle could be recorded by only one sensor placed at the ankle joint. Due to the degrees of freedom introduced to this PAFO, the chain elements are now able to rotate at the ankle joint as well as on the calf shell. Therefore the ankle movement cannot be accurately measured by only one sensor at the ankle, which explains the inaccurate data obtained. Of interest in general would be the overall efficiency of the system to confirm our assumption of 90% for the transmission. However, due to the inaccurate data measured from the ankle it would not make sense to calculate the overall efficiency of the system.

Therefore, only the efficiency of the motor is calculated. The efficiency in general is calculated as

$$\eta = \frac{P_{out}}{P_{in}} \tag{4.1}$$

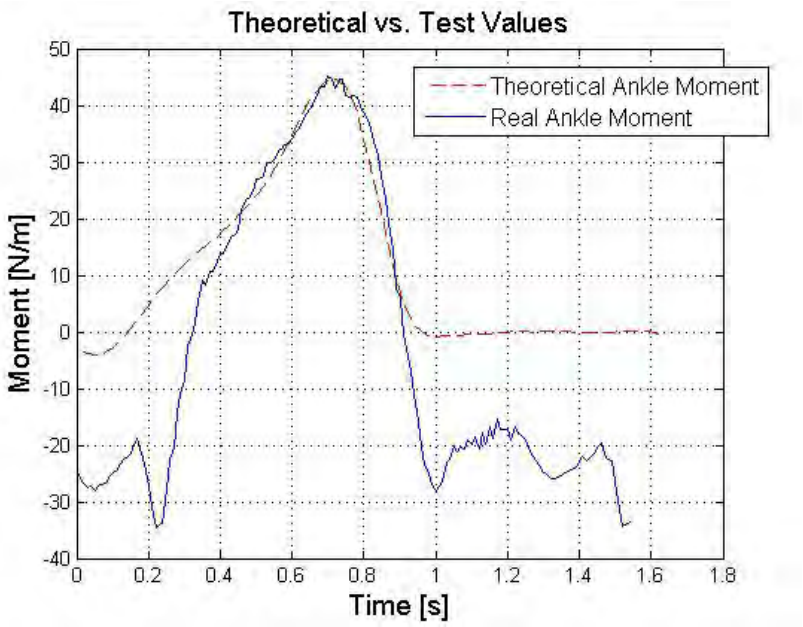

Figure 4.5: Real vs. theoretical ankle moment

where the output equals the mechanical power of the motor and the input the electrical power of the motor. The mechanical power of the motor can easily be calculated as

$$P_m = M \cdot \omega \tag{4.2}$$

where omega can be derived from the measured motor position. The moment M can then be calculated from

$$M = i_a \cdot K_m \tag{4.3}$$

where K_m represents the torque constant of the motor, with the unit of Nm/A.

The electrical power, representing the input in the efficiency equation, is calculated as

$$P_e = u_a \cdot i_a \tag{4.4}$$

where i_a is measured directly and u_a has to be calculated. In order to do so, we have to go back, taking a look at the motor circuit again from figure 3.13 on page 48. From there we see, that u_a can be derived from

$$u_a = R_a \cdot i_a + L_a \cdot \frac{di_a}{dt} + \frac{\omega}{K_v} \tag{4.5}$$

At this point it is important to take the values of the added inductors, which are used

to reach a current ripple, suitable for a switching frequency of $50kHz$, into account. Therefore R_a now consists of the internal resistance of the motor and the DCR of the added coils. The inductance can be neglected, as mentioned initially already, because $L << 1$. K_v still represents the speed constant of the motor, which is unchanged and ω can be derived from the motor position again.

In the following, figure 4.6 shows the electrical-, mechanical power and the efficiency of the motor. The data from the power graphs were processed with a moving average, to make it more visually obvious for the reader how the power levels behave. Therefore 8 terms were averaged and stored as one new value. The green curves represent the moving averaged curve while the blue ones show the original data and the red lines indicate the overall average. The mechanical power, shown in figure 4.6a presents peak power points of around $200W$ while the average power consumption is $41.2W$. The electrical power calculation (figure 4.6b) shows peaks of slightly more than $200W$ with an overall average of $48.6W$. The efficiency calculated from these two curves, presented in figure 4.6c, shows an overall average of 89% efficiency.

Besides behavior during walking, the second mode of the device, also referred to as pumping mode, was tested. In order to activate this mode, the second button on the user interface has to be pushed, causing the device to activate a sinusoidal movement of the nut. In this mode no data was collected. The frequency of the function was set to $0.5Hz$, while the amplitude and offset of the function were adjusted in a way to cover the whole range of movement of the ball screw nut. The movement felt nice and was not distracting for the test subjects.

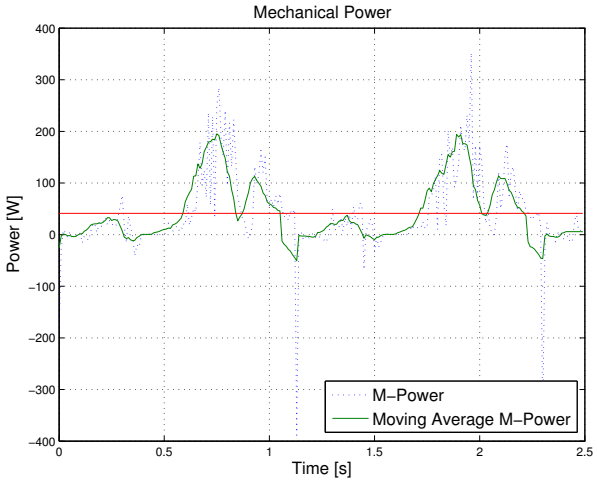

(a) Motor mechanical power over two consecutive cycles

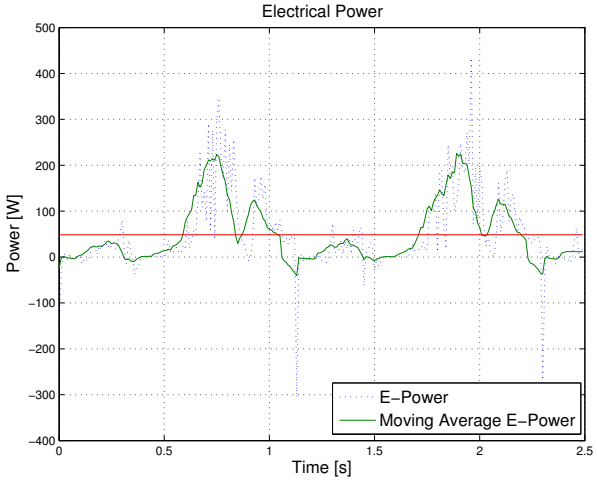

(b) Motor electrical power over two consecutive cycles

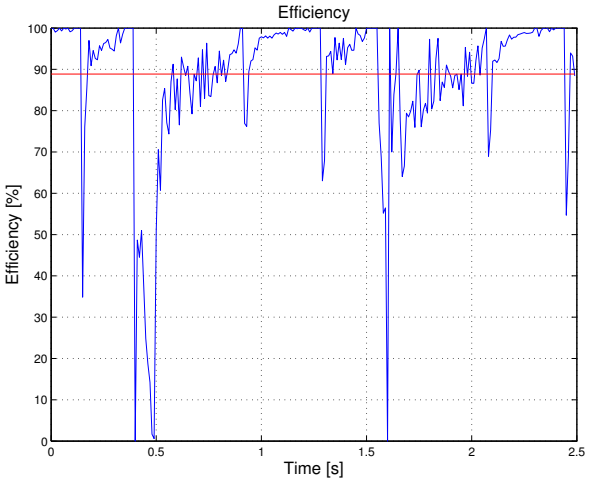

(c) Motor efficiency

Figure 4.6: Motor input and output power and efficiency over two consecutive cycles

5 Discussion and Outlook

Referring to the personal feedback from the subjects, the PAFO for diabetes patients already shows very promising results after the first prototype. One major concern, while adding degrees of freedom to such a device, is, if the necessary moments and forces can still be transferred from one part of the device to the other one. As the test data as well as the feedback of the test subjects point out, this problem was solved in a way, which does not influence the behavior of the device nor the gait behavior of the user. One other goal mentioned at the beginning of the thesis was, that the form factor is one major criteria. During modeling, special attention was paid to that topic. Supervisors and co-workers verified, that the form factor of this device is smaller than other devices of that kind built so far. Also the weight of $2.1kg$ is smaller than what has been developed before.

Earlier versions of PAFOs developed at the lab had lots of stray wires and external boxes containing all the electronics, making it almost impossible to classify the device as mobile and enabling the user to walk with it in daily life. Due to the development of small sized electronic boards and motor controllers, all of the devices could be mounted directly on the PAFO, minimizing the amount of wires to more or less only one cord connecting to the battery.

Furthermore, this is the first device which was modeled and laid out to support users up to $150kg$, opening it for use for a much wider spectrum of people than earlier devices. Due to the exchangeable spring at the actuator, it can also be adjusted to fit the user as well as possible.

Last but not least, the device is, referring the the collected feedback, comfortable to wear. This is mostly related to the added degrees of freedom, allowing the user to move the foot around freely, not feeling restricted.

However, despite all the positive feedback and all the accomplishments, there are also points for improvement and further development. First and most important for the user is to make the device even more comfortable. As mentioned, the calf shell was produced using a 3D printer which limited the size of the shell. Due to the reduced length and

the moments introduced to the shell due to the actuator, certain spots of the calf were affected by high pressure loads, making the device uncomfortable to wear over a longer period of time. Also the shell was only fixed in place by one velcro strap, giving the shell even more freedom to rotate and move. For future enhancements on that area, the shell should be custom fitted and made by a prosthetist. The longer the shell, the less the localized pressure. Also by increasing the length, another velcro strap can be added, minimizing the movement of the shell even further. Finally by adding padding to the inside of the shell and using another shell on the front, which covers a larger area of the shin, will cause a reduction in pressure as well, making the device even more comfortable to wear.

Also, the mounting of the actuator has to be improved. In order to do so, custom springs, which are shorter in length, have to be used allowing the mounting point to be placed in line of the axis of the spring. This will reduce the moments acting on the spring to almost zero extending the lifetime of all components of the actuator.

Because the PAFO is used on humans, it could be necessary to have the possibility to adjust the mounting point of the actuator. Due to the variety of shapes of patient's calves, an improvement can be made by making it possible to adjust the mounting point of the actuator on the calf shell by moving it sideways, ensuring that the actuator's axis is as close to a vertical line as possible. This makes sure that the effect of the force on the leverarm is optimal, increasing the overall efficiency of the device.

Also, the problem of accurately measuring the spring deflection has to be tackled. This can be done either by adding another rotational sensor on the joint between the calf shell and the chain slider connecting to the chain elements, or by not using an ankle angle sensor at all, but measuring the deviation of the length of the spring directly. The latter one is probably the preferred way of doing so, reducing the amount of wiring even more and increasing the quality of the measured data.

Also, the now used EC4-Pole 30 200W motor should be replaced with the EC4-Pole 22 which passed the motor calculation requirements. This decreases the weight of the device even further, but even more important, reduces the overall size. By using the EC4-Pole 22, also smaller inductors can be used reducing the form factor of the PAFO again and making it visually more appealing.

Because this device was a prototype, most of the parts were designed to last as long as possible, while still trying to reduce the size as much as possible. However, as shown during FEA, most of the parts can be sized down, not only reducing the weight of the device, but also making it look less frightening to the user.

Also it has to be verified, that pressure on the foot is reduced due to the use of the device and if so, by what magnitude. Therefore pressure or force sensors must be applied to the foot assembly, measuring the load of the user on the PAFO during gait.

Furthermore, it might be beneficial to enable the slider to be adjusted in height. the way the PAFO is configured right now, the slider allows the user to plantarflex easily, but dorsiflexion is limited. By making the slider adjustable in height, both movements can be served giving the user even more flexibility to move.

Last but not least, regarding the points of improvement, it should be considered to manufacture e.g. three different sizes of orthoses, covering different weight classes. By doing so e.g. a 80kg diabetic woman does not have to wear the much bigger and heavier version, designed for a 150kg male diabetic.

After all, taking into account all the feedback and the data collected, as well as the points of improvements found, one can say, that the device as a prototype was a success and elaboration should be continued.

Bibliography

Afsaneh Alavi, R. Gary Sibbald, Dieter Mayer, Laurie Goodman, Mariam Botros, David G. Armstrong, Kevin Woo, Thomas Boeni, Elizabeth A. Ayello, and Robert S. Kirsner. Diabetic foot ulcers: Part II. management. Journal of the American Academy of Dermatology, 70(1):21.e1–21.e24, January 2014. ISSN 0190-9622. doi: 10.1016/j.jaad.2013.07.048. URL http://www.sciencedirect.com/science/article/pii/S0190962213008219.

AST. Ball bearings - precision miniature bearings - industrial bearings | AST bearings, July 2014. URL http://www.astbearings.com/.

J.A. Blaya and H. Herr. Adaptive control of a variable-impedance ankle-foot orthosis to assist drop-foot gait. IEEE Transactions on Neural Systems and Rehabilitation Engineering, 12(1):24–31, March 2004. ISSN 1534-4320. doi: 10.1109/TNSRE.2003.823266.

Alexander Boehler. Mechanics, control and testing of a robotic ankle foot orhtosis for stroke rehabilitation, May 2008.

Alexander Boehler. MC710awa microprocessor boad SPECIFICATIONS, May 2014.

CANopen. CANopen USA - technology based on CANbus, CAN bus, controller area network, 2014. URL http://www.canopen.us/.

Comsol. Meshing considerations for linear static problems | COMSOL blog, July 2014. URL http://www.comsol.com/blogs/meshing-considerations-linear-static-problems/.

College Einstein. Diabetes facts and statistics | diabetes research center | albert einstein college of medicine, June 2014. URL https://www.einstein.yu.edu/centers/diabetes-research/facts-statistics/.

Barbara Ficarra. Technology robot power suit – hybrid assistive limb (HAL) to help nurses and patients : Health in 30, February 2009. URL http://healthin30.com/2013/02/technology-robot-power-suit-hybrid-assistive-limb-hal-to-help-nurses-and-patients/.

Karl-Heinrich Grote and Jörg Feldhusen. Dubbel Taschenbuch für den Maschinenbau. Springer, Berlin, auflage: 23. aufl. 2012 edition, September 2011. ISBN 9783642173059.

J. Hitt, AM. Oymagil, T. Sugar, K. Hollander, A Boehler, and J. Fleeger. Dynamically controlled ankle-foot orthosis (DCO) with regenerative kinetics: Incrementally attaining user portability. In 2007 IEEE International Conference on Robotics and Automation, pages 1541–1546, April 2007. doi: 10.1109/ROBOT.2007.363543.

Tim Holden. Tim holden quotes at BrainyQuote.com, 1957. URL http://www.brainyquote.com/quotes/quotes/t/timholden324207.html.

M.A. Holgate, T.G. Sugar, and A.W. Bohler. A novel control algorithm for wearable robotics using phase plane invariants. In IEEE International Conference on Robotics and Automation, 2009. ICRA '09, pages 3845–3850, May 2009. doi: 10.1109/ROBOT.2009.5152565.

K.W. Hollander and T.G. Sugar. A robust control concept for robotic ankle gait assistance. In IEEE 10th International Conference on Rehabilitation Robotics, 2007. ICORR 2007, pages 119–123, June 2007. doi: 10.1109/ICORR.2007.4428416.

William J Jeffcoate and Keith G Harding. Diabetic foot ulcers. The Lancet, 361(9368): 1545–1551, May 2003. ISSN 0140-6736. doi: 10.1016/S0140-6736(03)13169-8. URL http://www.sciencedirect.com/science/article/pii/S0140673603131698.

Keller-Kalmbach. Keller & kalmbach - home, July 2014. URL http://www.keller-kalmbach.com/.

Maxon. EPOS2 4012 hardware reference, January 2013.

Shoji Morimoto, H Tomyama, Y Hashimoto, M Ise, H Yoshida, and J Furusho. Development of MRF brake installed lower limb orthosis, May 2014. URL http://ot-world.com/e3731634/e3736354/e3732347/e3734118/e3734119/cg3735135/cg3735137/pub_export?lang=eng&itemid=3037&ts=1402973550.91&export_format=exportAbstract&ZMS_CHARSET=utf-8&download:int=1&btn=Exportieren.

Carlotta Mummolo, Luigi Mangialardi, and Joo H. Kim. Quantifying dynamic characteristics of human walking for comprehensive gait cycle. Journal of Biomechanical Engineering, 135(9):091006–091006, July 2013. ISSN 0148-0731. doi: 10.1115/1.4024755. URL http://dx.doi.org/10.1115/1.4024755.

L Nazarko. Causes and consequences of diabetes. British Journal of Healthcare Assistants, 3(11):534–538, November 2009. ISSN 1753-1586. URL http://search.ebscohost.com/login.aspx?direct=true&db=rzh&AN=2010472716&site=ehost-live.

Gene Ostrovsky. 'embracing the artificial limb', February 2005. URL http://www.medgadget.com/2005/02/embracing_the_a.html.

AM. Oymagil, J.K. Hitt, T. Sugar, and J. Fleeger. Control of a regenerative braking powered ankle foot orthosis. In IEEE 10th International Conference on Rehabilitation Robotics, 2007. ICORR 2007, pages 28–34, June 2007. doi: 10.1109/ICORR.2007.4428402.

G.S. Sawicki, K.E. Gordon, and D.P. Ferris. Powered lower limb orthoses: applications in motor adaptation and rehabilitation. In 9th International Conference on Rehabilitation Robotics, 2005. ICORR 2005, pages 206–211, June 2005. doi: 10.1109/ICORR.2005.1501086.

T.G. Sugar, Jiping He, E.J. Koeneman, J.B. Koeneman, R. Herman, H. Huang, R.S. Schultz, D.E. Herring, J. Wanberg, S. Balasubramanian, P. Swenson, and J.A. Ward. Design and control of RUPERT: A device for robotic upper extremity repetitive therapy. IEEE Transactions on Neural Systems and Rehabilitation Engineering, 15(3):336–346, September 2007. ISSN 1534-4320. doi: 10.1109/TNSRE.2007.903903.

Thomas G. Sugar. A novel selective compliant actuator. Mechatronics, 12(9–10):1157–1171, November 2002. ISSN 0957-4158. doi: 10.1016/S0957-4158(02)00021-1. URL http://www.sciencedirect.com/science/article/pii/S0957415802000211.

W. Svensson and U. Holmberg. Ankle foot orthosis control in inclinations and stairs. In 2008 IEEE Conference on Robotics, Automation and Mechatronics, pages 301–306, September 2008. doi: 10.1109/RAMECH.2008.4681479.

ThomsonLinear_1. Leas screws, ball screws and ball splines, July 2014. URL http://www.thomsonlinear.com/downloads/screws/Leadscrews_Ballscrews_Splines_cten.pdf.

ThomsonLinear_2. Specifying, selecting and applying linear BAll screw drives, June 2014. URL http://www.thomsonlinear.com/downloads/articles/specifying_selecting_applying_linear_ball_screw_drives_taen.pdf.

Michael Whittle. Gait analysis: an introduction. Butterworth-Heinemann, Oxford ; Boston, 3rd ed edition, 2002. ISBN 0750652624.

Michael W. Whittle. An Introduction to Gait Analysis, 4e. Butterworth-Heinemann, Edinburgh; New York, 4 edition edition, February 2007. ISBN 9780750688833.

WHO. WHO | diabetes, June 2014. URL http://www.who.int/mediacentre/factsheets/fs312/en/.

Katherine Xue. Harvard engineers design soft robotic exosuits to aid human movement | harvard magazine jan-feb 2014, February 2014. URL http://harvardmagazine.com/2014/01/wearable-robots.

A. Zelinsky. Robot suit hybrid assistive limb [industrial activities]. IEEE Robotics Automation Magazine, 16(4):98–98, 102, December 2009. ISSN 1070-9932. doi: 10.1109/MRA.2009.934836.

Affidavit

I declare that I have authored this thesis independently, that I have not used other than the declared sources / resources, and that I have explicitly marked all material which has been quoted either literally or by content from the used sources. This thesis has neither been presented, submitted to a different committee nor published.

Author

Dornbirn, 18.8.2014 Philipp Pasolli